CONTROLS ON DOLOMITIZATION OF THE UPPER ORDOVICIAN TRENTON LIMESTONE IN SOUTH-CENTRAL KENTUCKY

COLLIN JAMES GRAY

Department of Geological Sciences

APPROVED:

Dr. Katherine Giles, Ph.D., Chair

Dr. Richard Langford, Ph.D.

Dr. Matthew Johnston, Ph.D.

Charles Ambler, Ph.D.
Dean of the Graduate School

Dedication

I dedicate my thesis work to my family. My dedicated and loving parents, Michael and Deborah Gray have always supported me and provided words of encouragement during the struggles of my research. The support provided was second to none and I could not imagine reaching this point in my education without them. I also dedicate this thesis to my two brothers, Michael and Nathan Gray and my sister Nicole Gray. Without these role models I cannot imagine where my education would have ended. I will always appreciate the support provided by all three of you and consider you to be role models that I can always look up to.

CONTROLS ON DOLOMITIZATION OF THE UPPER ORDOVICIAN TRENTON LIMESTONE IN SOUTH-CENTRAL KENTUCKY

by

COLLIN JAMES GRAY, B.S. GEOLOGY

THESIS

Presented to the Faculty of the Graduate School of

The University of Texas at El Paso

in Partial Fulfillment

of the Requirements

for the Degree of

MASTER OF SCIENCE

Department of Geological Sciences

THE UNIVERSITY OF TEXAS AT EL PASO

December 2015

Acknowledgements

I wish to thank my committee whose time and expertise provided excellent input into my research. Dr. Katherine Giles, my M.S. supervisor provided guidance and provided endless suggestions and recommendations throughout my research while continuously motivating me to continue my education. Dr. Richard Langford donated countless hours providing recommendations and assistance throughout my research. Dr. Matthew Johnston donated his time, expertise, and guidance in the industry of oil and gas exploration.

I am in great debt of appreciation to West Bay Exploration Company for providing financial support throughout my research and for providing a project that would challenge my skills as a geologist. Employees of West Bay Exploration, my mentor Bill Van Sickel in particular, also delivered their input and personal suggestions from their renowned expertise in hydrothermally dolomitized hydrocarbon reservoirs while providing me with career guidance and assistance.

I would also like to thank the numerous organizations that provided funding in the form of grants and scholarships, which include the: American Association of Petroleum Geologists, Geological Society of America, West Texas Geological Society, Southwest Section of the American Association of Petroleum Geologists, and Society of Petrophysicists and Well Log Analysts.

I would like to thank numerous individuals who devoted their time, knowledge, and resources, which allowed for my research to be completed. Dr. Robert Goldstein at the University of Kansas donated his time, knowledge, and laboratory resources to allow for me to conduct a fluid inclusion analysis. Dr. Benjamin Brunner at the University of Texas at El Paso provided his time and expertise in geochemistry. Patrick, Gooding, Ryan Pinkston, and Ray Daniel at the Kentucky Geological Survey's Well Sample and Core Library provided their guidance and expertise while assisting me in the early stages of my research.

Finally, I would like to thank the faculty and students at UTEP who provided valuable feedback throughout my research and always made the Department of Geological Sciences feel like home.

Abstract

The Late Middle Ordovician Trenton Limestone is a highly productive carbonate hydrocarbon reservoir across the eastern United States. Enhanced secondary porosity and permeability within the Trenton Limestone generated by hydrothermal dolomitization (HTD) in Michigan and New York have allowed for extensive hydrocarbon reservoirs to be developed. In these areas, carbonate facies assemblages have been shown to significantly control the distribution of diagenetic alterations and influence the geometry and lateral continuity of reservoir-grade porosity and permeability. South-central Kentucky provides an exploratory region for post-depositional hydrothermal alteration due to its vicinity to the Appalachian-forming orogenic tectonism. Cool water carbonate deposition of the Trenton in Kentucky provides for a new setting composed of facies assemblages that are significantly different when compared to warm water carbonate hosts of the Trenton in New York, Ohio, and Michigan.

Results from outcrop and core analyses indicate that HTD is not facies-selective as the abundance of phosphate and marine hardgrounds in Kentucky's cool water carbonates are porosity-destructive. Rather than primary facies, controls of dolomitization through central Kentucky consist of a combination of fault and fracture networks, fluid injection pressures, homogenization temperatures, and basement fluid sources and sub-Trenton carrier beds. Dolomitization through the Trenton is characterized by vugular, interparticle, intraparticle, and fracture porosity, which are frequently restricted to near-fault and fracture margins.

Investigation of fluid inclusion microthermometric and stable isotope analyses indicate that fluids are sourced from deep Precambrian or Cambrian formations. Fluids generally range from 127°C to 107°C indicating that they are in fact hydrothermal (maximum burial temperatures

of 80°C through the Cincinnati arch region; Huff and Turkmenoglu, 1981) and have variable fluid compositions ranging from saline brines to $NaCl\text{-}H_2O\text{-}CaCl_2$.

Results of this study indicate that Kentucky provides for a setting that is highly susceptible to hydrothermal dolomitization and subsequent reservoir development, however cool water carbonates through the Trenton Limestone are not conducive to allow for reservoir-grade porosity and permeability development. The lack of depositional phosphate within warm water carbonates of the underlying Black River Group Carbonates does, however provide for a valid target to explore for HTD reservoir development in central Kentucky.

Table of Contents

List of Tables

List of Plates

List of Figures

Chapter 1: Introduction

The Trenton Limestone (locally known as the Lexington Limestone) is an Upper Ordovician carbonate succession that extends throughout the upper Midwest to eastern U.S. and has historically been highly productive in hydrocarbons (Hamilton-Smith et al., 1990). Trenton Limestone reservoirs have primarily been linked to fractured and dolomitized limestones associated with basement faulting (Black et al., 1981). The fault-related reservoirs are vertically extensive, but laterally restricted and difficult to predict (Davies & Smith, 2006).

Hydrothermal dolomitization within the Trenton Limestone has been shown to have had a substantial effect on reservoir development in Michigan, New York, and Ohio where secondary porosity and permeability result in highly productive hydrocarbon reservoirs. In hydrothermal dolomite (HTD) settings, deeply circulating basinal fluids are thought to migrate along basement-related fault and fracture networks so that regional tectonic controls are a key element of the system (Davies & Smith, 2006). Studies of fracture-induced hydrothermal dolomitization in warm-water carbonates of the Michigan Basin and western Canada show that specific facies fabrics such as cruziana-type burrows may be preferentially dolomitized and lead to enhanced lateral extent of reservoir-grade porosity and permeability (Grammer et al., 2010).

Fractured and dolomitized Ordovician reservoirs have been identified in south-central Kentucky (Hamilton-Smith et al., 1990; Petroleum Information, 1990; Harris et al., 2006), but the nature and controls on the dolomitization have not been studied in detail. Outcrops of the Trenton Limestone exposed in northern Kentucky have been hydrothermally dolomitized along faults and fractures related to the Lexington Fault System (Reid et al., 2004). During the Ordovician, Kentucky was in the foreland of the Taconic orogenic belt, which may have reactivated basement structures and provided a conduit for secondary fracture-induced hydrothermal dolomitization in the region (Pope and Read, 1997).

This study documents and characterizes the nature of Trenton Limestone dolomitization in the subsurface of south–central Kentucky (Clinton and Cumberland counties) and compares it

to correlative outcrops in northern Kentucky in an attempt to determine the overriding controls (geochemical, stratigraphic, and structural) on dolomitization in the area and increase predictability of reservoir quality and distribution through the cool-water carbonate facies assemblages found in the area. This study tests the hypothesis that hydrothermal dolomitization within the Trenton Limestone is present and has influenced hydrocarbon production in south-central Kentucky and dolomitization may be more extensive in facies that exhibit increased primary porosity and permeabilities. The documentation of HTD and other controls on reservoir attributes in Kentucky will provide a new concept to predictably focus hydrocarbon exploration throughout the region. Characterization of trends in depositional and diagenetic facies within the Trenton Limestone will ideally lead to increased predictability of reservoir development and improved success in hydrocarbon exploration and production through the southern Appalachian foreland area of North America. This study also provides insight into the potential for the development of cool water carbonate-hosted HTD reservoirs in other regions across the globe.

1.1 HYDROTHERMAL DOLOMITIZATION

Hydrothermal dolomitization is an important diagenetic process in hydrocarbon reservoir development because of its tendencies to enhance porosity and permeability in otherwise low-porosity limestone formations. Two forms of dolomite replacement (saddle void-filling and matrix-replacive) are present in prolific hydrocarbon reservoirs of hydrothermally dolomitized carbonates. Hydrothermal void-filling cement produces saddle dolomite and subsequently develops minor amounts of decreased porosity and permeability due to the large crystals and their curved, irregular shapes while matrix-replacive dolomite tends to provide a much more drastic increase in porosity and permeability through the replacement of calcite with the smaller (atomic radius) magnesium (Davies and Smith, 2006).

Within the study area, HTD has been linked to the reactivation of basement-faults and Mississippi Valley-type ore deposits in western Kentucky's Fluorspar District have been interpreted to be derived from fluid flow into Mississippian carbonates as a result of extensive

faulting through the New Madrid Seismic Zone (Black et al., 1981). Additionally, historical production from south-central Kentucky has been attributed to fractured limestones with minor amounts of dolomite hinting at the possibility of additional undiscovered fault systems in the subsurface (Harris et al., 2006). The presence of faults and the structural nature of the region create an extremely favorable geologic setting for hydrothermal alteration.

Models of HTD that utilize open fracture networks to initiate vertical fluid flow have been developed for states such as Michigan and New York where excellent reservoir development within warm-water carbonates has occurred. Migration of magnesium-rich fluids into the Ordovician Trenton Limestone where vertical migration is halted and lateral brine migration into the host facies occurs (Figure 1.1). Results of this interaction frequently lead to diagenetic fabrics such as zebra fabrics, brecciated zones, vugular porosity, and intercrystalline matrix porosity along the fracture networks with saddle (baroque) dolomite crystal growth in open vugs and fractures. Fluid inclusion microthermometry, cathodoluminescence microscopy, strontium isotope analysis, and stable isotope analysis are common tools utilized to determine salinity, temperature, paragenesis, and $\delta^{18}O_{dolomite}$ within dolomitized zones to determine geochemical controls and subtle irregularities between HTD bodies. Further variations include variable mineralogies including fluorspar, barite, sphalerite, and calcite, which vary based on fluid compositions and sources being derived from deep brine circulation.

Geometries of diagenesis are severely limited by the geometry of fracture networks, timing of fluid migration, host facies pore geometries, and fluid injection pressures. One of the most well-known HTD reservoirs is the Albion-Scipio field in southern Michigan, which is approximately 35 miles long, is less than 1 mile wide, and occurs in the Trenton-Black River Group Carbonates (Ells, 1962). Outcrops in central New York occur along en echelon fractures that developed along a strike-slip fault system, which were likely active during the Taconic Orogeny and led to the formation of three dolomite bodies stretching approximately 170 feet along strike yet only reach a maximum of three feet wide (Slater and Smith, 2012).

Consequently, geometries of diagenesis are highly variable; however lateral extent relative to length (strike plane of parent fractures) is unanimously restricted.

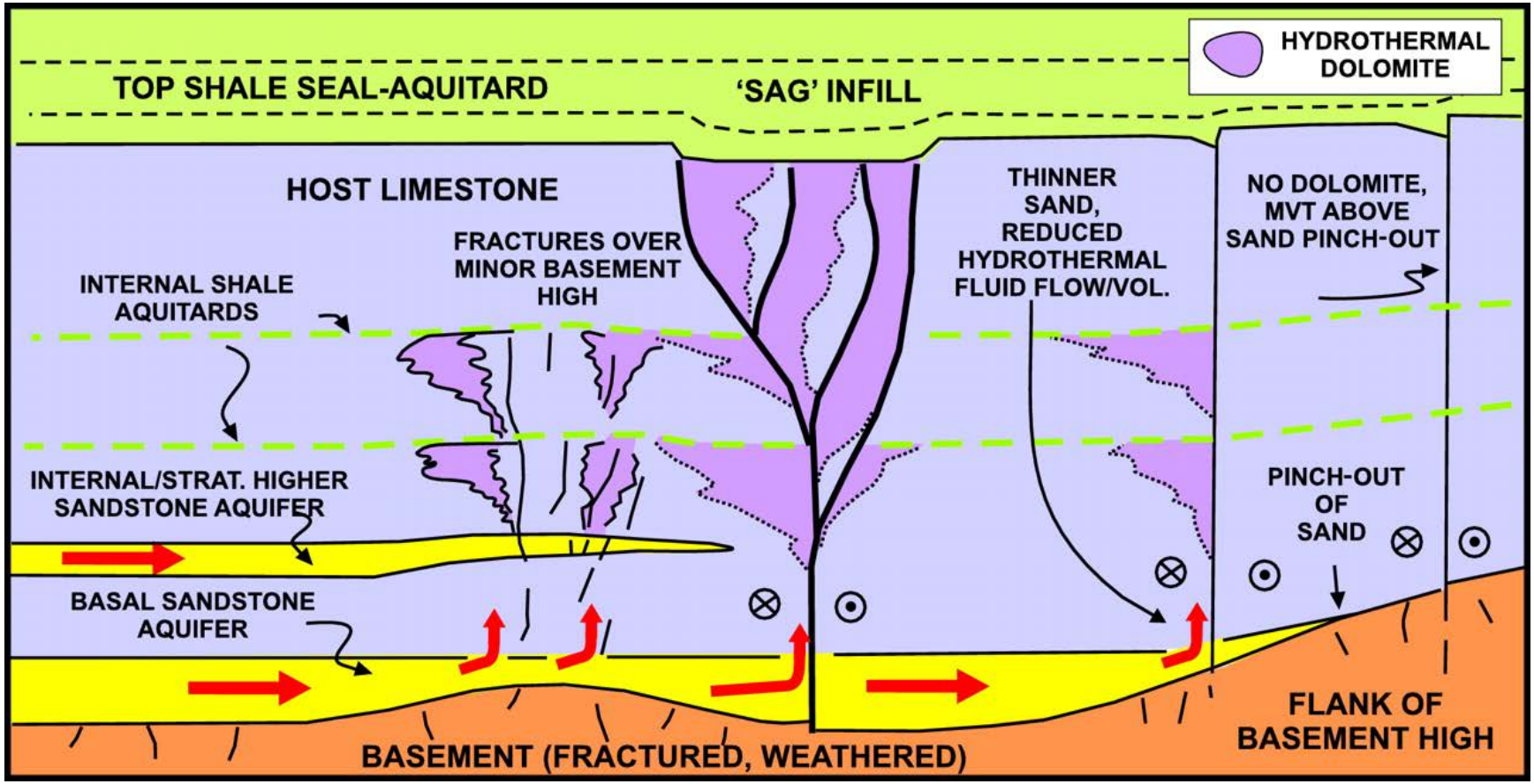

Figure 1.1 A model illustrating features associated with hydrothermal dolomite reservoir development. Fluid migration along porous and permeable carrier beds flows vertically along reactivated fault planes into the host limestone where aquitards limit vertical fluid flow forcing lateral fluid migration. The 'Sag' at the contact of the hydrothermal dolomite and top shale seal results from solution collapse within the dolomitized reservoir and is a distinguishing characteristic of hydrothermal dolomite reservoirs that can frequently be observed on reflection seismic profiles (From Davies and Smith, 2006).

Chapter 2: Geologic Setting

2.1 Regional Structure

The Precambrian Basement in Kentucky can be subdivided into three prominent provinces; the Granite-Rhyolite Province, the Middle Run Formation, and the Grenville Province (Figure 2.1; Greb and Solis, 2010). The Grenville Front is a large thrust sheet that trends generally north-northeast and directly underlies the Lexington Fault System, which is composed of predominantly steeply dipping normal faults with minor thrust and strike-slip faults dispersed through the system (Greb and Solis, 2010). Two negative Cambrian structures transect Kentucky; the Rough Creek Graben to the west and the Rome trough to the east (Figure 2.2). The Rough Creek Graben is a dogleg feature located on the Reelfoot Rift that trends approximately W-E and developed during Cambrian rifting and opening of the Iapetus Ocean (Potter et al., 1995). The Rome trough is a northeast trending negative structure that also resulted from Cambrian rifting and experienced subsidence during the Late Cambrian (Gao et al., 2000). Seismic studies of Precambrian and Cambrian rocks through Kentucky have revealed that normal faulting is the dominant structure through central Kentucky (Brett et al., 2012). Major fault systems that transect the study area include the Lexington, Kentucky River, and Irvine-Paint Creek fault systems, which are often associated with local mineralization adjacent to fractures (Weir et al., 1984).

Three major tectonic pulses developed the structural framework of the central Kentucky area through the Paleozoic: the Taconic, Acadian, and Alleghanian orogenies. The Taconic orogeny (Late Ordovician) formed during plate convergence of eastern North America and South America during the closing of the Iapetus Ocean. The Taconic orogeny can be subdivided into three tectonophases; the Blountian, Vermontian, and the Chatfieldian (Brett et al, 2012). Deformation in Central Kentucky associated with the Taconic orogeny (Chatfieldian tectonophase) led to the development of the N-NE trending Cincinnati arch, which extends from central Tennessee to Ohio (Figure 2.1). The northern termination under the Jessamine dome

marks the point where the Cincinnati arch bifurcates into the Kankakee and Findlay arches (Silurian and Devonian development), which trend W-NW and N-NE, respectively (Brett et al., 2012; Weir et al., 1984). The Cincinnati arch separates the Illinois basin (present day geometry formed during the Late Cretaceous uplift of the Pascola arch) from the Appalachian basin and consists of three prominent positive structures; the Jessamine dome, the Cumberland saddle, and the Nashville dome (Catacosinos et al., 1996). The Jessamine dome structural high was a fault-bounded positive feature during Trenton deposition (Borella and Osbourne, 1978; Weir et al., 1984). Trenton Limestone deposition occurred along the northeast trending Lexington platform within the Appalachian basin during the Late Ordovician. The Lexington platform was bound to the west by the Sebree trough and to the southeast by the Taconic foreland (Martinsburg foredeep) while the platform plunged slightly northeast. Subsidence in the Sebree trough was likely initiated during early stages of the Taconic orogeny when Taconic flexure led to reactivation of the Rough Creek Graben (Kolata et al., 2015). Trenton Limestone deposition was continuous along the Lexington platform, however dramatic thinning to approximately 150-200 feet is observed near the Jessamine dome of Central Kentucky and further thinning of the interval (completely absent near the center of the trough) occurs in the adjacent Sebree trough (caused by intertounging with deep water facies of the Clays Ferry Formation) indicating that arch development was synchronous with Trenton deposition (Brett et al., 2012). Taconic orogenic stresses induced a second period of subsidence through the Rome Trough, which closely followed deposition of the Trenton Limestone (Borella and Osborne, 1978; Cable and Beardsley, 1984; Weir et al., 1984). Historic hydrocarbon production within the Trenton has been from the Cumberland saddle region focused around Clinton and Cumberland counties. Tectonic flexure and dormant basement fault reactivation likely occurred during the later stages of the Taconic orogeny or during the Acadian and Alleghanian orogenies of the Late Devonian and Permian, respectively (Brett et al., 2012).

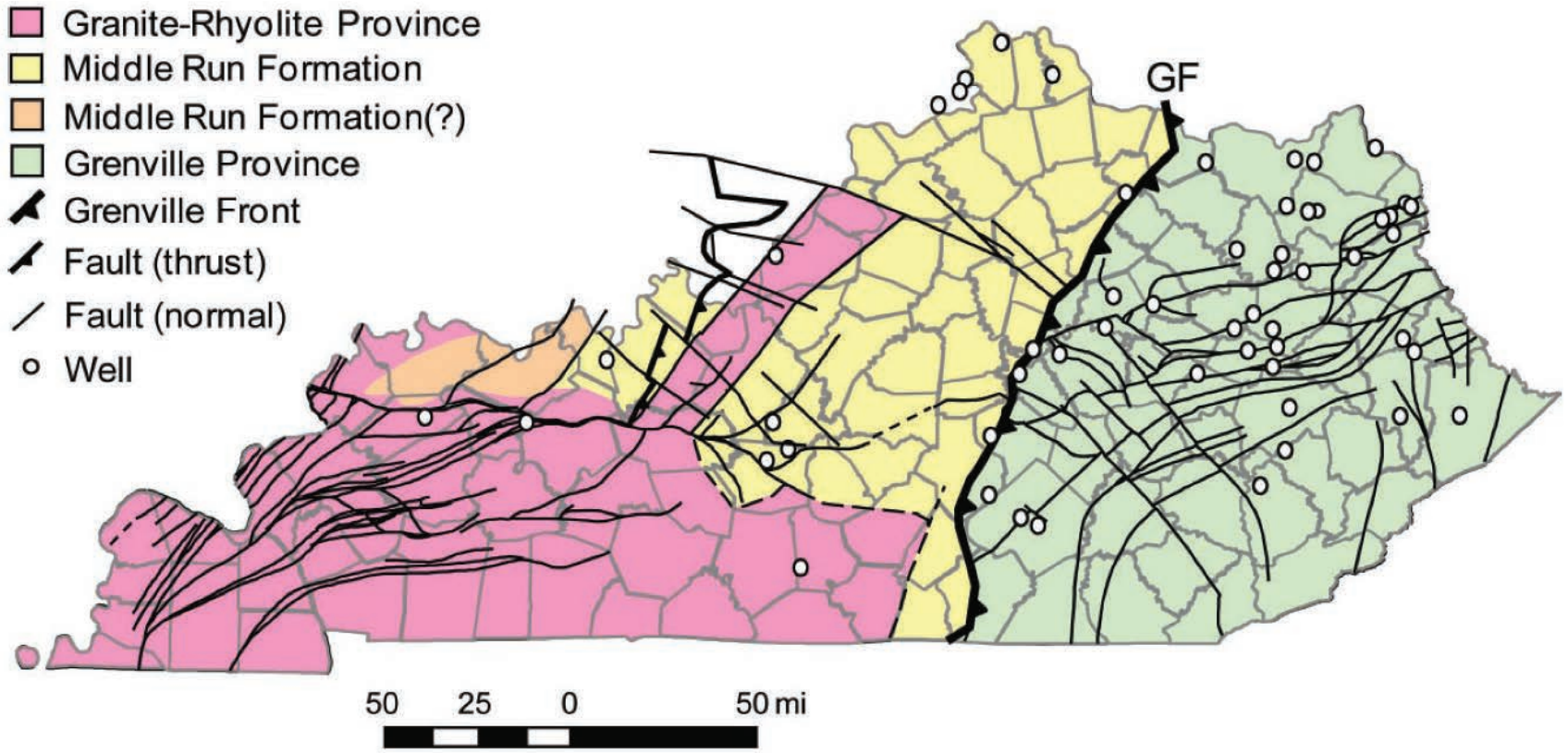

Figure 2.1 Map illustrating the four Precambrian compositional provinces in the subsurface of Kentucky. The Grenville Front is marked by a large thrust fault that very closely follows the path of the Cincinnati Arch through central Kentucky. Note the abundance of normal faulting through central Kentucky (From Greb and Solis, 2010).

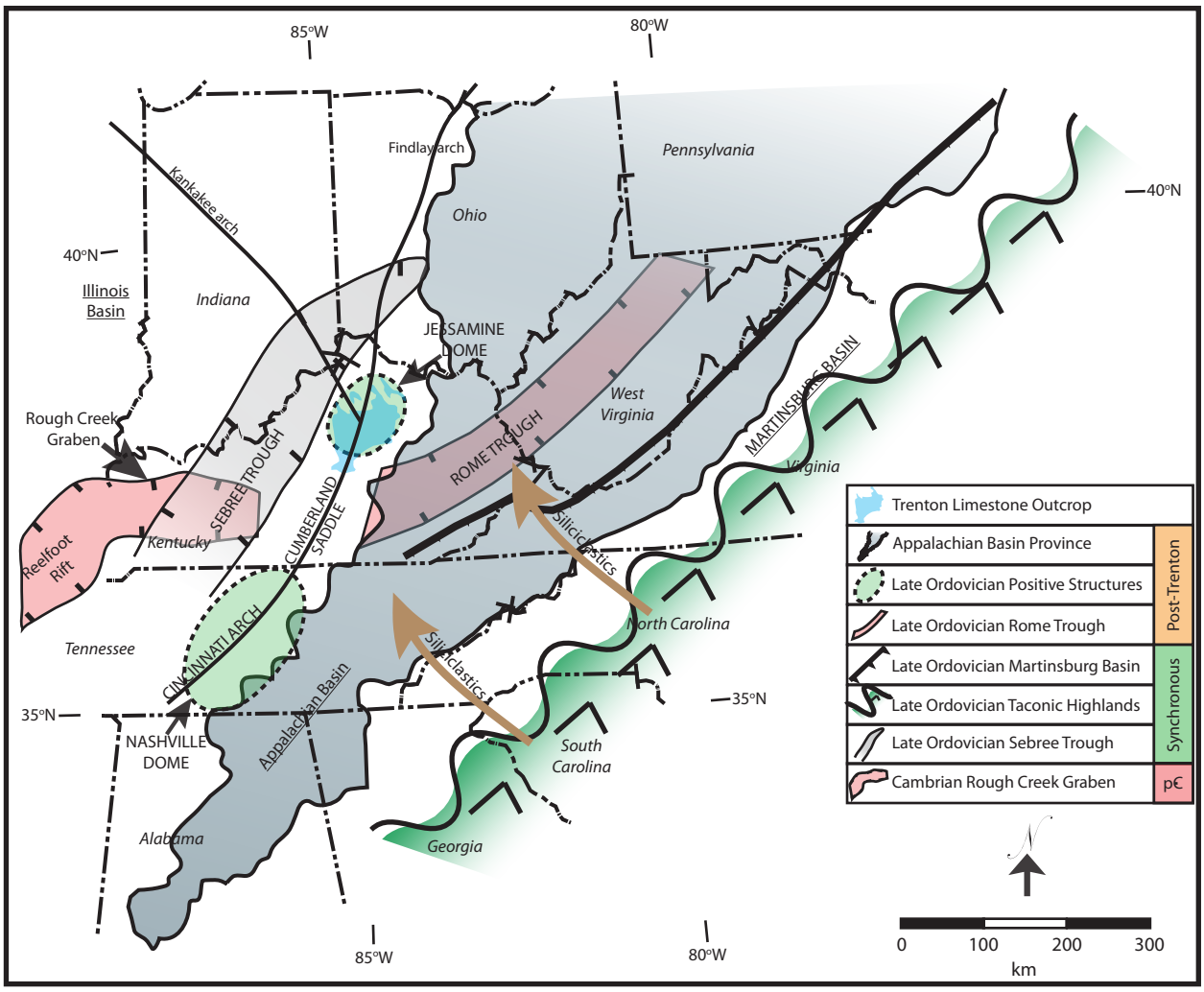

Figure 2.2 A map illustrating principal structures through present-day Kentucky (Modified from Brett et al. 2012; Modified from Kolata et al., 2001; Modified from Pope et al., 2009).

2.2 COOL WATER CARBONATE DEPOSITION

Deposition of the Ordovician Trenton Limestone of south-central Kentucky occurred along a high-energy ramp environment where cool-water carbonate deposition occurred within a foreland basin associated with the Taconic orogeny (Pope and Read, 1997). Paleogeographic reconstructions (Figure 2.3) place the study region at approximately 20°S to 30°S latitude in a subtropic to temperate climate (Blakey, 2011; Wilde, 1991). Changes in oceanic currents caused by the Taconic orogenic uplifts and flexural downwarping allowed cool polar currents to upwell into the foreland basin resulting in widespread deposition of cool-water carbonate facies (Wilde, 1991; Pope and Read, 1997; Blakey, 2003).

Pope and Read (1997) recognize six shallow-ramp carbonate facies within the Trenton Limestone (along the Cincinnati arch) in Kentucky, which include: fenestral lime mudstone, restricted skeletal wackestone/packstone, skeletal grainstone, nodular skeletal wackestone/ packstone and shale, thin bedded skeletal packstone and shale, and even bedded shale and calcisiltite (Figure 2.4). Tidal flat and subtidal environments that developed over the Cincinnati arch/forebulge depozone (known as the Lexington platform) contain fenestral mudstone, grainstone shoals, lagoonal wackestones/packstones, open marine mid-ramp packstones, basinal rhythmites and wackestones, and condensed sections (hardground surfaces representing sediment-starved intervals).

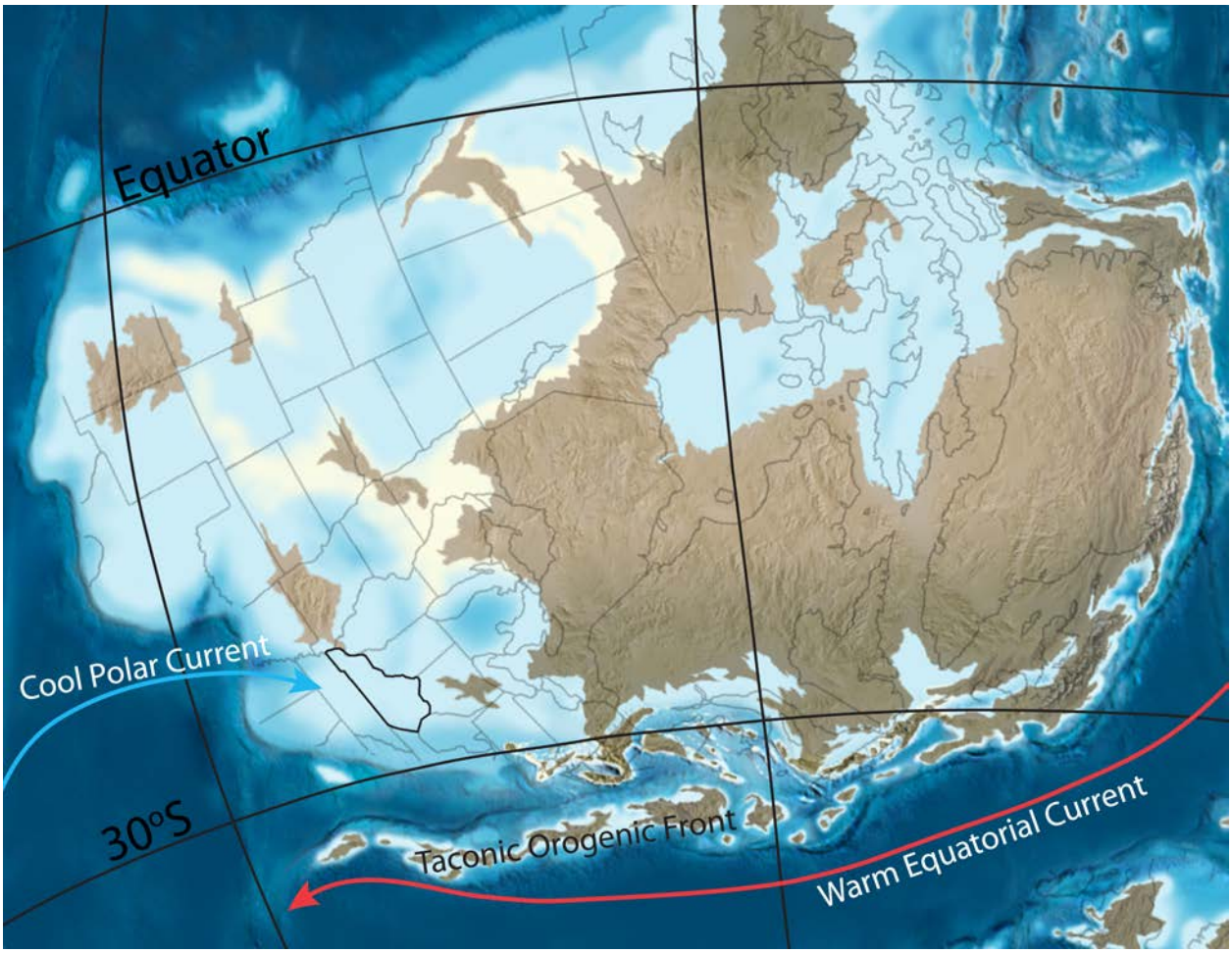

Figure 2.3 A paleogeographic reconstruction of Kentucky illustrating ocean currents during Late Ordovician Trenton deposition. Cool phosphate-rich polar upwelling onto the Lexington Platform resulted in heterozoan carbonate deposition (Modified from Blakey, 2011 and Wilde, 1991).

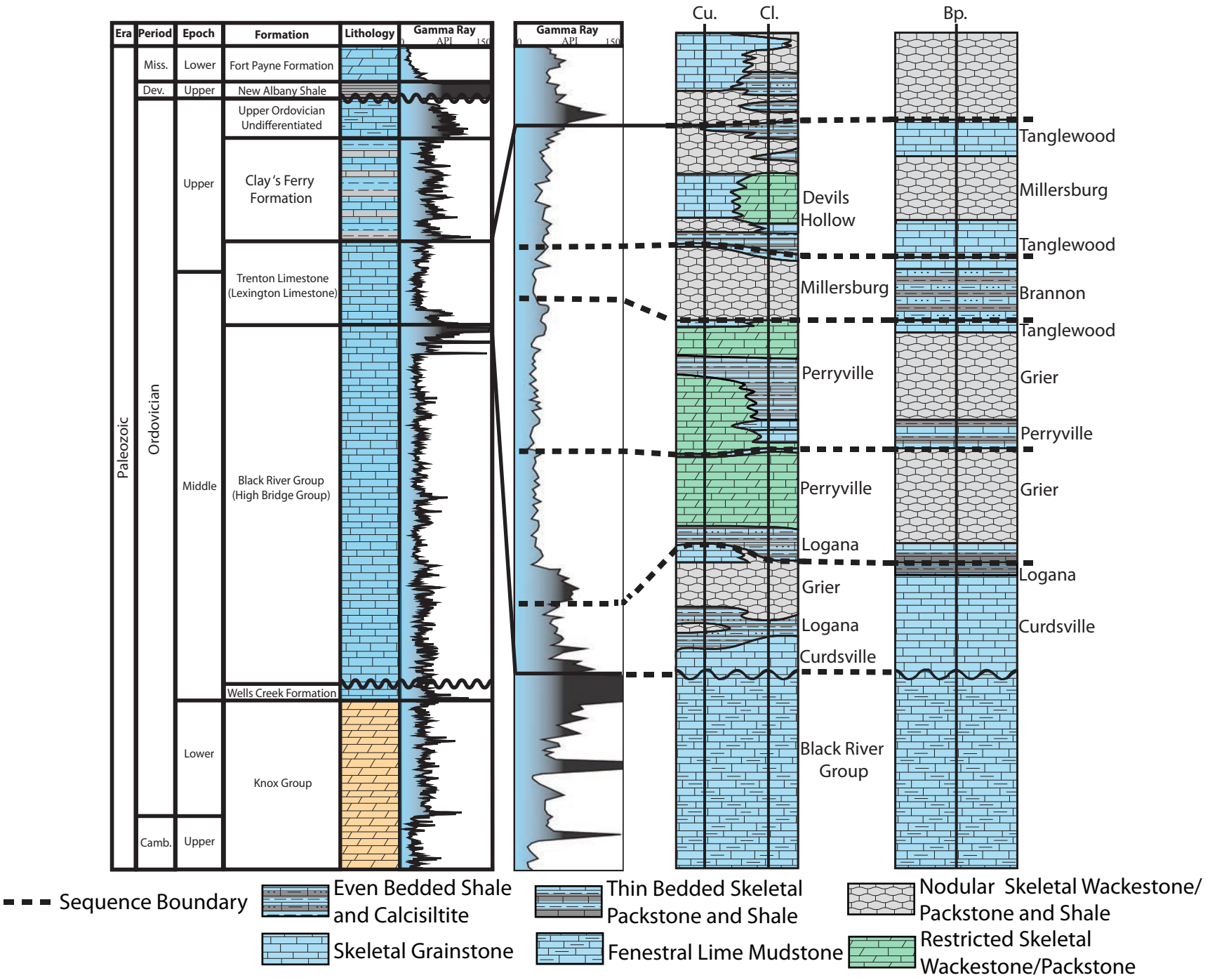
Era
Period
Epoch
Formation
Lithology
Gamma Ray
0 API 150
Paleozoic
Miss.
Lower
Fort Payne Formation
Dev.
Upper
New Albany Shale
Ordovician
Upper Ordovician Undifferentiated
Upper
Clay's Ferry Formation
Trenton Limestone (Lexington Limestone)
Middle
Black River Group (High Bridge Group)
Wells Creek Formation
Lower
Knox Group
Camb.
Upper
Gamma Ray
0 API 150
Cu.
Cl.
Bp.
Tanglewood
Devils Hollow
Millersburg
Tanglewood
Millersburg
Brannon
Tanglewood
Perryville
Grier
Perryville
Perryville
Grier
Logana
Logana
Grier
Logana
Curdsville
Curdsville
Black River Group
Sequence Boundary
Even Bedded Shale and Calcisiltite
Skeletal Grainstone
Thin Bedded Skeletal Packstone and Shale
Fenestral Lime Mudstone
Nodular Skeletal Wackestone/ Packstone and Shale
Restricted Skeletal Wackestone/Packstone

Figure 2.4 A stratigraphic chart displaying Ordovician strata and their typical gamma ray signatures through central Kentucky. Note the strong gamma ray signatures at the base of the Trenton; these are k-bentonites that mark the contact between the Trenton and Black River formations. The expanded sections to the right display typical facies assemblages that Pope and Read (1997) observed in core through the Trenton in south-central (Cu. and Cl.) and north-central Kentucky (Bp.) with sequence boundaries indicated by black dashed lines and corresponding members listed to the right side of the facies (Modified from Pope and Reade, 1997).

2.3 UPPER ORDOVICIAN STRATIGRAPHY

The Trenton Limestone has been documented as both Late Middle and Late Ordovician in age due to its intertonguing with the overlying Clays Ferry Formation towards the northwest (Weir et al., 1984). Locally (through central Kentucky) the Trenton is referred to as the Lexington Limestone, which can be further subdivided into various local members: Curdsville, Logana, Grier Limestone, Brannon, Perryville Limestone, Tanglewood Limestone, Sulfur Well, Millersburg, Greendale Lentil, Stamping Ground, and Devils Hollow Members (Figure 2.5; Weir et al., 1984). The top of the Trenton occurs at the transition to the more shaley Clays Ferry Formation (Weir et al., 1984). Underlying the Trenton is the Black River Group Carbonates locally known as the High Bridge Group, which consists of subtidal and intertidal sequences of fenestral micrites indicating deposition in a subtropical warm-water environment (Weir et al., 1984). The contact between the Black River Group and the overlying Trenton is marked by the top of the Mud Cave K-bentonite (also known as the Millbrig or T-4). The Mud Cave is the upper of two prominent and generally continuous (only absent across structural highs) K-bentonites in the upper Black River Group and is at least two feet thick across much of Kentucky while the underlying Pencil Cave bentonite is located 16 to 30 feet below the top of the Black River (Weir et al., 1984). Both bentonites provide excellent marker horizons through both drilling and petrophysical logging due to their strong radioactivity, lack of porosity, and uniformity across much of Kentucky and northern Tennessee. The contact between the Black River Group and the Trenton Limestone marks the transition from tropical-type to temperate-type carbonate deposition (Brett et al., 2012).

The Curdsville Member of the Trenton is the basal member that directly overlies the Mud Cave K-bentonite where the Mud Cave is present and unconformably overlies the Tyrone (upper Black River/High Bridge Group) where the Mud Cave is absent such as across much of the Jessamine dome (Weir et al., 1984). It's well log signature is recognized as having natural gamma ray readings of 20-30 API decreasing up in the member, bulk density readings of 2.60-2.70 g/cm^3 generally increasing towards the top of the member as it becomes increasingly clean

limestone, and generally decreases in porosity up in the section again due to the decreasing bentonite content. The unit consists of mostly abraded brachiopod and trilobite allochems and encrusting bryozoans and generally does not contain micrite. This resulted from deposition in a high energy environment where fossil abrasion and micrite winnowing resulted from wave action within a mid-ramp open marine setting. Cressman (1973) suggests marine transgression and corresponding depositional deepening upward through the section.

The Logana Member overlies the Curdsville in northern Kentucky and consists of interbedded petroliferous limestone and shale (Pope and Read, 1997). The member ranges in thickness from approximately 30 feet in northern Kentucky's Jessamine dome region to being absent in southern Kentucky due to the southward shallowing of water depths on the Lexington platform (Pope and Read, 1997). Deposition was beneath normal wave base within a basinal-deep ramp setting where the lack of biodiversity and burrowing organisms allowed for preservation of thin beds. The member can be recognized in well log analysis as exhibiting gamma ray values of 35 to 60 API (generally higher values than the underlying Curdsville Member), bulk density ranging from 2.60 to 2.70 g/cm^3, and porosity values below 5%.

The Grier Limestone Member is the most prominent and continuous member of the Trenton. It ranges in thickness from 150 feet in the Jessamine dome region to approximately 80 feet near Clinton and Cumberland counties (Brett et al., 2012). The Grier disconformably overlies the Logana and Curdsville in northern and southern Kentucky, respectively (Brett et al., 2012). It is an irregularly bedded massive lime packstone to wackestone and contains abundant normal marine allochems consisting of ostracodes, bryozoans, brachiopods, gastropods, crinoids, echinoids, and trilobites. Phosphatized hardgrounds are frequent through the lower and middle portions of the section and intraclasts from the hardgrounds can be found in throughout the lime packstones and wackestones. Deposition was in a shallow, moderate to low-energy mid-ramp open marine environment near normal wave base (Pope and Read, 1997). The lack of significant accumulations of micrite indicate that it was either winnowed away by wave or current action or

was simply not present as many of the organisms formed well cemented hardgrounds. The well log signature is recognized as having a low, clean gamma ray curve, bulk density ranging from 2.70-2.79 g/cm^3, and total porosity generally less than 3%.

The Perryville Limestone Member overlies the Grier Limestone Member and consists of three beds; the Faulconer bed, Salvisa bed, and Cornishville bed, which consist of dominantly calcarenite, fenestral micrite, and shaley nodular wackestone and packstone, respectively (McLaughlin et al., 2004). The lowest stratigraphic bed, the Faulconer calcarenite, is increasingly common and extensive south through the Cincinnati Arch where deposition was in a high energy, normal marine environment that contains authigenic quartz and has well developed trough and planar crossbeds in outcrops near the Jessamine dome region (McLaughlin et al., 2004). The Salvisa bed (fenestral micrite) reaches a thickness of about fifteen feet and likely developed during sparse periods of low energy in a tidal flat setting where micrite development was extensive near the central regions of the Lexington platform (McLaughlin et al., 2004). The capping Cornishville bed (shaley nodular wackestone and packstone) is common throughout the Cincinnati Arch region and is very similar in appearance to the Grier Member however it generally contains a higher amount of evenly bedded shale relative to the Grier (Brett et al., 2012). The Perryville Limestone has a well log signature exhibiting increased gamma ray signatures relative to the underlying Grier Member, bulk densities generally display a slight decrease in their signature with values ranging from 2.72-2.68 g/cm^3, and have porosity values generally below 4%.

The Tanglewood Limestone Member is only present in the northern regions of the Cincinnati Arch and generally parallels the Lexington Platform-Sebree Trough margin (Pope and Read, 1997). The unit is a skeletal grainstone that was deposited in a high energy shoal environment and consists of abraded bryozoans, brachiopods, echinoids, and crinoids that ranges in thickness from being absent to reaching a maximum of 100 feet near Frankfort, KY (Cressman, 1973).

The Brannon Member consists of evenly bedded calcisiltite and shale with increasing shale content north and west towards the Sebree trough where increased accommodation space along the deep ramp led to increased shaliness (Brett et al., 2012). The unit is largely missing in the southern subsurface and is most prevalent in the Jessamine dome region where it reaches a maximum thickness of approximately 30 feet (Cressman, 1973). The Brannon is not present south of the Jessamine dome region and appears to intertongue with the Millersburg Member and the Clay's Ferry Formation northwest towards the Sebree trough (Pope and Read, 1997). The high shale-to-carbonate ratio suggests deposition in low energy basinal environments that were not conducive to biological activity that would have mottled and destroyed the bedding. Well log signatures display increasing gamma ray signatures up through the section caused by increasing shale content, bulk density values decrease to values ranging from 2.70-2.65 g/cm^3, and porosity values display slight increases up to 5%.

The Sulfur Well Member disconformably overlies the Tanglewood or Brannon Members in varying localities across the Jessamine dome region and directly overlies the Grier or Perryville Members south of the Lexington River Fault System (Cressman, 1973). The member is very similar in appearance to the Grier Member; however it is almost entirely composed of encrusting bryozoans that may have led to the development of hardgrounds through the interval, which reaches a maximum thickness of approximately 35 feet and thins to the south where distinction from the underlying Grier becomes trivial (McLaughlin et al., 2004). Deposition in a high energy shallow shelf environment led to the development of abundant encrusting bryozoans and fragments of brachiopods echinoids and crinoids are common. This unit can be recognized from the Brannon Member on well logs as having a very low and clean gamma ray curve, increasing in bulk density to 2.70-2.72 g/cm^3, and exhibiting very low porosities (less than 2%). In regions where the interval directly overlies the Grier or Tanglewood, the lack of distinguishing well log characteristics between units makes recognition extremely difficult.

The Stamping Ground Member consists of a thin (maximum thickness of 15 feet) bed of interbedded shale and nodular limestone that is only present in the Jessamine dome region of northern Kentucky (Cressman, 1973). The member is very similar in appearance and in well log signatures to the Brannon Member; however the limestone-to-shale ratio is generally higher in the Stamping Ground. Deposition occurred in a storm-dominated deep ramp environment that was conductive to trilobite and brachiopod niche spaces. As a result, characteristic gamma ray signatures are relatively low (below approximately 50 API) while bulk densities range from 2.72-2.65 g/cm^3 and total porosity is generally below 3%.

The Greendale Lentil Member consists of 10-15 feet of irregularly bedded limestone and shale that grade into the Tanglewood calcarenite in all directions (Weir et al., 1984). The unit is present in northern Kentucky and has a similar appearance and well log signature as the Millersburg Member (Weir et al., 1984).

The Devils Hollow Member consists of approximately 15 feet of grainstone-packstone composed of abraded gastropods that is overlain by approximately 10 feet of wackestone containing abundant ostracodes and peloids (Cressman, 1973). Deposition occurred in a tidal flat and in shoaling environments near Frankfort, Kentucky, however it thins and pinches out into the Tanglewood to the west and north and is overlain by the Millersburg to the south and north of the Tanglewood extent (Cressman, 1973; Pope and Read, 1997).

The Millersburg Member is a prominent unit that makes up the upper section of the Trenton. Reaching a maximum thickness of approximately 90 feet, the member is composed of interbedded shale and nodular limestone that increases in shale content up through the section where the member intertongues with the overlying Clays Ferry Formation (Cressman, 1973). The Millersburg directly overlays the Devil's Hollow Member to the east and south and truncates due to transitions into higher energy depositional facies south of Jessamine dome (Weir et al., 1984). The wackestones consist of bryozoans, brachiopods, and trilobites and phosphatic marine hardgrounds litter the section, which suggest deposition in moderate to low-energy deep ramp

normal marine environments near storm wave base. The unit has a well log signature that shows moderate to low gamma ray signatures, bulk densities generally show decreasing density up through the member decreasing from 2.72 to 2.66 g/cm^3, and neutron porosity shows increasing porosities up to nearly 4% caused by increasing shale content.

2.4 SEQUENCE STRATIGRAPHY

Deposition was largely controlled by varying eustatic sea-level patterns as the Cincinnati arch was passive during Trenton deposition (Pope et al., 2009). As a result, two third-order depositional sequences (durations are typically one to a few million years) have been recognized in the late Mowhawkian Series of the Sandbian Stage, which consist of the M5 and M6 sequences which can be further segregated into six third-order sequences; the M5A, M5B, M5C, M6A, M6B, and M6C sequences (Figure 2.5; Brett et al., 2012). These sequences provide for very useful tools to correlations outside of Kentucky south into Tennessee and northeast along the Trenton ramp.

The M5A sequence constitutes the base of Trenton deposition and is represented as a TST (transgressive system tract)-HST (high stand system tract) through the Curdsville and Logana Members which transitions into a FSST (falling stage system tract) in the lowermost Grier Member (Brett et al., 2012). The M5B sequence begins in the lower Grier Member with a TST that reaches a HST in the middle section of the Grier where the M5B sequence terminates (Brett et al., 2012). The M5C sequence begins during upper Grier deposition with a TST grading into a MFS (maximum flooding surface), which can be recognized by abundant hardground surfaces (McLaughlin et al., 2004). The HST and FSST of the M5C are represented by the interbedded shales and fenestral micrite of the Faulconer Bed of the Perryville Limestone Member. The M6A sequence begins with a TST in the Salvisa Bed of the Perryville Limestone Member and continues to a MFS at the top of the Cornishville Bed of the Perryville Limestone Member marked by hardground development (McLaughlin et al., 2004). The HST of the M5A sequence correlates to the lower Brannon Member's interbedded shale and calcisiltite and the

FSST may correlate to the lower Sulfur Well. The M6B sequence is marked by a TST and subsequent MFS represented by hardground development in the Sulfur Well Member (Brett et al., 2012). The following HST correlates to deposition of the Devils Hollow Member. The M6C sequence begins with a TST associated with the Millersburg Member, which continues into a MFS in the middle and upper Millersburg. Deposition of the Clays Ferry Formation occurred during the HST of the final M6C sequence (Brett et al., 2012).

2.5 DIAGENETIC MODIFICATION

Diagenesis through the Trenton Limestone was primarily linked to rapid early burial leading to the development of stylolite surfaces, calcite cementation in marine and meteoric phreatic environments (where rapid burial did not occur), dolomitization due to the very minor restriction within the Taconic foreland, phosphatization and pyritization through hardground surfaces, and silicification. Paragenetic sequence analyses indicate that numerous stages of diagenesis and porosity evolution have occurred ranging from early marine cementation to various pulses of dolomite and hydrothermal mineral emplacement in faulted and fractured intervals.

Phosphatization along marine hardground (condensed sections) surfaces is common particularly during HST and during maximum flooding surfaces of third order sequences (Brett et al., 2012). Hardgrounds occur primarily through the Grier, Millersburg, and Cornishville beds and frequently contain abundant brachiopods, bryozoans, and ostracodes that have undergone extensive mineralization. Iron oxides and phosphate are frequent through the hiatus surfaces (reducing conditions), which likely result from upwelling into the Taconic foreland (Martinsburg foredeep) and Sebree troughs while climatic changes led to a transition from tropical to temperate carbonate sedimentation (Holland and Patzkowsky, 1996). Hardground surfaces typically produce sharp irregular upper boundaries that are entirely phosphatized and frequently display signs of oxidation, which tend to fade away within 4 cm below the surface. In other cases where hardground development was over a more prolonged period, hardground surfaces

develop into highly mineralized surfaces that exhibit very limited amounts of porosity (microporosity) and no permeability and are highly cemented for up to 5 inches. The lack of porosity and permeability in all hardground surfaces becomes increasingly important during initiation of hydrothermal fluid flow and dolomitization as these surfaces act as aquitards to limit vertical and lateral fluid migration.

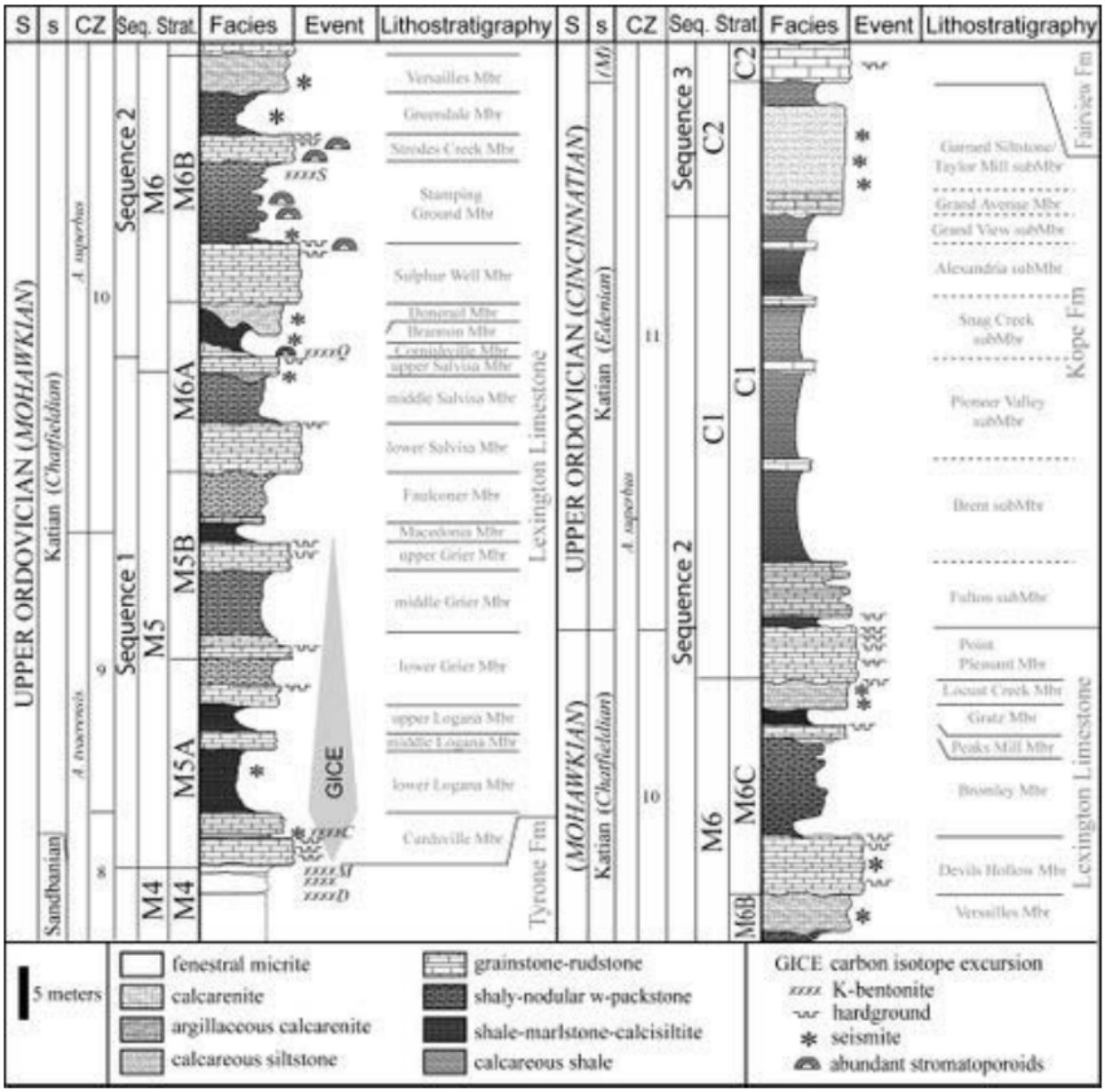

Figure 2.5 A stratigraphic chart illustrating the M5A through M6C sequences through the Trenton and the correlative members as commonly observed marking sequence boundaries (From Brett et al., 2012)

Chapter 3: Methodology

3.1 Outcrop Studies

The study involved both outcrop and subsurface datasets from north-central and south-central Kentucky (Figure 3.1). Fieldwork consisted of sampling various hydrothermally dolomitized zones in the Trenton Limestone that outcrop in north-central Kentucky. Outcrops documented by the Kentucky Geological Survey provided directions to the localities, which consist of dolomitized road cuts that have been attributed to fracturing along the Lexington Fault System (Black et al., 1981). Outcrops were located in Shelby and Fayette counties where hydrothermal dolomite is present in a variety of facies assemblages through the Trenton Limestone (Black et al., 1981; Reid et al., 2004). Correlations between facies assemblages that exhibit variations in lateral distance from fractures were documented throughout the outcrops and samples of the vertical limit, lateral limit, central mineralized interval, zebra fabrics, vuggy precipitates, and matrix-replacive dolomite were collected. Measured sections were developed utilizing measuring tapes and vertical and lateral sampling of facies and diagenetic variations allowed for the generation of polished hand specimens for further analysis. Billets were cut from the acquired samples, which were converted into thin sections by Spectrum Petrographics Inc. and Petrographic Services for detailed petrographical analysis where paragenetic sequences, porosity evolution and diagenetic pervasiveness were documented. Viewing extent of mineralization through the various facies assemblages allowed for conclusions and models for the observed diagenetic alterations to be generated.

Hand specimens were polished utilizing a 1000 grit silicon carbide to provide detailed analysis at the hand specimen scale, which were combined with core samples and photographed prior to the generation of thin section billets.

Further fieldwork consisted of core observation at the Kentucky Geological Survey's Well Sample and Core Library where cores were selected based on location and availability of well logs to decipher the Trenton top and base as well as recognition of variations in bulk

density, porosity, natural radioactivity, and resistivity that would be indicative of mineralized zones. Clinton and Cumberland counties were the focus for core analysis due to the abundance of hydrocarbon production that has occurred through the Ordovician carbonates. Cores and cuttings were then observed proceeding north along the Cincinnati Arch towards the sampled road cuts in Fayette County. Utilizing the facies associations and sequence stratigraphic framework outlined by Pope and Read (1997), observed diagenesis was correlated to specific depositional facies that allowed for correlations between outcrop and core analyses. Samples were collected from cores that displayed variable amounts of mineralization, which were converted into thin-sections for petrographic analysis.

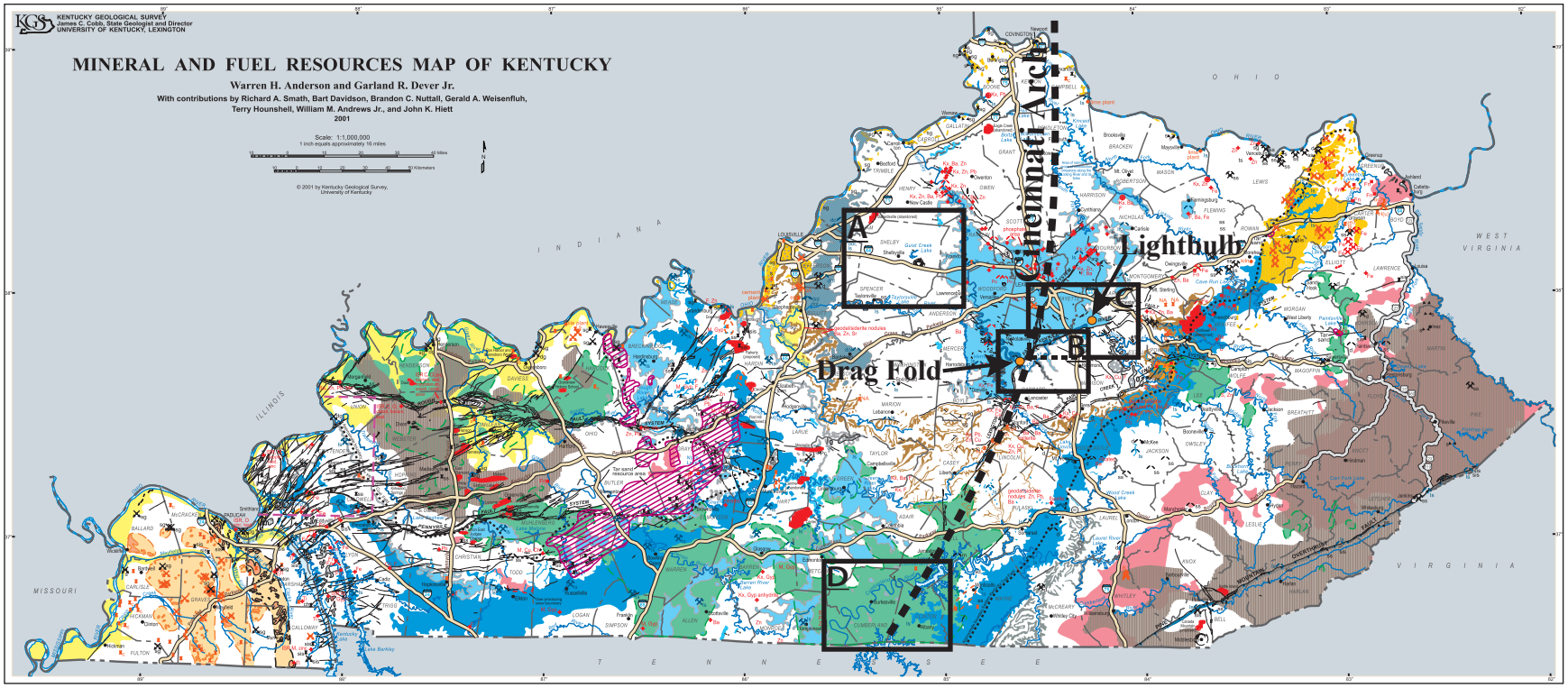
KENTUCKY GEOLOGICAL SURVEY
James C. Cobb, State Geologist and Director
UNIVERSITY OF KENTUCKY, LEXINGTON
MINERAL AND FUEL RESOURCES MAP OF KENTUCKY
Warren H. Anderson and Garland R. Dever Jr.
With contributions by Richard A. Smath, Bart Davidson, Brandon C. Nuttall, Gerald A. Weisenfluh, Terry Hounshell, William M. Andrews Jr., and John K. Hiett
2001
Scale: 1:1,000,000
1 inch equals approximately 16 miles
© 2001 by Kentucky Geological Survey, University of Kentucky
Cincinnati Arch
Lightbulb
Drag Fold
A
B
C
D
INDIANA
ILLINOIS
MISSOURI
OHIO
WEST VIRGINIA
VIRGINIA
TENNESSEE


A
Bardstown (abandoned)
OLDHAM
C-1287
SHELBY
Guist Creek Lake
Shelbyville
Frankfort
C-1286
SPENCER
Taylorsville
Taylorsville Lake
Lawrenceburg
B
Nicholasville
FAULT
KENTUCKY
Kentucky
DRF
GARRARD
C
FAYETTE
CLARK
Winchester
C-201
RIVER
C-106
LB
KENTUCKY
C-201
D
LFE
Cumberland River
C-295
Burkesville
C-1220
CLINTON
CUMBERLAND
C-511
Albany
C-1221

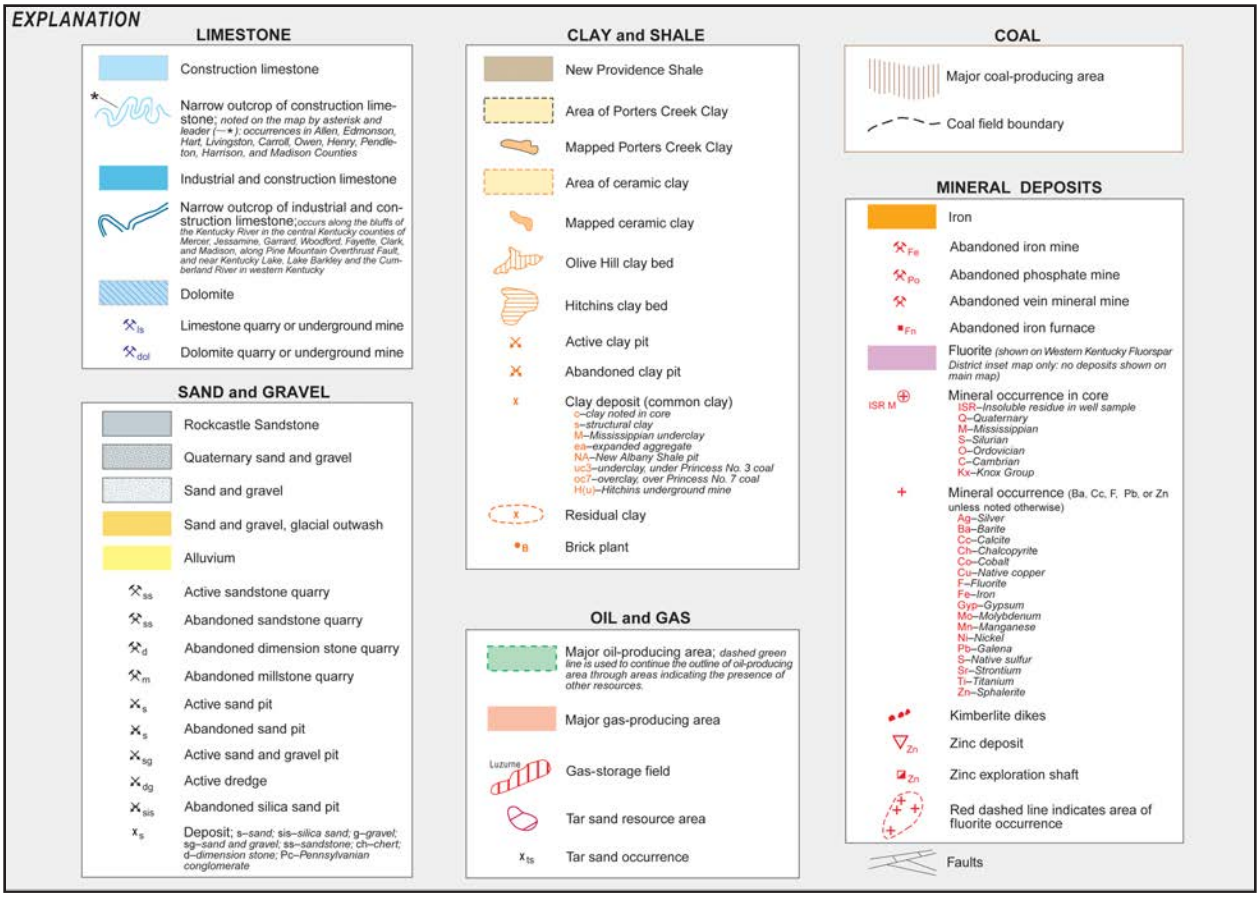

Figure 3.1 An index map illustrasting sample locations across central Kentucky. An aproximate trace of the Cincinnati arch is indicated by the dashed line and hydrocarbon production in south-central Kentucky is indicated by green. Black boxes highlight regions where samples were collected including; A-northwestern cores, B-drag fold outcrop, C-lightbulb outcrop and northern cores, and D-southern cores (Modified from Anderson and Dever, 2001).

3.2 PETROGRAPHY

Petrographical analysis consisted of the utilization of 64 thin sections slides that were half-stained with alizarin red S and potassium Ferricyanide to delineate calcium carbonate (limestone) from calcium-magnesium carbonate (dolomite) and ferrous iron. The slides were ground to a thickness of 30 micrometers and had coverglass coverings mounted with permanent acrylic cement. Analysis consisted of utilizing a Leica Compound Light Microscope with polarizing capabilities. Thin-section photomicrographs were captured with a Leica DFC295 digital microscope color camera to help document paragenetic sequences.

3.3 STABLE ISOTOPE ANALYSIS

Stable isotope analysis consisted of analyzing carbon and oxygen isotopes in both core and outcrop samples. Samples were collected using a dremel to observe variations from unaltered primary fabrics into dolomitized vugs/fractures. A total of three core samples were used for isotopic mapping, which consisted of using a grid-like pattern of twelve sample points focused around vugs lined with saddle dolomite. This method was utilized to attempt to determine fluid flow conduits and to observe how isotopic values varied spatially away from the point of maximum diagenetic alteration. Fourteen additional samples were acquired from outcrop and core specimens to observe spatial variations in geochemical signatures. Approximately 200 micrograms of carbonate were collected utilizing a dremel and pulverized to a size of 150 μm using a mortar and pestle prior to sending to IsoLab at the University of Washington for $\delta^{13}C$ and $\delta^{18}O$ analysis. IsoLab utilized a Kiel III Carbonate Device fixed to a Finnigan Delta Plus Isotope Ratio Mass Spectrometer (IRMS) to analyze the samples. Results from $\delta^{18}O_{dolomite}$ were corrected to account for oxygen fractionation factors, which adjusted the correction from -0.8‰ to -1.2‰ with methods suggested in Kim et al. (2015). Results of the fifty analyzed samples were compared to those documented by Patchen et al. (2005) and Young et al. (2005) to compare trends in geochemical signatures of hydrothermal dolomites south through the Appalachian Basin region. In addition to comparisons between $\delta^{18}O$ values through

dolomites, trends in $\delta^{13}C$ from primary calcium carbonates were analyzed and compared to carbon isotope sequence stratigraphic studies conducted by Young et al. (2005) through the Trenton Limestone interval in eastern and central North America (Figure 3.2).

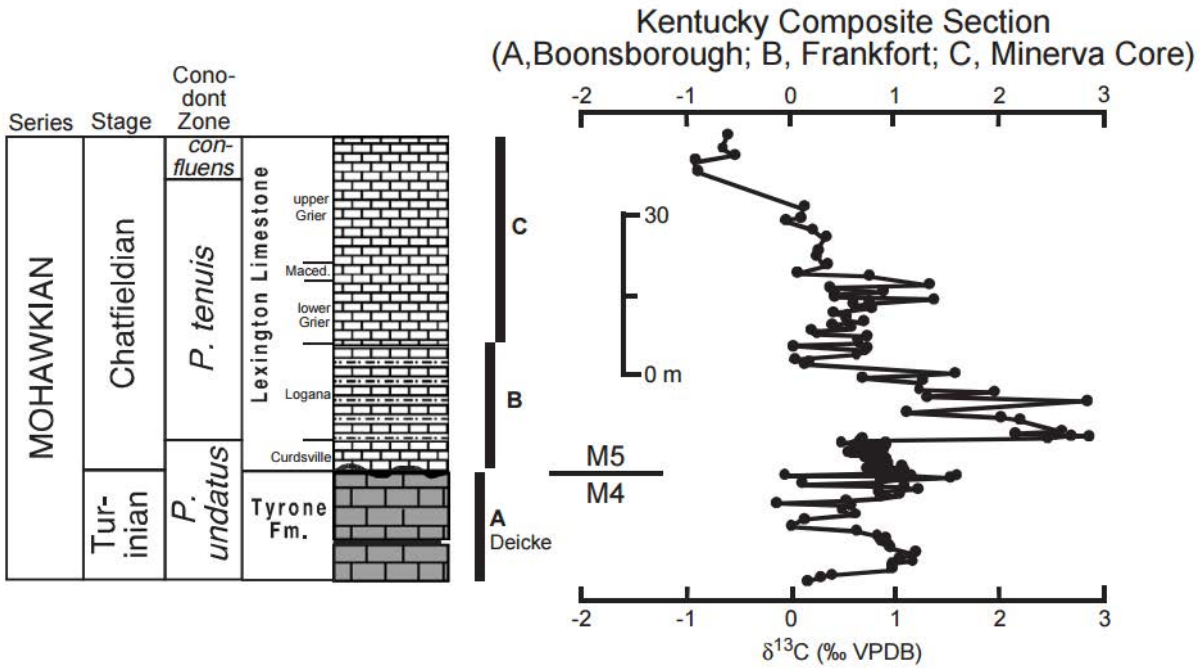

Figure 3.2 A measured composite section of illustrating the utilization of $\delta^{13}C$ to conduct sequence stratigraphic analysis through the Trenton in north-central Kentucky (From Young et al., 2005).

3.4 FLUID INCLUSION MICROTHERMOMETRY

Fluid inclusions consist of liquids and gasses that become trapped within minerals during imperfect crystal development (Goldstein & Reynolds, 1994). Analysis of fluid/vapor composition through inclusion freeze-thaw (phase change) trends allowed for the determination of temperature and salinity of fluids that were present during mineral formation. Goldstein and Reynolds (1994) recognize three categories of fluid inclusions; primary, secondary, and pseudosecondary, which consist of host mineral inclusions, healed fracture/diagenetic inclusions, and host fracture inclusions that form during host crystallization and necking down, respectively. The primary focus for this analysis were primary inclusions, and to a lesser extent secondary inclusions in an attempt to compare unaltered limestone and hydrothermal dolostone occurrences.

Initially, primary fluid inclusion assemblages in dolomite and calcite were documented using an Olympus BX60 microscope with 1.25x, 4x, 10x, and 40x lenses and magnification adjustments of 1, 1.25, 1.6, and 2 fold that was equipped with a 100 watt high pressure mercury burner to observe epifluorescence within inclusions and a Q Imaging QICAM Fast 1394 microscope camera. Assemblages were photographed, described, sketched, and evidence of primary or secondary origin was documented (Figure 3.3). Next, the glass surface of the thick section was marked using a permanent marker to delineate the fluid inclusion assemblage targeted for microthermometric analysis. A low speed thin section saw with a diamond infused blade was utilized to remove the assemblage. The resulting cubes measured approximately 4mm x 4mm x 2mm, which were then submerged in acetone for one hour to remove the rock from the glass slide. A Linkam THMSG 600 heating/cooling stage was utilized to conduct the microthermometric analysis. The "cycling method" documented in Goldstein & Reynolds' *Systematics of Fluid Inclusions in Diagenetic Minerals* was utilized to ensure precise temperatures of entrapment were documented. Following the determination of temperature of entrapment (Th), cooling runs were conducted to determine eutectic temperatures (temperature of first melt, Te) and final melt temperatures (Tm). Liquid Nitrogen was used to freeze fluid

inclusions, which were then evaluated utilizing Table 1 and Table 2 to determine chemical compositions and weight percent salinity of the inclusion assemblages (Goldstein and Reynolds, 1994). Utilizing these two methods, homogenization temperatures and fluid compositions were determined and compared to Late Middle and Upper Ordovician marine environments and hydrothermal dolomites documented by Patchen et al. (2005).

3.5 SUBSURFACE MAPPING

Well logs available from the Kentucky Geological Survey's Oil & Gas Records Database were utilized to conduct subsurface mapping of the Trenton Limestone. All available LAS files were downloaded and analyzed with Petrel E&P Software Platform to document structural and isopach variations. Characteristics of the Trenton interval were documented to attempt to recognize areas that may exhibit fractures, increased porosity, or deviations in well log signatures. Key attributes that are commonly indicative of fractures and/or vugular porosity include spikes in density corrections, spikes in bulk density, increase in neutron and density porosity, and separation of microresistivity and deep resistivity tools. Basemaps of Kentucky and the known faults were imported and well locations were plotted to help determine areas of particular interest for core analysis and to assist in outcrop-subsurface correlations.

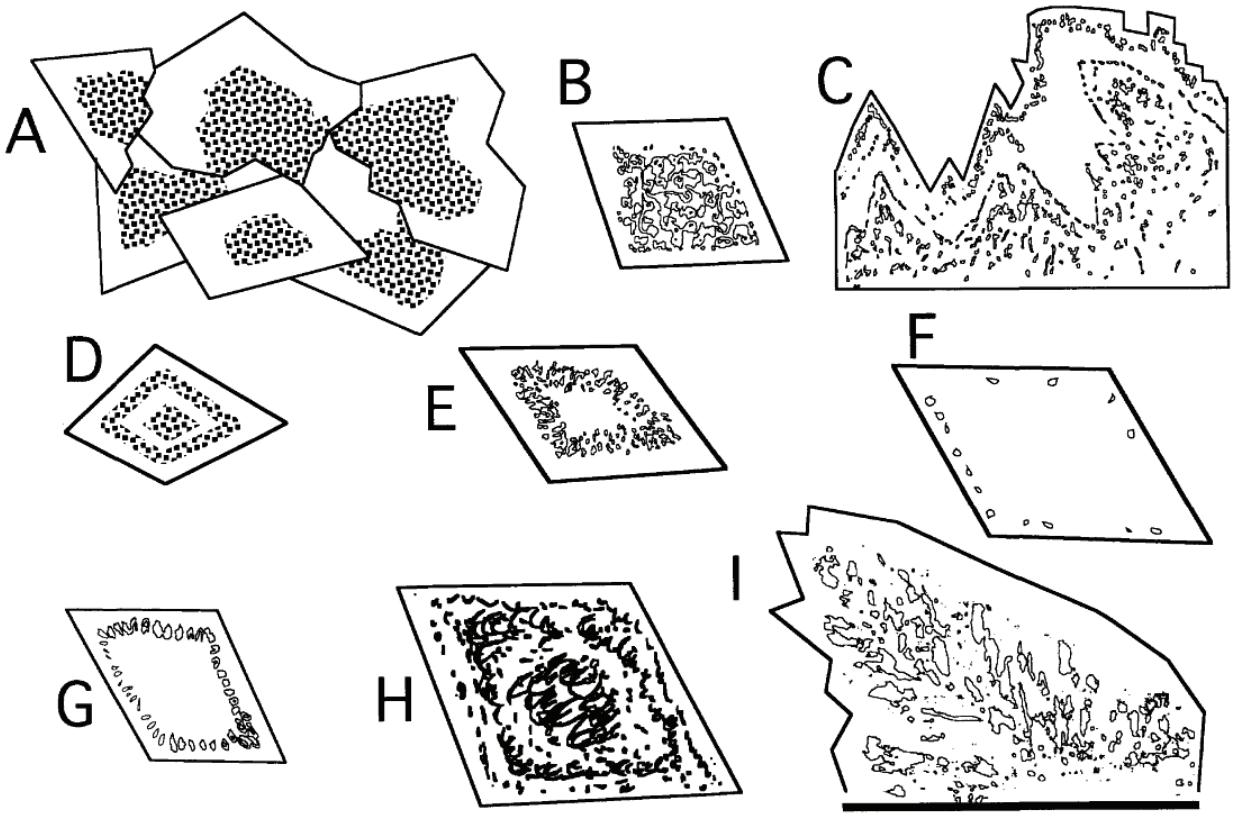

Figure 3.3 Illustrations displaying variations in primary fluid inclusion geometries that occur within dolomites (From Goldstein and Reynolds, 1994).

Chapter 4: Outcrop Analysis

Two outcrops in northern Kentucky termed the "Lightbulb Locality" and the "Drag Fold Locality" were analyzed to determine extent and character of dolomitization. Outcrops were selected based on previous work that was completed by Black et al. (1981) that indicated locations, presence of dolomite, presence of structural influences, and the stratigraphic formations that hosted mineralization.

4.1 THE LIGHTBULB LOCALE

The Lightbulb locality is located approximately five miles southwest of Winchester, KY along highway 627 S/Boonesboro Rd and consists of a road-cut through the Trenton Limestone revealing a hemispherical body of hydrothermal dolomite (Figure 4.1 and Figure 4.2). Dolomitization is most prevalent along the northwest side of the road cut where an oblique-normal fault allowed for vertical fluid migration into the Trenton interval. Dolomitization is most prevalent directly adjacent to the fault plane where fluid migration transitioned from near vertical to horizontal (bed-parallel) migration. The dolomitized body is approximately 30 feet wide by 35 feet tall and terminates laterally into unaltered Trenton Limestone and vertically into a low porosity phosphatic marine hardground of the Millersburg Member of the Trenton Limestone. Solution collapse associated with magnesium replacement of calcite in the dolomitized body is recognized by a "sag" in the capping marine hardground, a characteristic trait of HTD reservoirs in the Michigan and Appalachian basins (Davies and Smith, 2006).

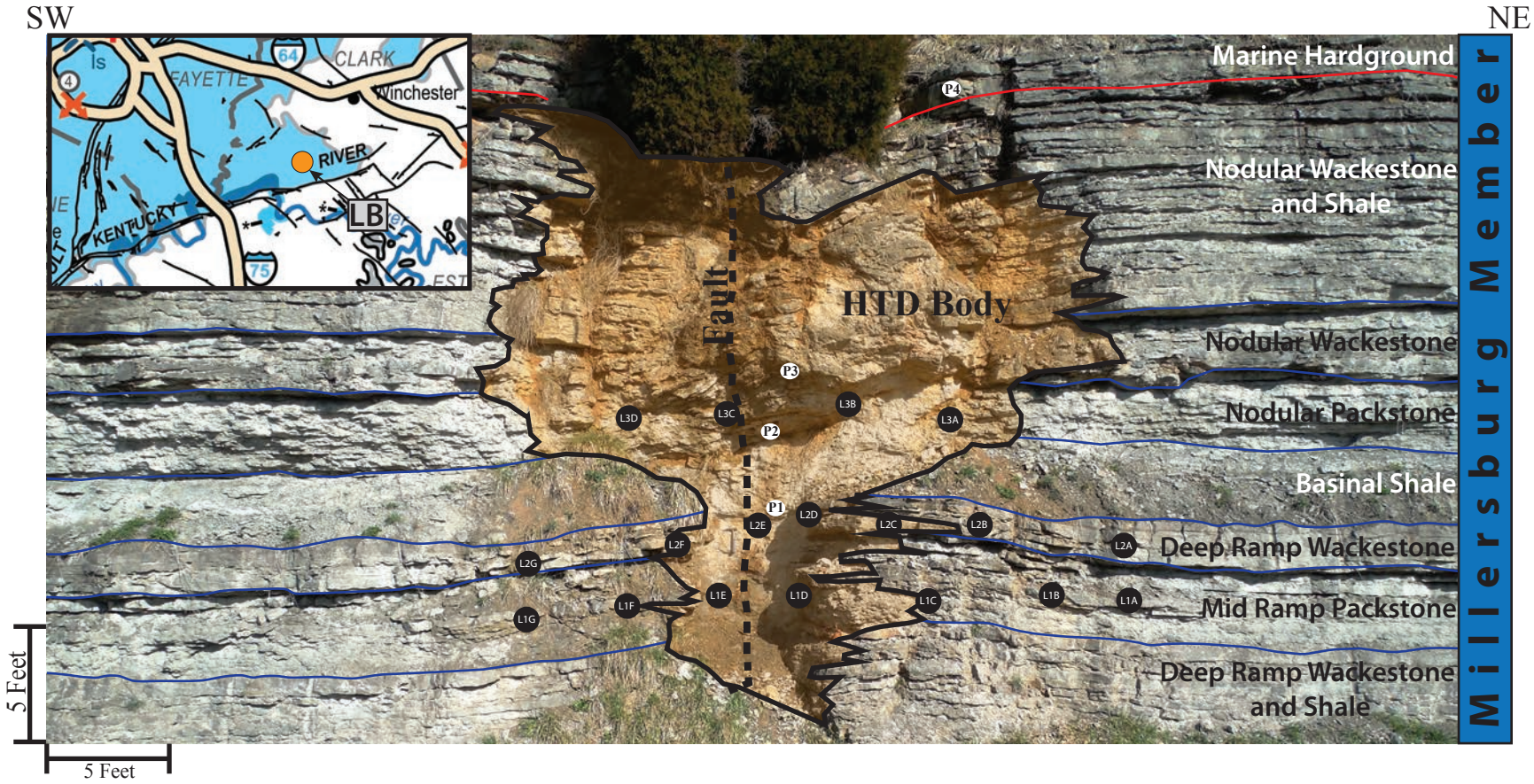

Figure 4.1 Outcrop photograph of the northwest side of the roadcut at Lightbulb locality with sample locations illustrated by black circles and polished slab locations indicated by white circles. An approximate trace of the fault plane is indicated by the dashed line and the dolomitized body is shaded orange.

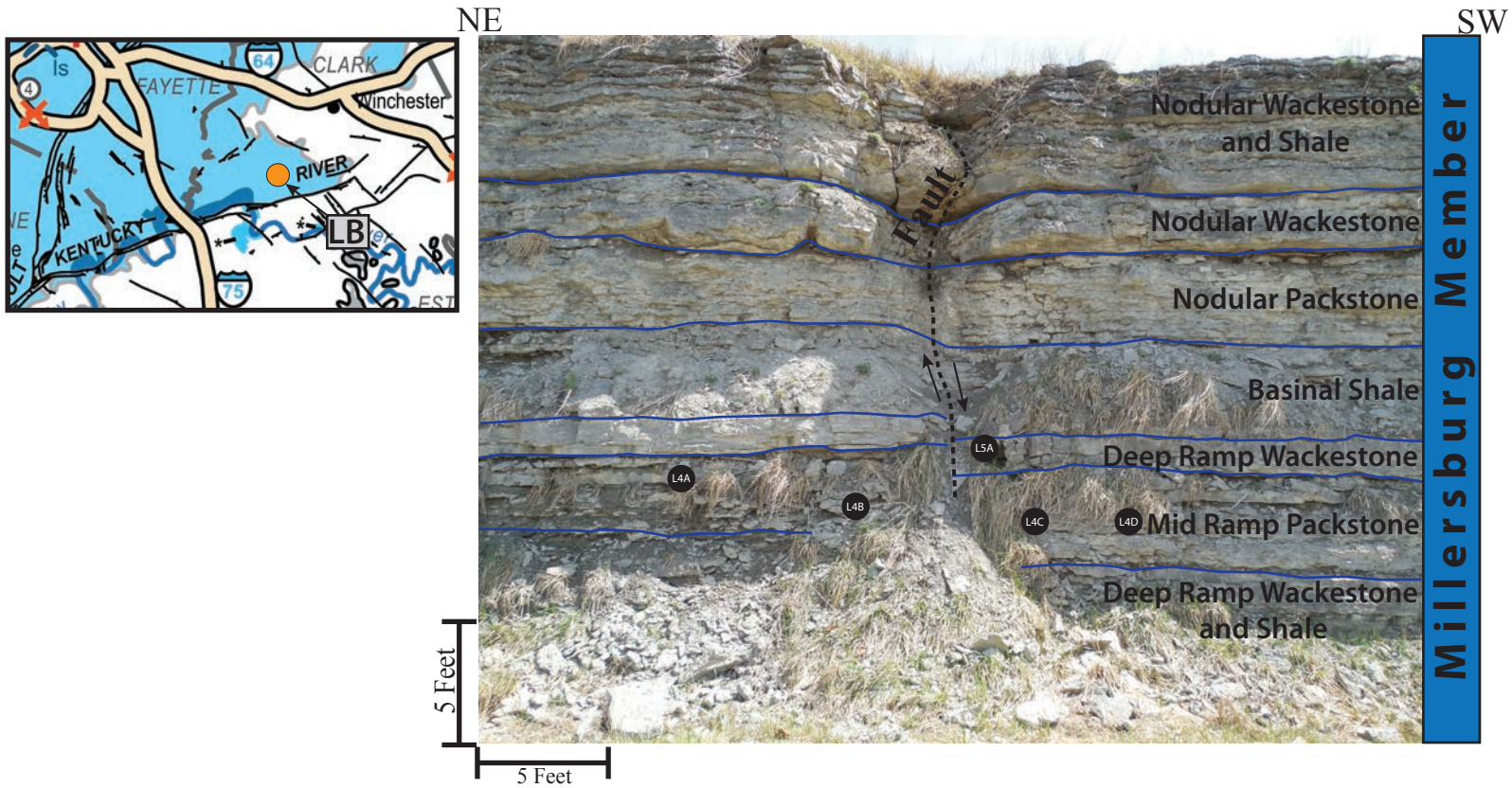

Figure 4.2 Outcrop photograph of the southeast side of the road cut at the Lightbulb locality with sample locations illustrated by black circles. A trace of the fault plane is indicated by the black dashed line.

The Lightbulb locality is influenced by an oblique-normal fault with approximately one foot of vertical offset. This fault has been interpreted to be a possible limb of a negative flower structure that is responsible for the development of the Stoner Branch Dolostone, a HTD body within the Upper Ordovician Calloway Creek Limestone and Garrard Siltstone (Black et al., 1981). This structure is the result of the Boonesboro Fault, which trends E-NE and is a part of the Kentucky River Fault System (Black et al., 1981). The fault plane truncates at the top of the outcrop suggesting that the timing of alteration was penecontemporaneous with the final stages of fault displacement.

Three distinct cool-water low-energy shallow marine carbonate depositional facies from Pope and Read (1997) of the Millersburg Member make up the outcrop. Sequences are one-to-two meters thick and consist of shallow marine packstones grading upwards into shallow marine wackestones capped by thin phosphatic hardgrounds with thin shale interbeds. Sequences within the outcrop generally thin and shale interbeds increase in abundance vertically through the road cut.

Basal packstones (L1A-L1G and L4A-L4D from Plate 1) contain bioclasts of bryozoans and echinoids with minor amounts of bivalves, ostracodes, red algae, trilobites and intraclasts within a microcrystalline matrix of cloudy calcite (Figure 4.3). There is a lack of micrite in the matrix, which instead is dominated by cloudy calcite spar, poikilotopic calcite that is highly twinned, and syntaxial overgrowths nucleating on echinoid plates. The observed heterozoan fauna support Pope and Read's (1997) interpretation of deposition in a normal marine shallow subtidal environment that was supplied by nutrient-rich cool water upwelling. The abundance of bryozoans suggests that deposition occurred on firm substrates that allowed for encrusting bryozoans to thrive (Scholle and Ulmer-Scholle, 2003). In these shallow marine environments micrite was winnowed due to wave action and cementation was relatively rapid following deposition as evidenced by the lack of sutured grain boundaries and early compaction fabrics (Scholle and Ulmer-Scholle, 2003). Syntaxial overgrowths and poikilotopic twinned calcite

suggest that neomorphism resulted from increased solution temperatures supplied from a burial connate environment (Scholle and Ulmer-Scholle, 2003).

Echinoid wackestones form the middle facies (L2A-L2G and L5A from Table 3) of the deepening-upward sequences (fifth or sixth order TST of the M6C sequence; Brett et al., 2012). Wackestones are composed of echinoids, ostracodes, trilobites, brachiopods and intraclasts hosted in a matrix of cloudy calcite spar (Figure 4.4). Deposition occurred near storm wavebase in a moderate energy deep ramp setting (Pope and Read, 1997) where high energy storm events induced intraclast reworking. Cementation occurred in a marine phreatic environment, which limited the development of compaction structures.

Finally, the marine hardgrounds that cap each sequence were deposited at the MFS of the fifth or sixth order M6C sequence (Brett et al., 2012) and are composed of phosphatic intraclasts, trilobites, and bryozoans. This facies exhibits very minor amounts of microporosity within cryprocrystalline and crystalline phosphate and shows minor signs of oxidation. The hardground that caps the outcrop is significantly thicker (4 inches) than the underlying 0.5 inch fifth and sixth order hardgrounds, which likely represents a third order composite MFS. Cementation was synsedimentary and occurred in a marine phreatic environment.

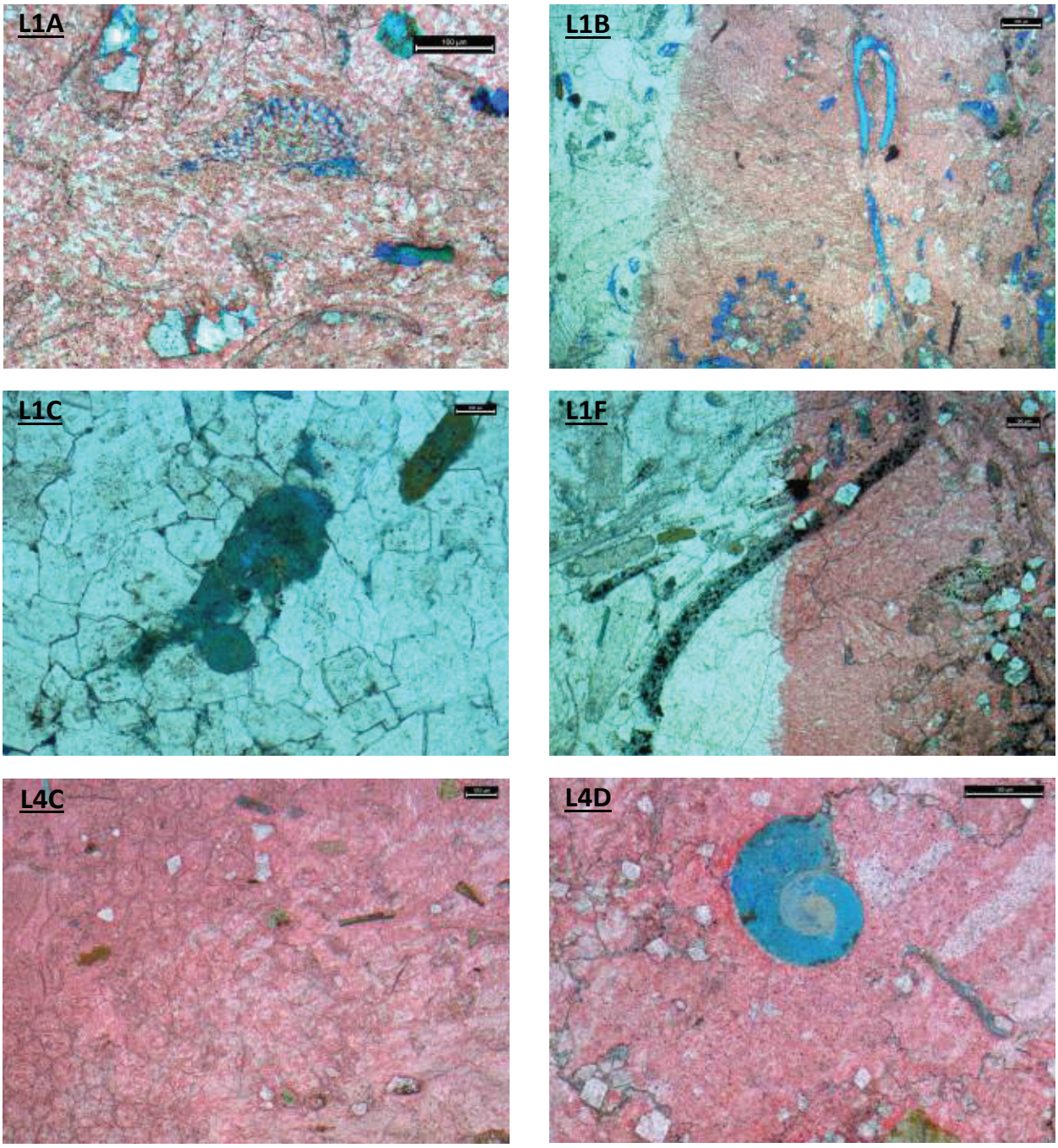

Figure 4.3 Samples from a moderate energy mid-ramp environment that make up the Millersburg Member at the Lightbulb Locality that have not been subjected to hydrothermal dolomitization due to their lateral distance from the fluid-supplying fault plane. (L1A) Moldic porosity within a solenoporoid red algal allochems with a thin trilobite fragment near the bottom of the image. (L1B) Moldic porosity development in trilobites and bryozoans resulting from early-stage fluid dissolution caused by decreasing distance from the fluid-supplying fault plane. (L1C) Phosphatized echinoids have been reworked as intraclasts throughout the Millersburg are largely unaffected by dolomitization. (L1F) Pyritization of a trilobite fragment and of zooecial walls in the bottom right corner. Pyrite fills microbored holes through the chitin that makes up the

trilobite fragment. (L4C) Ghost textures of a bryozoan within a neomorphosed matrix. Note the lack of primary porosity that may have been partially occluded during burial connate neomorphism. (L4D) A planispiral or evolute coil foraminifer that was phosphatized from cool polar upwelling ocean currents resulting in microporosity development through the central chamber.

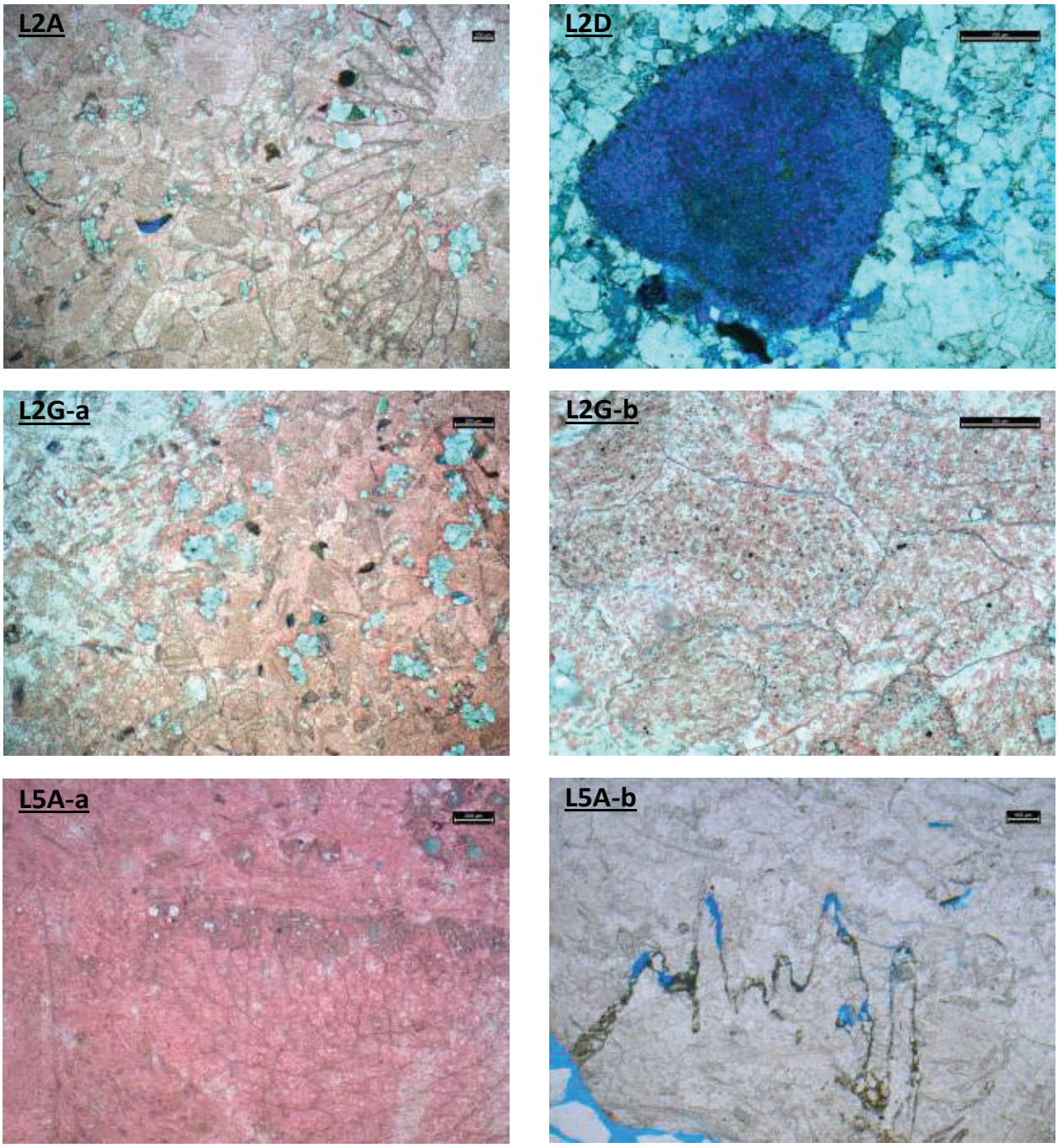

Figure 4.4 Photomicrographs of samples deposited in a moderate energy deep ramp environment of the Millersburg Member. (L2A) Subplanar calcite cement with minor amounts of subplanar dolomite filling primarily moldic pore spaces. On the right side of the image is a bryozoan that has undergone minor neomorphism from burial connate fluids. (L2D) A fragment of phosphatized solenoporoid algae within a hydrothermally dolomitized matrix. Minor porosity is preserved from dissolution of calcite walls following phosphate precipitation within large circular voids. (L2G-a) Abundant trilobite and ostracode fragments within a cloudy subplanar matrix of calcite. Some calcite crystals exhibit twinning surfaces that formed during neomorphism of the primary fabric. Calcite twins are indications of elevated temperatures of precipitation.

Early stage dolomite cements (unstained) can be observed filling moldic porosity. (L2G-b) A red algal solenoporoid fragment is observed within a subplanar to nonplanar calcite matrix. Neomorphism gives the allochems a "ghost" appearance. (L5A-a) A bryozoan that displays minor dolomite and phosphate alteration in the outermost zooecia. In the upper right corner of the figure circular phosphatized bryozoan zooecia and be observed. (L5A-b) An unstained section displaying a high-amplitude stylolite that is oriented in a non-bed-parallel direction indicating that development likely occurred during faulting at the early stages of dolomite emplacement. Phosphate and minor pyrite are observed following the surface that is associated with minor amounts of porosity enhancement.

The Lightbulb locality consists of 12 individual diagenetic events that are correlative to porosity enhancement, porosity destruction, and non-porosity affecting (Figure 4.5). Following deposition of the Trenton on the Lexington platform, marine phreatic and cementation occluded much of the depositional porosity. Coeval with deposition and cementation was phosphatization of marine hardgrounds (condensed sections/ hiatus surfaces), which were supplied with phosphate from cool, nutrient-rich upwelling from the Martinsburg foredeep and Sebree trough (Young et al., 2005). The following stages consist of eogenetic fracture generation following lithification and compaction of the cool water carbonates. Fracture generation allowed for the earliest stage of fluid migration to initiate, which led to the development of moldic porosity. Allochems of trilobites and bryozoan zooecia were preferential to eogenetic porosity development, however the porosity was quickly occluded by early dolomite cements. At the mesogenetic stage elevated temperatures and pressures led to calcite recrystallization into poikilotopic twinned calcite, which was followed by Stage II dolomitization (minor alteration). This stage led to minor volumes of increased porosity development and remained mimetic among the host facies. Progressively nearer to the fault plane, fine matrix dolomitization (highly altered) becomes extremely prevalent as this stage is fabric-destroying as the high fluid injection pressures present during the mesogenetic stage forced hydrothermal brines into the matrix. Fine matrix dolomitization is the most porosity-enhancing event in the Lightbulb's diagenetic history. This increase in porosity led to solution collapse of the dolostone body and directly led to the development of vugular, intercrystalline, and intracrystalline porosity. Following the mesogenetic solution collapse and large increase in porosity and permeability, saddle dolomite growth within large vugs/ pore spaces began while hydrothermal fluid cooling commenced. Saddle dolomite growth is an intercrystalline and vugular porosity-destructive process, however intracrystalline porosity generation is common due to crystal imperfections associated with the curved crystal faces. During uplift, iron-rich fluid flow caused neomorphism of fine matrix dolomites within a reducing environment (Scholle and Ulmer-Scholle, 2003). The

final stage of paragenetic sequence analysis revealed meteoric phreatic calcite cementation within the center of late-stage saddle dolomite cemented vugs, which was emplaced during the final stages of uplift and exhumation.

Diagenetic facies of the Lightbulb locality can be split into five distinct groups, which tend to grade from minor diagenesis at the lateral extent of dolomitization into pervasive highly altered facies (nonmimetic) near the fault plane in the middle of the outcrop. Facies exhibiting varying degrees of diagenesis are characterized as exhibiting very minor alteration (approximately 15 lateral feet from the fault plane), minor alteration (15 to 10 feet away from the fault plane), moderate alteration (approximately 10 feet away from the fault plane), high alteration (generally 5 to 10 feet from the fault plane), and very high alteration (within 5 feet of the fault plane).

At the lateral limit of fluid migration, diagenesis has occurred in the form of grain-selective dissolution to create moldic porosity (very minor alteration; L1A and L1B in Table **3**). Allochems that underwent fabric-selective dissolution include trilobites and bryozoan zooecia (Figure 4.3 L1B) of the moderate energy mid-ramp and moderate energy deep ramp wackestone and packstone facies of the Millersburg Member (Pope and Read, 1997). Minor subplanar, porosity-occluding dolomite cements occur within moldic pore spaces along the margin of the pervasively dolomitized unit (L1B, L2A from Table 3). The porosity-destructive dolomite cements exhibit well-developed medium sized rhombic and subplanar dolomite crystals that display unit extinction. The lack of significant sweeping extinction through the dolomite most likely resulted from fluid cooling with increasing distance from the fault plane, indicating that the cements were not emplaced from significantly elevated fluid temperatures.

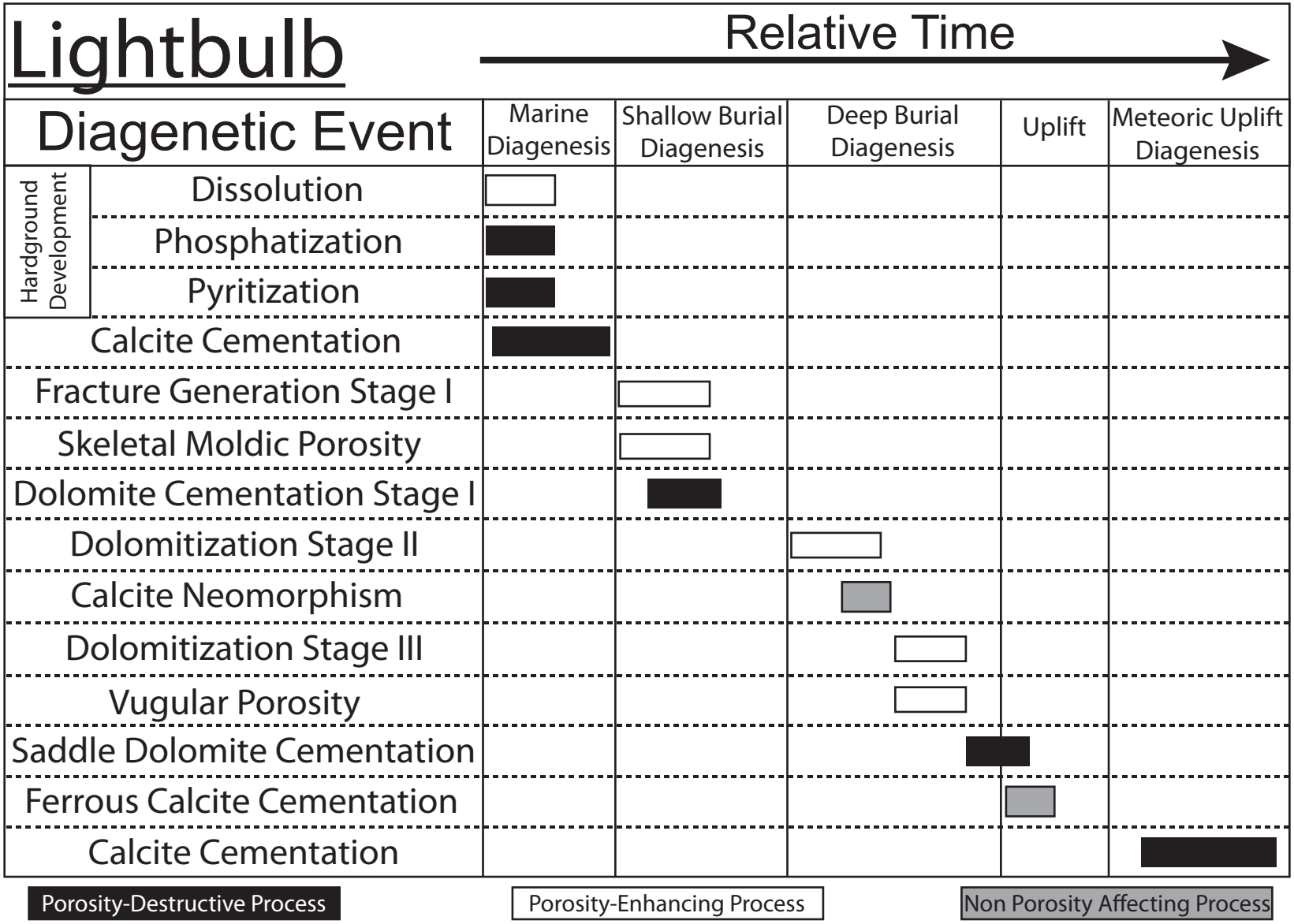

Figure 4.5 Paragenetic sequences observed at the Lightbulb locality.

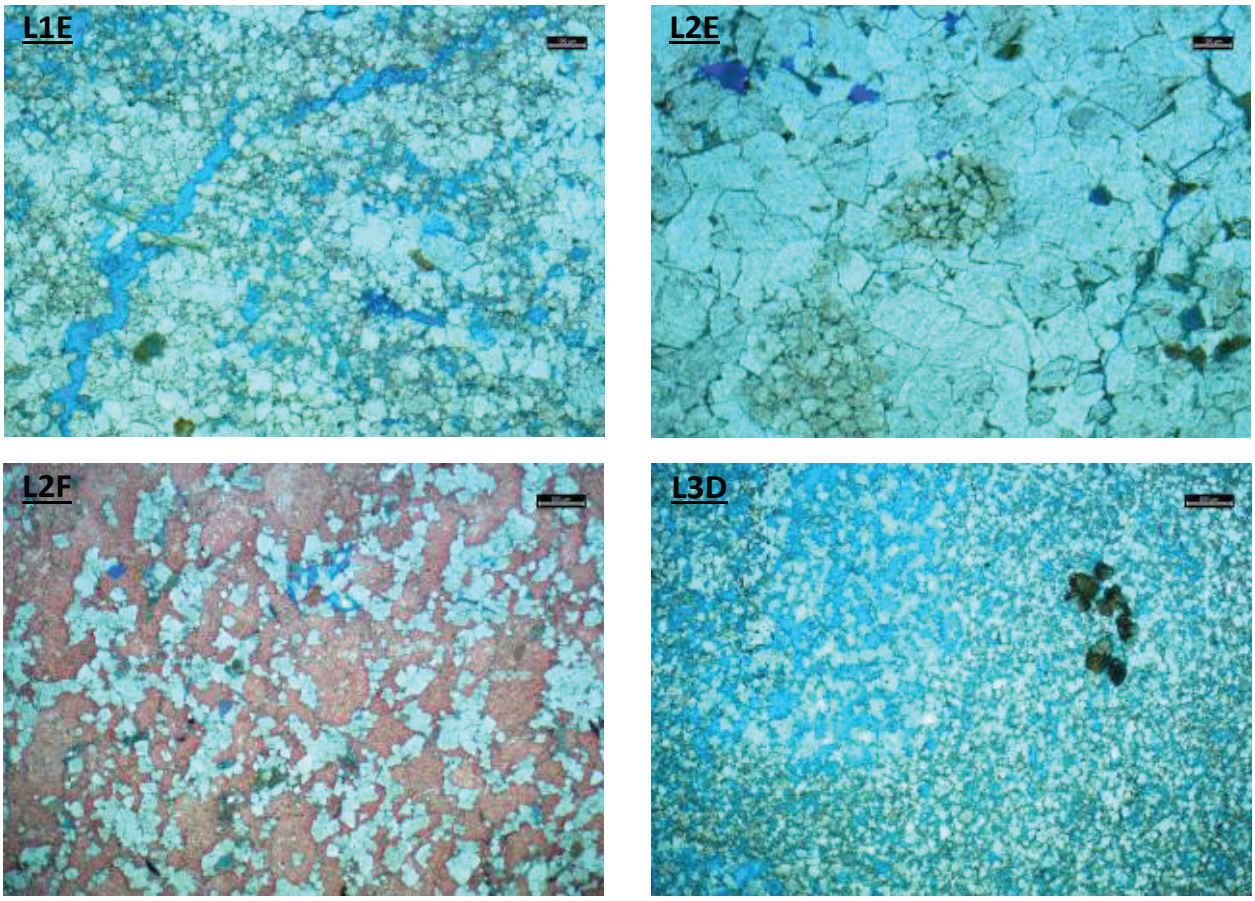

Figure 4.6 Photomicrographs illustrating Stage I through Stage III dolomitization. (L1E) Matrix dolomitization and a late stage open fracture lead to significant porosity development and destroy primary fabrics. Dolomite is subplanar to planar and leads to excellent intercrystalline porosity development. (L2E) Stage I moldic dolomite cements remain unaffected by pervasive Stage III dolomitization and are commonly associated with moldic cements with very minor porosity within the Stage III matrix that exhibits excellent intercrystalline porosity. (L2F) Stage II dolomitization near the margin of dolomite-country limestone where minor amounts of porosity development can be observed. (L3D) Excellent porosity development through the fabric-destructive Stage III dolomitization. Phosphatized echinoid clasts remain unaffected by Stage III dolomitization and generally contain significantly less porosity than the surrounding dolomite matrix.

Near the margin of dolomite-country limestone, fine dolomite spar can be observed propagating into the host limestones. Dolomitization exhibits sweeping extinction under cross polarization, is mimetic (fabric-preserving), and results in minor amounts of increased intercrystalline porosity (minor alteration; L1G and L2F from Table 3; Figure 4.6 L2F). In addition, an increase in fracture density is observed along the dolomite-country limestone margin. Sweeping extinction and the relationship of dolomite to fractures suggests that dolomites were supplied from hydrothermal fluid migration, which is confirmed through fluid inclusion microthermometric analysis (see Chapter 7 for fluid inclusion results).

Complete matrix dolomitization occurs as samples near the fault plane (moderate alteration; L1C-L1E, L2B-L2E, L3A-L3D in Table 3). Dolomite is finely crystalline, displays sweeping extinction under cross polarization, is nonmimetic and unimodal, and results in extensive intercrystalline and vugular porosity development (Figure 4.6). Remnant moldic dolomite cements are preserved and are recognized as having no porosity and having closely spaced medium subplanar crystals. The extent and pervasiveness of dolomitization tends to increase towards the fault plane where vugular porosity development is most prevalent.

The final hydrothermal facies composes the central portion of the outcrop and consists of coarsely crystalline saddle dolomite cements (highly altered; L1D, L2C, L3A, and L3B in Table 3). Crystalline saddle (baroque) dolomites nucleate at the margin of vugular pore spaces and extend towards the center of voids (Figure 4.7). The dolomites are generally porosity-destructive, however very minor amounts of intracrystalline porosity can be observed within individual crystals. Dolomite crystals display sweeping/undulose extinction under cross polarization and frequently contain moderate-to-well developed crystal zonation (caused by variations in fluid inclusion densities). Crystal growth is only possible due to the significant increase in porosity caused by the preceding (moderately altered) stage of dolomitization, which opened large vugular pore spaces to allow for coarsely crystalline saddle growth.

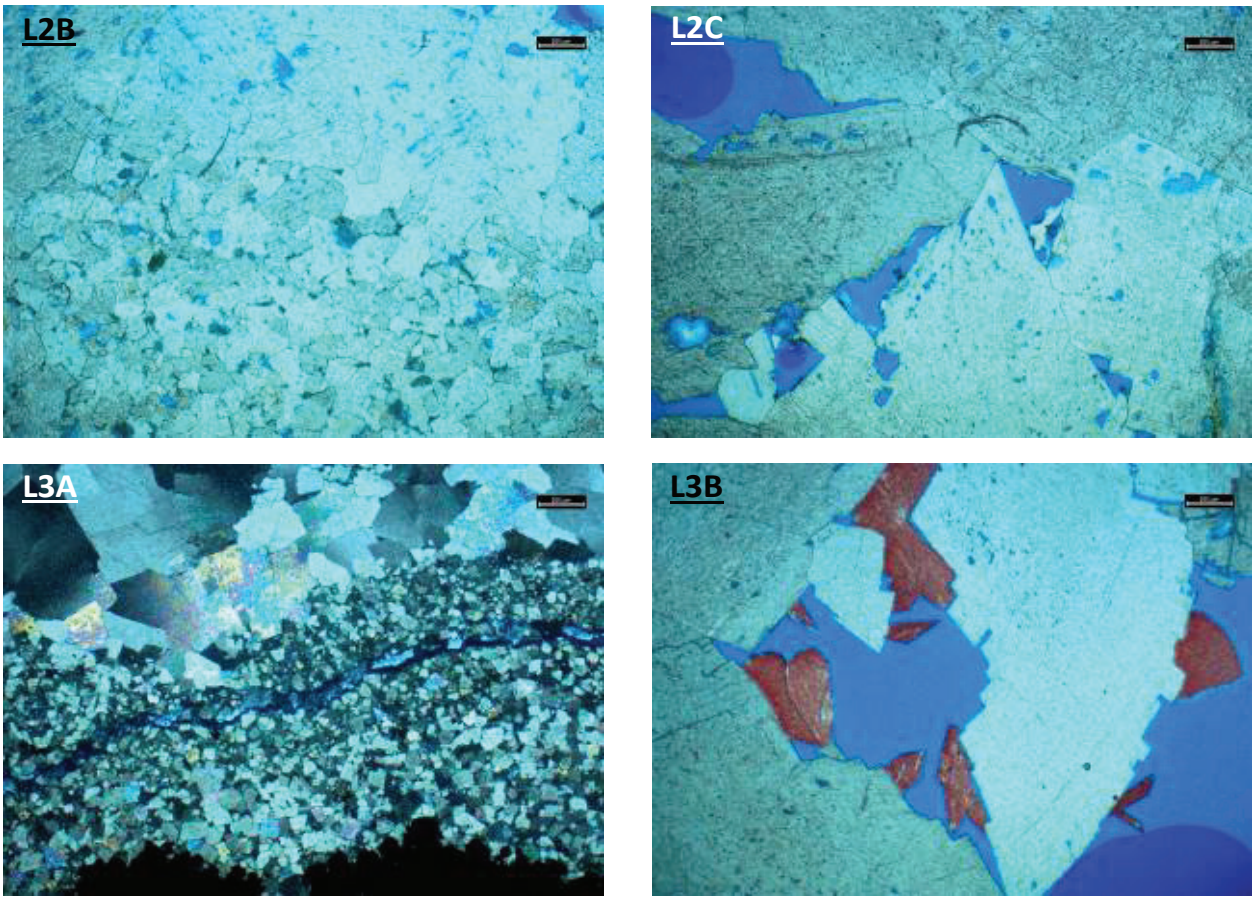

Figure 4.7 Photomicrographs illustrating the transition from Stage III through late stage calcite cementation. (L2B) Stage III dolomitization at the base of the image transitions into coarse subplanar dolomite cements that exhibit minor intercrystalline and intracrystalline porosity. (L2C) Intercrystalline porosity development resulting from curved crystal faces that form in Stage IV dolomites. Imperfect crystal structures associated with saddle dolomite crystals also commonly result in intracrystalline porosity. (L3A) Transitions from phosphatized allochems at the base of the figure into Stage III matrix dolomites with a quartz-healed fracture through the middle of the matrix and finally into saddle dolomite cements at the top of the figure. Saddle dolomites display well developed sweeping extinction caused by the imperfect crystal habit. (L3B) Late stage saddle dolomite crystal displaying a curved crystal face that extends into a vug. Late stage meteoric calcite (stained red) cements are observed near vugular porosity.

Very highly altered facies are only observed in sample L3C where medium to finely crystalline matrix dolomite appears to have been neomorphosed by iron-rich fluids giving the saddle and matrix dolomites a rusty appearance (Figure 4.8). Scholle and Ulmer-Scholle (2003) present similarly appearing dolomites that were replaced by calcite filled with iron oxide inclusions and were interpreted to originate from telogenetic meteoric alteration.

In conclusion, the Lightbulb locality exhibits five distinct levels of mineralization, which appear to have been induced by fluid migration along the fault plane. Pope and Read's (1997) moderate energy mid-ramp and moderate energy deep ramp facies (other than hardground surfaces) do not appear to have significant impacts on dolomitization; however hardground surfaces tend to resist secondary mineralization and the lack of porosity and permeability led to the hardgrounds acting as aquitard surfaces. A major control on the extent of dolomitization appears to have been fluid injection pressures, which appear to have been significant as bed-parallel zebra fabrics line the dolomite-limestone margin and degree of alteration decreases with increasing distance from the fault plane.

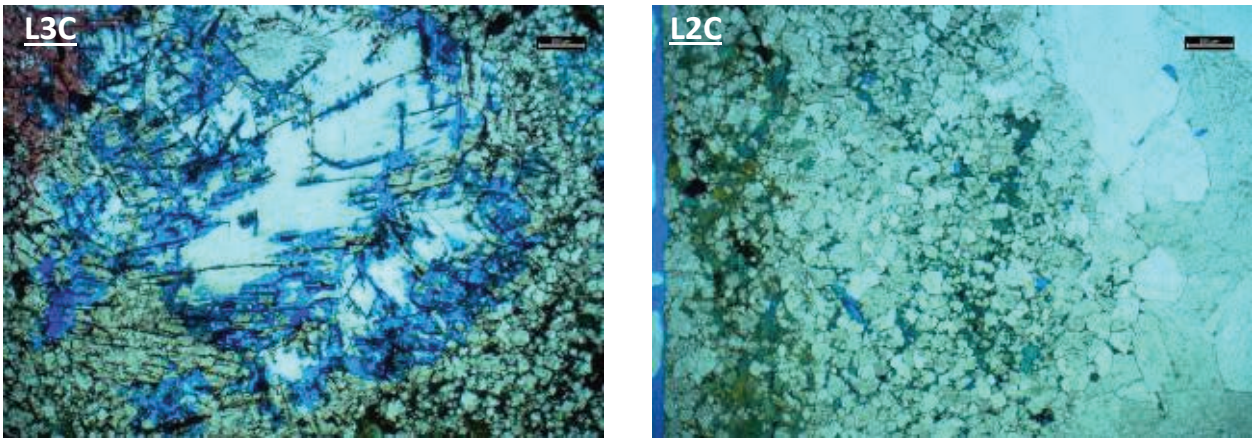

Figure 4.8 Late stage Fe and PO4-rich meteoric fluid migration results in very limited porosity occlusion. (L3C) Neomorphosed coarsely crystalline Stage IV dolomite and Stage III dolomites exhibit rusty appearances resulting from iron-rich meteoric fluid migration. (L2C) Late Stage V fluid migration led to limited quantities of phosphate cements to develop along fracture and intercrystalline porosity. Pyrite and phosphate tend to favor precipitation in Stage III dolomites due to the increased porosity that allowed for efficient fluid migration.

4.2 THE DRAG FOLD LOCALE

The Drag Fold locality is located approximately three miles south of Camp Nelson, KY along N US Highway 27. The outcrop is almost entirely covered in vegetation due to the highly fractured nature of the Trenton Limestone (fractures allow for enhanced weathering and erosion that provided space for vegetative growth), which has led to outcrop dimensions of approximately 40 feet wide by 10 to 15 feet tall (Figure 4.9). Conjugate fracturing in the Trenton Limestone is the result of tensional stress caused by extension near the hinge of the fold (Twiss and Moores, 1994), which terminates against the N-S trending Lexington Fault System. Mineralization is limited to a very narrow margin in the center of the outcrop where extensive conjugate fracturing provided fluid-flow conduits through the Trenton Limestone. Dolomite and calcite-healed fractures cover the outcrop; however matrix dolomitization is restricted to a narrow margin near the middle of the outcrop exposure.

The Drag Fold locality consists of four depositional facies that confirm interpretations from work conducted by Pope and Read (1997) within the lower Millersburg Member including low-energy deep ramp, moderate energy deep ramp, high energy deep ramp, and high energy shallow shelf depositional facies that are characterized by normal marine wackestones, packstones, and boundstones.

A bryozoan boundstone (high energy shallow shelf facies from Pope and Read, 1997) makes up the base of the exposed outcrop as a very thin interval (approximately one foot thick) of nodular-bedded limestone (D4C from Table 3; Figure 4.10). The boundstone contains echinoids, ostracodes, trilobite fragments, and peloids and micrite is largely absent. Cloudy calcite spar and microspar cements fill the facies, which precipitated in a marine phreatic environment. Marine phreatic cementation likely provided firm substrates that allowed for bryozoan anchoring (Scholle and Ulmer-Scholle, 2003). Storm events are likely responsible for the lack of micrite and also provide mechanisms that allowed for transportation and reworking of the observed allochems into the shallow shelf where they became trapped within encrusting bryozoans.

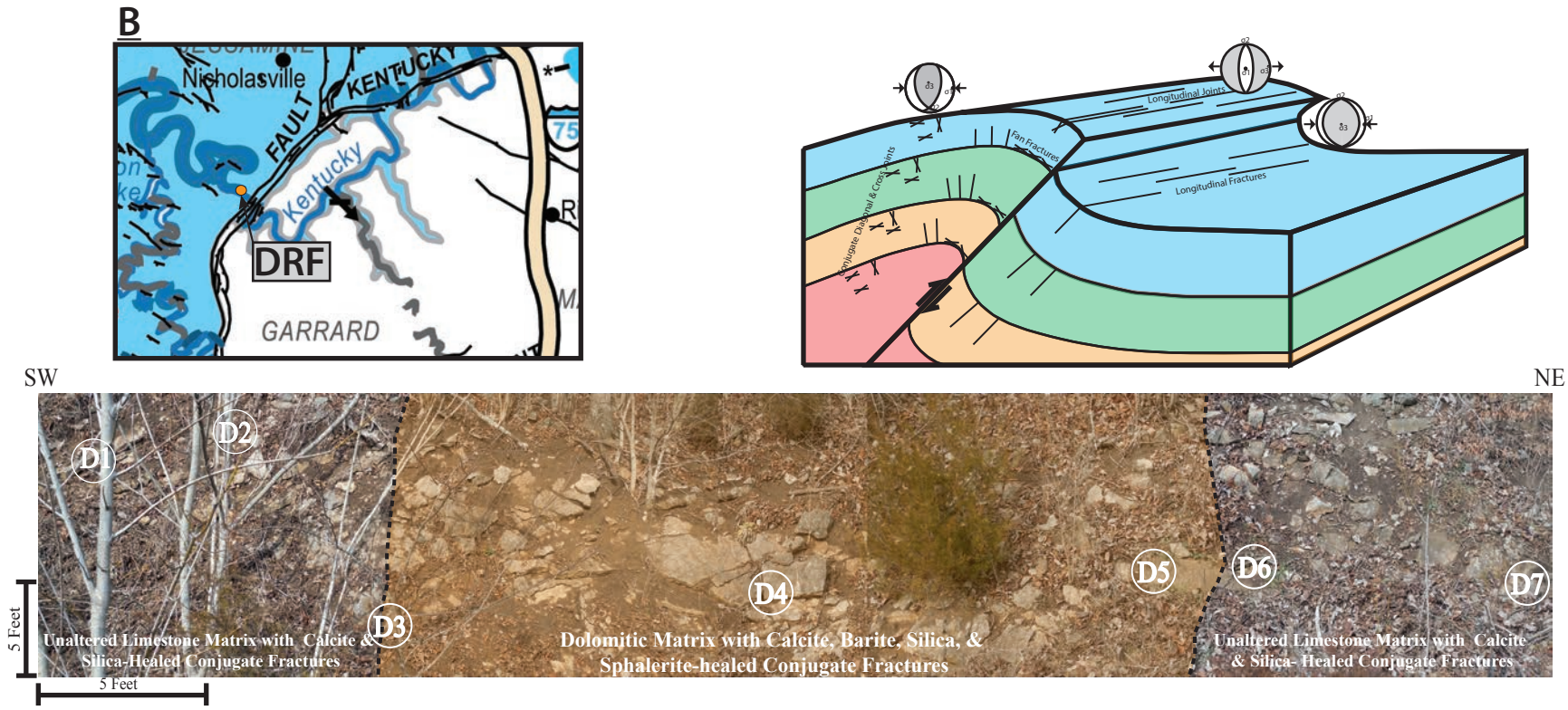

Figure 4.9 A composite outcrop photograph from the Drag Fold Locality with sample locations illustrated by white circles and the dolomitic zone is shaded orange. The location of the outcrop is indicated by the white circle on the figure in the upper right corner. A schematic stress diagram in the upper left illustrates how conjugate fracturing along the drag fold occurs (Modified from Patchen et al., 2005; Modified from Twiss and Moores, 1994).

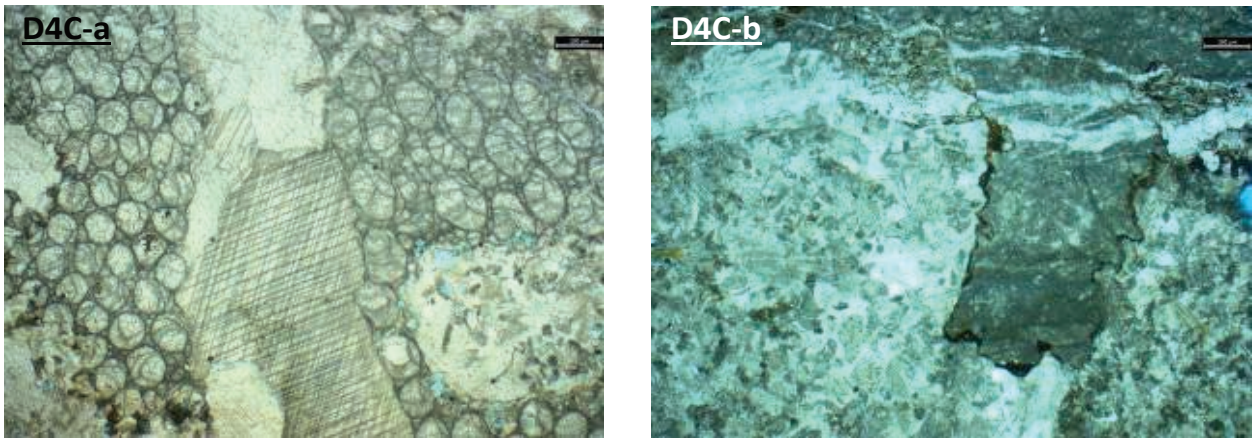

Figure 4.10 Photomicrographs of sample D4C that illustrate primary fabrics such as the bounding nature of bryozoans that developed in high-energy shallow shelf environments. (D4C-a) An encrusting bryozoan that also contains one intraclast in the bottom left within an unstained section of thin section D4C. Encrusting bryozoans developed on hard substrates in high energy shallow marine environments. One calcite-healed fracture is observed in the center of the photograph that contains poikilotopic, highly twinned calcite. (D4C-b) A low amplitude stylolite surface that separates a micritic upper facies from the peloidal, grain-rich lower facies. A calcite-healed fracture crosscuts the upper portion of the stylolite surface indicating that bed-parallel stylolite development likely occurred during burial and not during structural deformation.

Moderate energy deep ramp wackestones (D1A-D2A in Table 3; Figure 4.11) contain abundant brachiopods and trilobites that are frequently fractured and less frequent echinoids have been replaced by cryptocrystalline phosphate. A matrix of up to 25% microspar is transected by minor stylolite surfaces and preserves horizontal laminations. The presence of compaction structures such as fractured grains and the development of stylolite surfaces indicate that rapid burial occurred prior to cementation, which likely occurred in a meteoric phreatic or burial connate environment. The presence of microspar suggests that neomorphism of depositional micrite into microspar occurred, which supports the influence of increased temperatures and pressures induced from a deep burial connate environment (Scholle and Ulmer-Scholle, 2003).

Peloidal wackestones (D2B-D4B and D5A-D5B in Table 3) contain peloids, brachiopods, ostracodes, and echinoids hosted within a matrix of up to 50% micrite that occasionally displays horizontal laminations. Occasional thin beds (less than 1 inch thick) of brachiopod coquina composed of small (up to 2 centimeters across) that have been silicified and are very well cemented can be observed. The lack of biodiversity within these units indicates that conditions produced highly segregated niche spaces, a result of large quantities of cold water upwelling along a low-energy deep ramp environment. The lack of sutured and concavo-convex grain boundaries paired with preservation of horizontal laminations supports synsedimentary cementation in the marine phreatic realm (Figure 4.12; Scholle and Ulmer-Scholle, 2003).

High-energy mid-ramp wackestones (D5C-D6B in Table 3) make up the top of the outcrop. Allochems within the facies include echinoids, bryozoans, ostracodes, brachiopods, trilobites, gastropods, and intraclasts, which are hosted in a matrix of up to 20% micrite (Figure 4.13). Styolite surfaces are well developed throughout the facies, however significant compaction at grain boundaries or through fractured grains was not observed. Minor amounts of poikilotopic calcite exhibit highly twinned crystal faces where allochems are not present. Collectively the variety of allochems is indicative of deposition in a high-energy normal marine environment (near normal wave base; Scholle and Ulmer-Scholle, 2003). The lack of

compaction structures and presence of cloudy calcite spar are indicative of marine phreatic cementation, which underwent later neomorphism in a burial connate environment resulting in highly twinned poikilotopic calcite (Scholle and Ulmer-Scholle, 2003).

At the Drag Fold locality 12 stages diagenetic events are recognized (Figure 4.14) beginning with early marine phreatic calcite cementation and hardground development (involves phosphatization, dissolution, and pyritization). Eogenetic chalcedony replacement favored trilobite skeletal fragments which transitioned into brittle deformation with Stage I fracturing. The porosity-enhancing stage allowed for the development of matrix dolomitization (minor alteration) directly adjacent to open Stage I fractures. Upon reaching maximum burial (mesogenetic) fluid sourcing changed in composition to initiate precipitation of ferrous calcite and bladed barite, which cemented Stage I fractures. During late-middle mesogenetic alteration, Stage II fracturing allowed for barite, ferrous calcite, and fluorite precipitation from hydrothermal fluid migration. Elevated injection pressures allowed for the influx of these hydrothermal fluids to penetrate into the matrix and flow along the base of stylolite surfaces where minor chalcedony mineralization can be observed. Stage II fractures offset Stage I calcite and fluorite-healed fractures and allowed for a final stage of fluid migration to occur. Coeval precipitation of hydrothermal dolomite and sphalerite marked the final stages of mesogenetic alteration. Telogenetic alteration is recognized as a final stage of fracturing (Stage V), which was caused by unroofing and exhumation of overlying strata causing a relaxation of the country rock. Aside from minor pyrite development along the margin of the fractures, the Stage V fractures remain open and account for the only porosity present in the Drag Fold locality.

The Drag fold locality contains dolomite in very minor amounts, which tends to follow fracture planes and does not initiate matrix dolomitization as observed in the Lightbulb locale. Dolomitization and diagenesis are primarily located along healed fractures and along conjugate brecciated zones. Degrees of diagenesis are again characterized based on relative alteration, which range from minor alteration, moderate alteration, high alteration, and very high alteration.

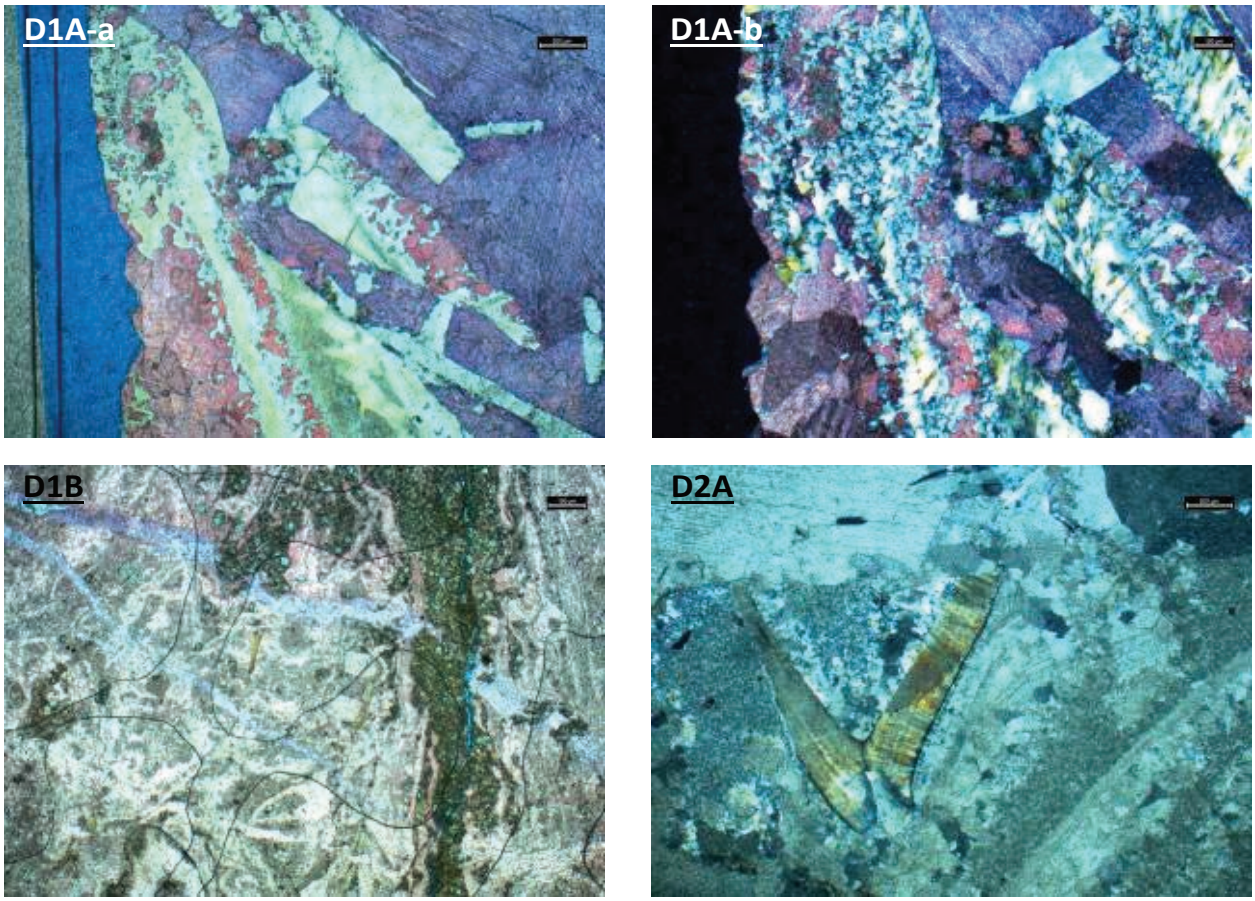

Figure 4.11 Photomicrographs of the highly neomorphosed Millersburg Member from the Drag Fold Locality. (D1A-a) A chalcedony-replaced trilobite "shepards hook" that indicates deposition in a deep ramp environment with limited siliciclastic input. Chalcedony replacement likely occurred during shallow burial neomorphism. (D1A-b) A view of D1A-a under cross polarization making the neomorphosed matrix of subplanar calcite and poikilotopic ferrous calcite readily distinguishable. (D1B) A primary micritic matrix has been neomorphosed into microspar and two stages of fracturing are evident; one early stage fracture cementation with ferrous calcite and a second fracture event that supplied magnesium and phosphate-rich fluids to precipitate fine crystalline dolomite microspar that cross-cuts the early ferrous calcite-healed fracture. (D2A) A chalcedony-replaced trilobite fragment that has microcrystalline quartz nucleating on the stratigraphic up side of the allochems. Calcite microspar fills the matrix that has been highly neomorphosed.

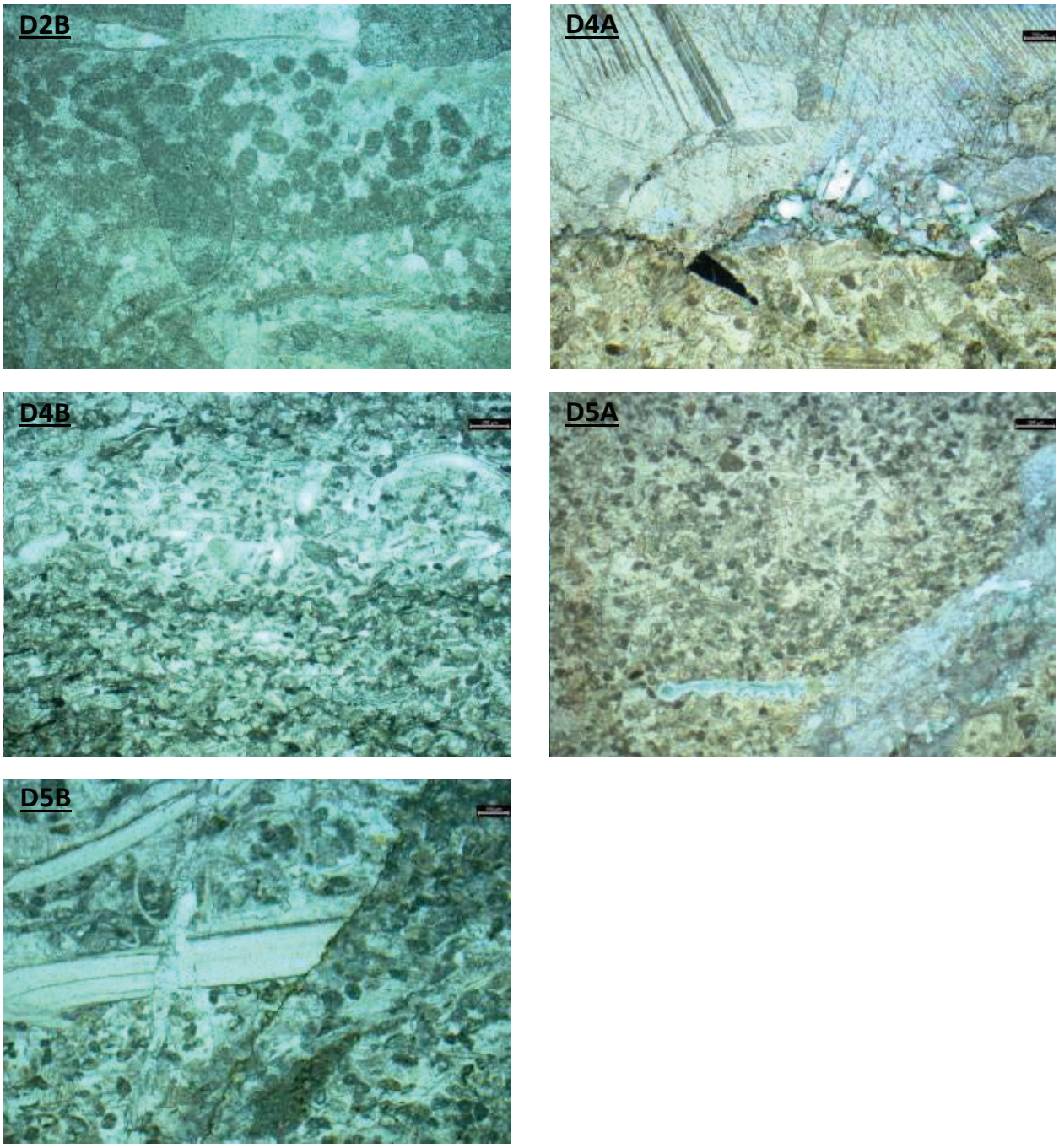

Figure 4.12 Photomicrographs displaying primary fabrics of peloidal wackestones deposited in a low energy deep ramp environment that was subjected to occasional storm reworking and prolonged periods of low energy deposition. (D2B) An unstained section that exhibits large peloids that are concentrated within a cloudy nonplanar matrix of calcite spar. (D4A) A low-amplitude stylolite surface that exhibits mineralization and separates the overlying poikilotopic twinned calcite from an ostracode and echinoid-rich wackestone at the base of the photograph. (D4B) An unstained section that illustrates well-developed horizontal laminations of peloids, trilobites, ostracodes, and echinoids with alternating volumes of micrite versus cloudy calcite spar. (D5A) A packstone composed of predominantly peloids and echinoids. Near the bottom right

corner is a fracture that has been healed by ferrous calcite and chalcedony. Additionally, a trilobite fragment has been replaced by chalcedony at the margin of the healed fracture. (D5B) A peloidal packstone that has a pyritized fracture displacing a large trilobite fragment.

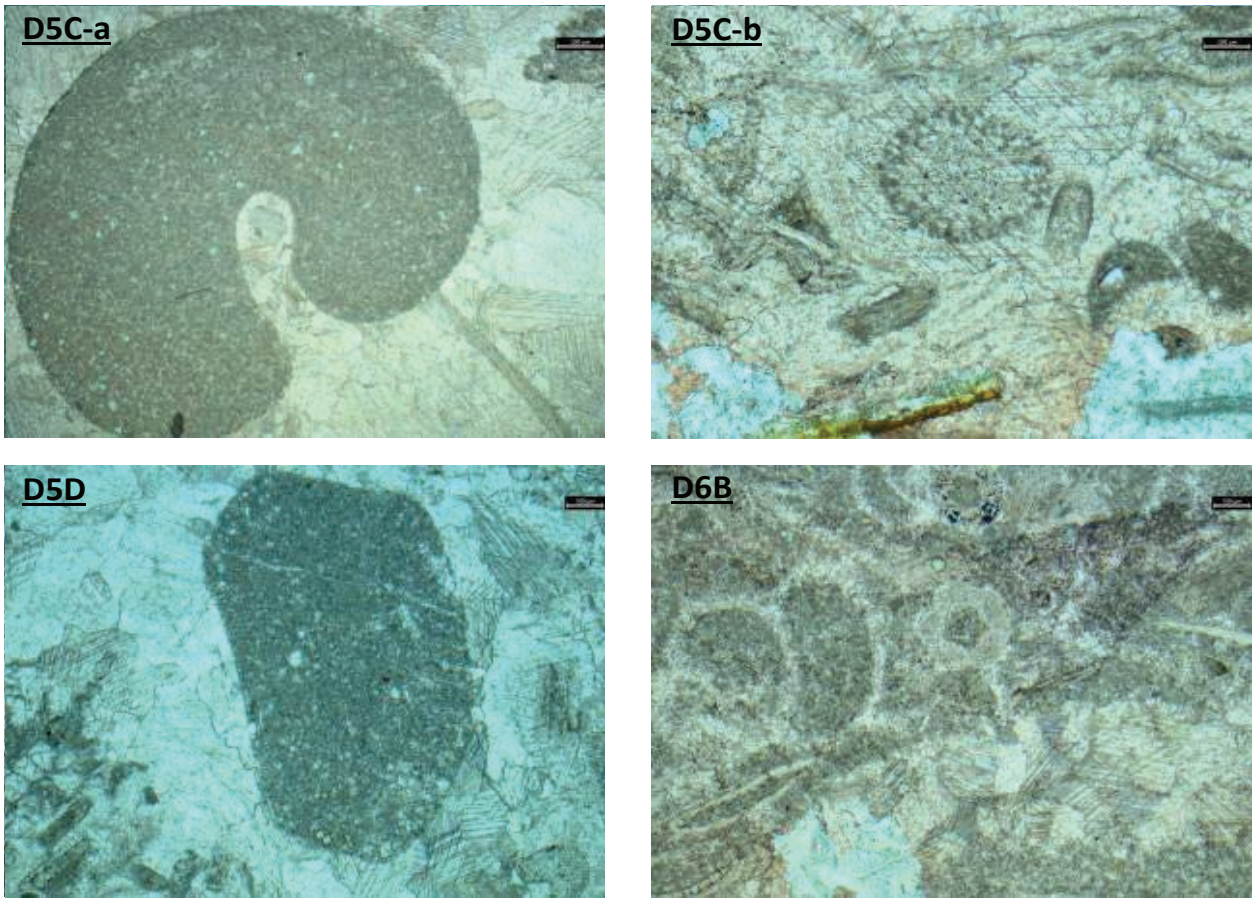

Figure 4.13 Photomicrographs of wackestones that were deposited in high energy mid-ramp environments. (D5C-a) A cut through a gastropod that is filled with a weakly dolomitized micritic matrix embedded within a subplanar matrix of twinned calcite. (D5C-b) An echinoid that has a twinned syntaxial overgrowth that likely developed during neomorphism in a burial connate environment. Minor chalcedony is observed in the bottom corners (unstained). (D5D) A subrounded extraclast of micrite that has been weakly dolomitized and very weakly pyritized embedded in a matrix of nonplanar cloudy calcite that frequently exhibits mineral twinning. (D6B) Allochems of gastropods and crinoid stems embedded within a matrix of microspar that developed as a result of neomorphism of the primary micritic matrix. One crinoid stem at the top of the picture exhibits early stages of pyritization through the outer stem wall. Minor chalcedony cementation within a chalcedony and calcite-healed fracture can be observed near the base of the photograph.

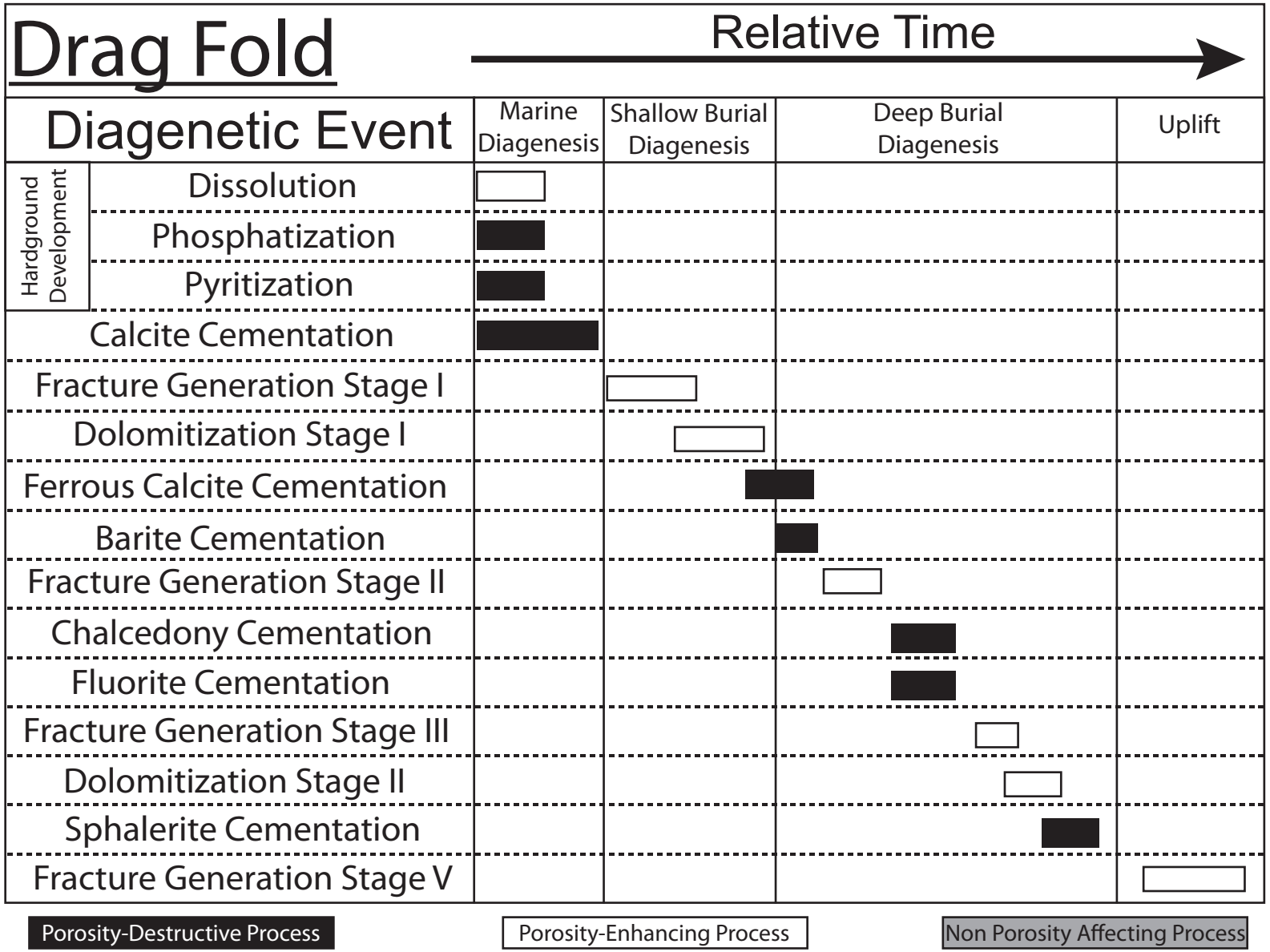

Figure 4.14 Paragenetic sequences observed at the Drag Fold locality.

Minor alteration is observed through chalcedony replacement of trilobite shell fragments (Figure 4.15 D5C). Chalcedony has a radiating tendency that exhibits pseudo-uniaxial extinction under cross polarization. Minor megaquartz cements can frequently be observed nucleating on the exterior of chalcedony-replaced trilobite fragments. Minor alteration occurred during early burial diagenesis.

Moderate alteration consists of early stage fractures that have fine matrix-replacing dolomites along the fracture margins. Dolomites are unimodal and finely crystalline, occur as subplanar to planar rhombic crystals that exhibit intracrystalline and minor intercrystalline porosity, and exhibit sweeping extinction under cross polarization (Figure 4.15 D5C). Fracture generation appears to have allowed for magnesium-rich hydrothermal brine migration that induced dolomitization. Extent of dolomitization is severely limited due to the lack of primary porosity within the host carbonates in combination with the lack of evidence for high-pressure fluid injection.

Highly altered facies consist of bladed barite, ferrous calcite, and fluorite precipitation within open fractures and intercrystalline porosity (D2A, D1A, D5C, D6A, D1B, and D6B in Table 3; Figure 4.15 D1B, D1A). Ferrous calcite is poikilotopic and is highly twinned whereas fluorite has high relief and is littered with fluid inclusions. Further, fluorite exhibits abundant two phase fluid inclusions and the crystal shape tends to mimic the shape of the open porosity that it fills. In addition to healing fractures, the fluorite and minor amounts of chalcedony can be observed along stylolite surfaces, which may have acted as aquitards to limit vertical fluid migration. Ferrous calcite and fluorite appear to have precipitated shortly after barite precipitation and all three are indicative of elevated temperatures and reducing conditions (Scholle and Ulmer-Scholle, 2003).

Very high alteration consists of facies exhibiting minor matrix dolomitization and the emplacement of sphalerite (D2B in Table 3; Figure 4.15 D2B). Dolomite occurs as subplanar crystals with a cloudy appearance and exhibit sweeping extinction under cross polarization while

sphalerite has a cloudy yellow appearance in transmitted light. Both minerals are indicative of hydrothermal fluid flow and are commonly observed in Mississippi Valley Type (MVT) ore deposits (Scholle and Ulmer-Scholle, 2003).

In conclusion the highly fractured Drag Fold locality exhibits varying degrees of alteration that have resulted in an abundance of minerals that commonly are associated with MVT ore bodies. The lack of pervasiveness in alteration indicates that fluid injection pressures were not elevated (caused by the lack of a vertical aquitard) and mineralization is limited to near-fracture horizons. The lack of primary porosity and permeability through the depositional facies of the Millersburg further restricted matrix fluid migration and matrix alteration. The high variability of secondary mineralogies (sulfides and sulfates) relative to those observed at the Lightbulb locality may have resulted from variable fluid compositions. Results of the low-pressure mineralization did not lead to reservoir grade porosity or permeability development indicating that injection pressures, primary porosity, and primary permeability had significant impacts on the character of mineralization.

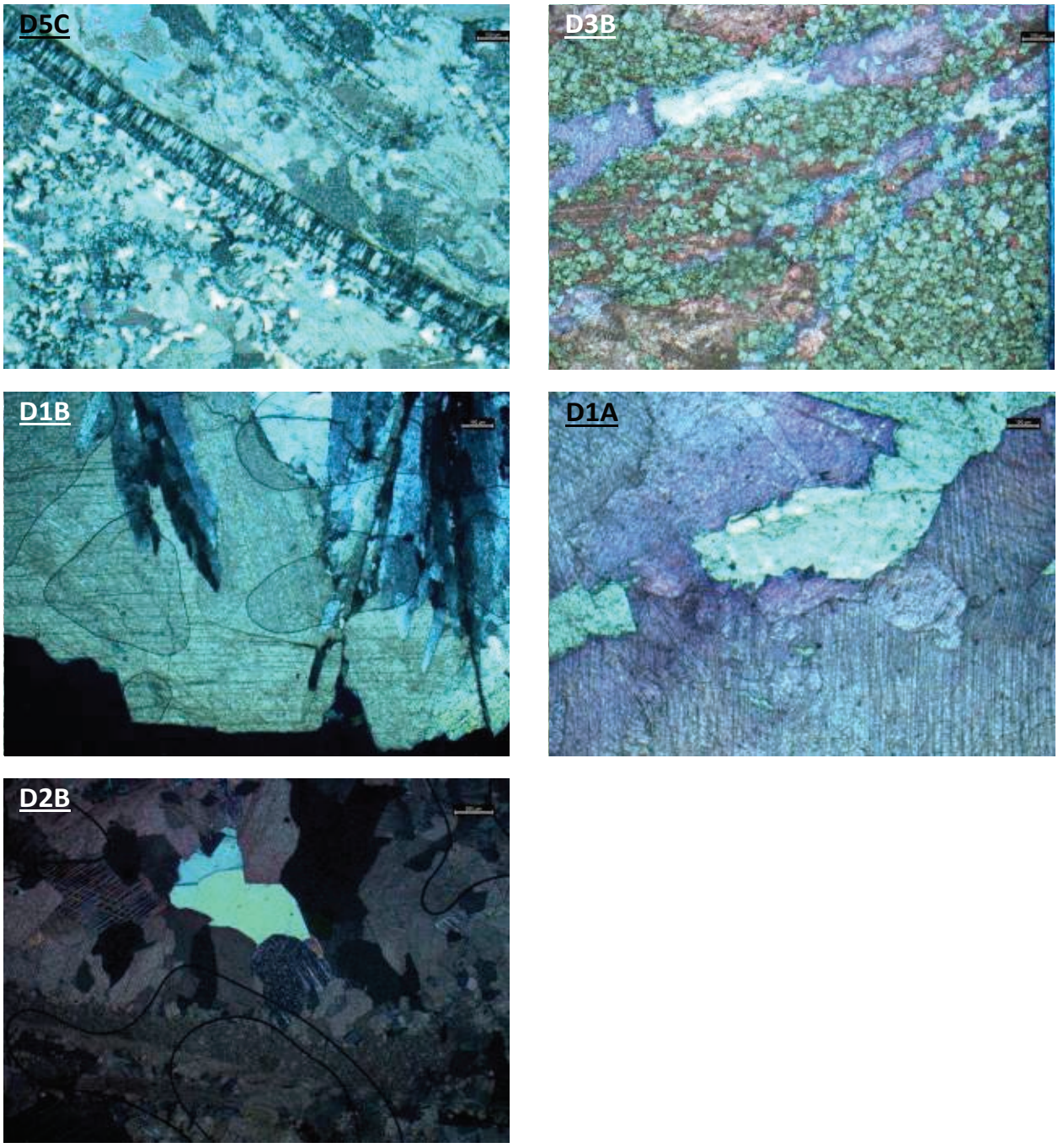

Figure 4.15 Minor through highly altered facies through the Drag Fold outcrop can be recognized based on crystal habit and cross-cutting relationships. (D5C) Chalcedony replacement during Stage I was grain-selective and initially replaced trilobite fragments prior to filling porosity and precipitating along stylolite surfaces. (D3B) Matrix dolomitization initiated with early stage fracturing and occurs as subplanar to planar dolomites located near the margin of early fractures. (D1B) Bladed barite precipitation occurred during deep burial diagenesis, which was closely followed by poikilotopic calcite and fluorite mineralization. Bladed crystal habits indicate that significant porosity development must have occurred following the development of Stage II fractures to allow for bladed crystal growth in porous void spaces. (D1A) Poikilotopic ferrous

calcite (stained purple) precipitation was coeval with fluorite cementation, which mark the waning stages of highly altered diagenesis (late mesogenetic). (D2B) Sphalerite occurs in association with hydrothermal dolomite within intercrystalline pore spaces and has a dull-pale yellow appearance.

Chapter 5: Core Analysis

A total of nine cores that exhibited signs of secondary mineralization were sampled in an attempt to determine the origin and controls of observed diagenetic fabrics. Cores hereafter are identified based on the Kentucky Geological Survey's sample call number identification. Northwestern cores (C-1286 and C-1287) are located in Shelby County where a cryptoexplosive structure known as Jeptha Knob is situated. This is a spherical structure of faults that may have resulted from an impact structure, cryptoexplosive event, or from a cryptovolcanic structure (Black et al., 1981). Northern cores (C-201, C-200, and C-106) all originated from Clark County near the Kentucky River Fault System.

Cores observed in south-central Kentucky (southern cores) include C-295 of Cumberland County, and C-511, C-1220, and C-1221 of Clinton County. Major structural features in Clinton and Cumberland counties are very poorly defined relative to those along the Lexington Fault System, Kentucky River Fault System, and the Irvine-Paint Creek Fault System. Relatively small structures are interpreted to be present through Clinton and Cumberland counties and previous workers have developed maps of possible fault systems based upon surface linear features to attempt to locate fractured intervals through the subsurface (Haney, 1990).

5.1 NORTHWESTERN CORES

Cores C-1286 and C-1287 from Jeptha Knob were completely dolomitized and even while utilizing the white card method (utilized to distinguish primary fabrics in highly dolomitized units), primary fabric identification is trivial (Folk, 1987). Both cores exhibited dolomitization through the entire Trenton interval. Distinguishable primary fabrics were limited to phosphatized echinoid plates and bryozoan zooecia, which were observed in sample C-1287-1.

Sample C-1286-1 is a crystalline carbonate composed of unimodal equant dolomite rhombs that are nonmimitec (aside from ghost textures of pyritic styolite surfaces, Figure 5.1 C-1286-1b) and exhibit sweeping extinction (Figure 5.1 C-1286-1a). Dolomitization resulted in a significant amount of porosity development in the form of vugular, intracrystalline, and

intercrystalline porosity, which is occasionally occluded by isotropic fluorite that have high relief in thin section. The pervasive nonmimetic nature of dolomitization suggests that fluid injection was under significant pressure and fluid cooling likely occurred extremely rapidly to account for the lack of late-stage saddle (baroque) dolomite cements. Fluorite cements are late stage and are located within intercrystalline pore spaces. Rhombic dolomite crystals do not appear to have been affected by stylolite development, which provides evidence for early stylolite development prior to hydrothermal fluid injection.

Diagenesis of the Trenton in core C-1286 began during the mesogenetic stage where compaction and burial resulted in stylolite generation (Figure 5.2). Telogenetic faulting and fracturing initiated highly pressurized fluid migration into the Trenton host resulting in pervasive matrix dolomitization that was associated with a significant increase in porosity. Intercrystalline, intracrystalline, and vugular porosity development resulted from the high pressure Mg-charged brine injection. Upon solution cooling, minor fluorite and coarsely crystalline equant dolomite cements precipitated within intercrystalline pore spaces.

Sample C-1287-1 consists of multiple stages of dolomitization, both primary and secondary. Early moldic dolomite cements occur as very fine grained nonplanar crystal fabrics that result in no increase in porosity (Figure 5.3 C-1287-1). Phosphatic echinoids and bryozoans are preserved within the matrix and are frequently associated with minor amounts of very fine euhedral crystals that appear opaque in thin section. Planar euhedral (porosity enhancing) and planar subhedral (non-porosity affecting) crystal fabrics characterize the dolomites and both fluorite and megaquartz are observed within intercrystalline pore spaces indicating that precipitation postdated dolomitization.

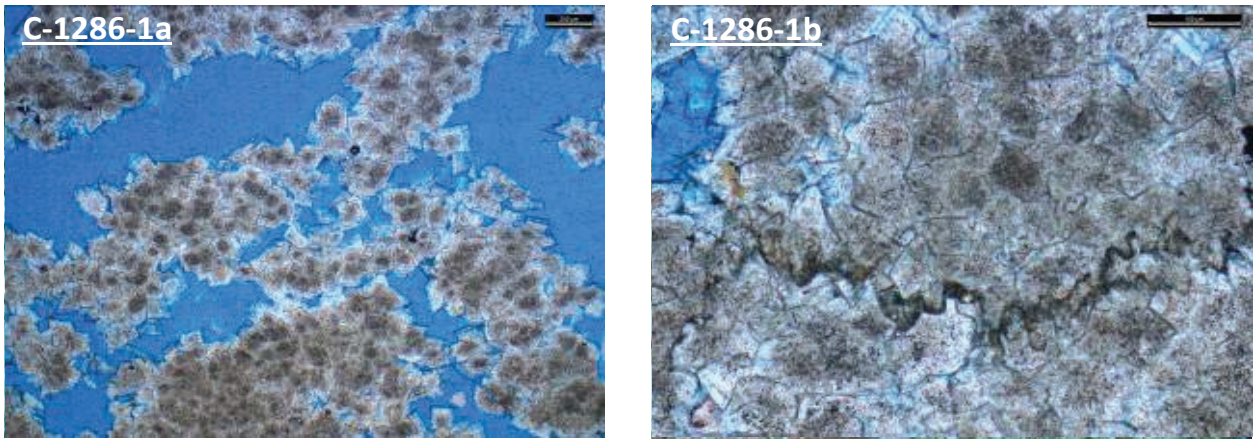

Figure 5.1 Photomicrographs from C-1286 that illustrate the pervasive dolomitization that has destroyed the majority of primary fabrics and resulted in excellent porosity development. (C-1286-1a) Vugular, intercrystalline, and intracrystalline porosity development resulting from hydrothermal dolomitization. Note how coarse saddle dolomite cements are not present, which indicates that dolomite emplacement likely occurred in a near-surface environment where solution cooling was extremely rapid. (C-1286-1b) A stylolite surface that does not appear to have an influence on subplanar dolomites that appear to have utilized the surface for points of crystal nucleation.

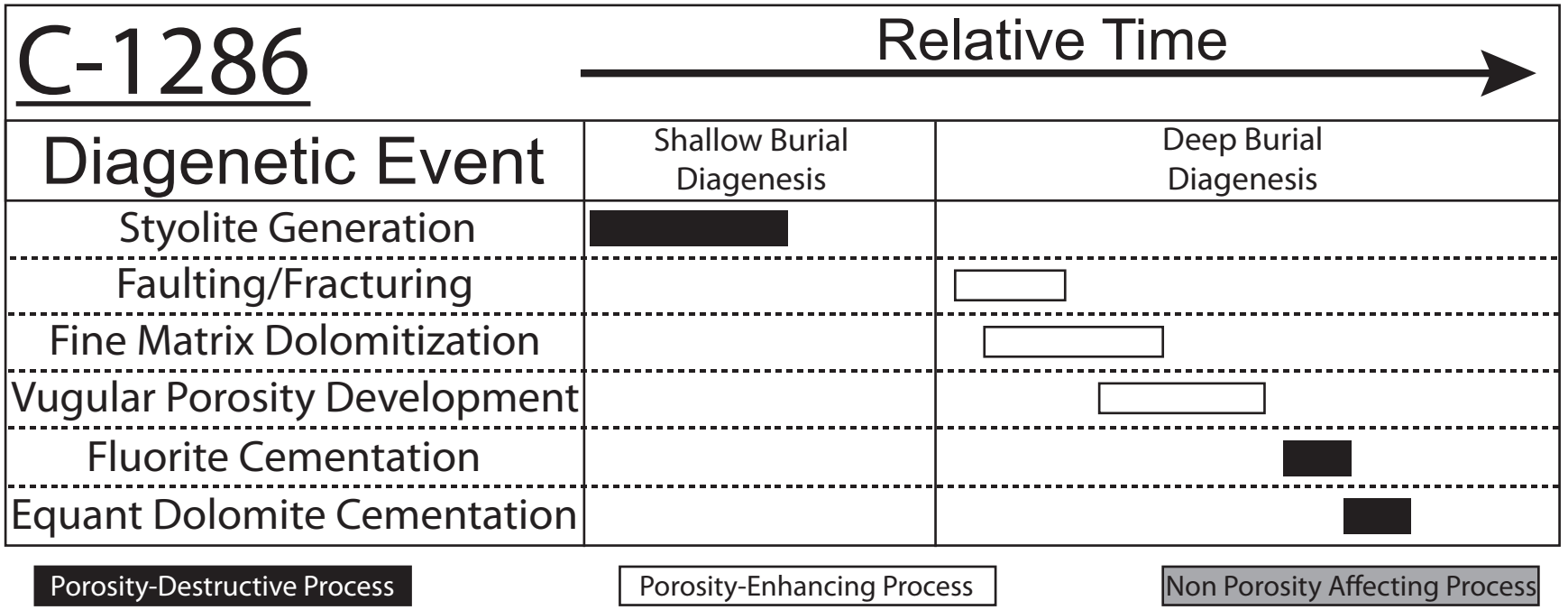

Figure 5.2 Paragenetic sequences observed in core C-1286.

Sample C-1287-2 is more similar in appearance to sample C-1286-1 as primary fabrics have been destroyed (nonmimetic) as a result of high pressure hydrothermal fluid injection. Dolomite is primarily euhedral and tends to develop into fabrics that are associated with significant quantities of intercrystalline porosity. Saddle dolomite and fluorite cementation can be observed where vugular and large intercrystalline pore spaces were developed indicating that precipitation postdated matrix dolomitization and vugular porosity generation (Figure 5.3 C-1287-2).

The Trenton in core C-1287 contains intraclasts from marine hardground surfaces that underwent telogenetic phosphatization (Figure 5.4). Mesogenetic grain selective dissolution was closely followed by planar subhedral dolomite cementation that frequently occluded the majority of moldic porosity. Stylolite generation followed moldic cementation marking the end of mesogenetic diagenesis. Faulting and fracturing initiated telogenetic diagenesis by allowing high pressure fluid migration that resulted in fine planar euhedral dolomitization. Megaquartz cementation occurred in voids within planar subhedral dolomite cements. During the late telogenetic stage penecontemporaneous fluorite and saddle dolomite cements precipitated within remaining moldic pore spaces and along pyritized and phosphatized stylolite surfaces.

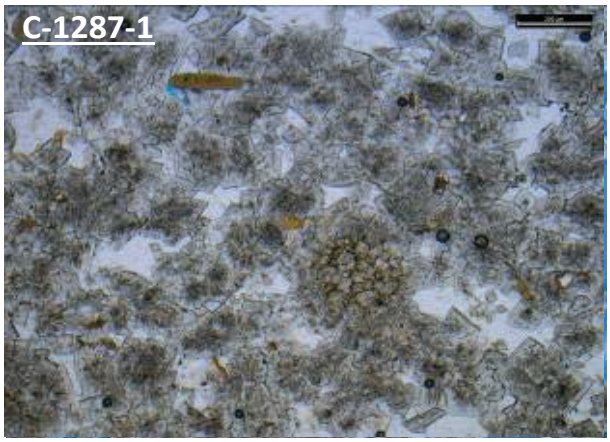

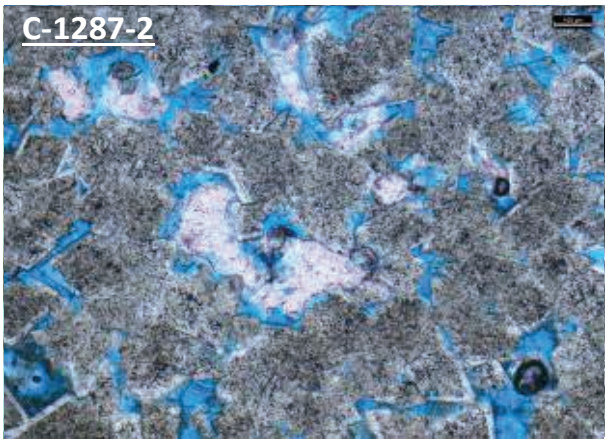

Figure 5.3 Secondary fabrics displaying pervasive mineralization of the host carbonates. (C-1287-1) Three distinct stages of mineralization; moldic dolomite cementation, non-mimetic matrix dolomitization, and late stage porosity-destructive quartz cementation can be observed through the section. (C-1287-2) A view displaying very cloudy equant dolomite that produces intercrystalline porosity with late stage fluorite cements within open pore spaces. Note the high relief of fluorite and the abundance of fluid inclusions relative to the matrix dolomites that display very precise mineral zoning.

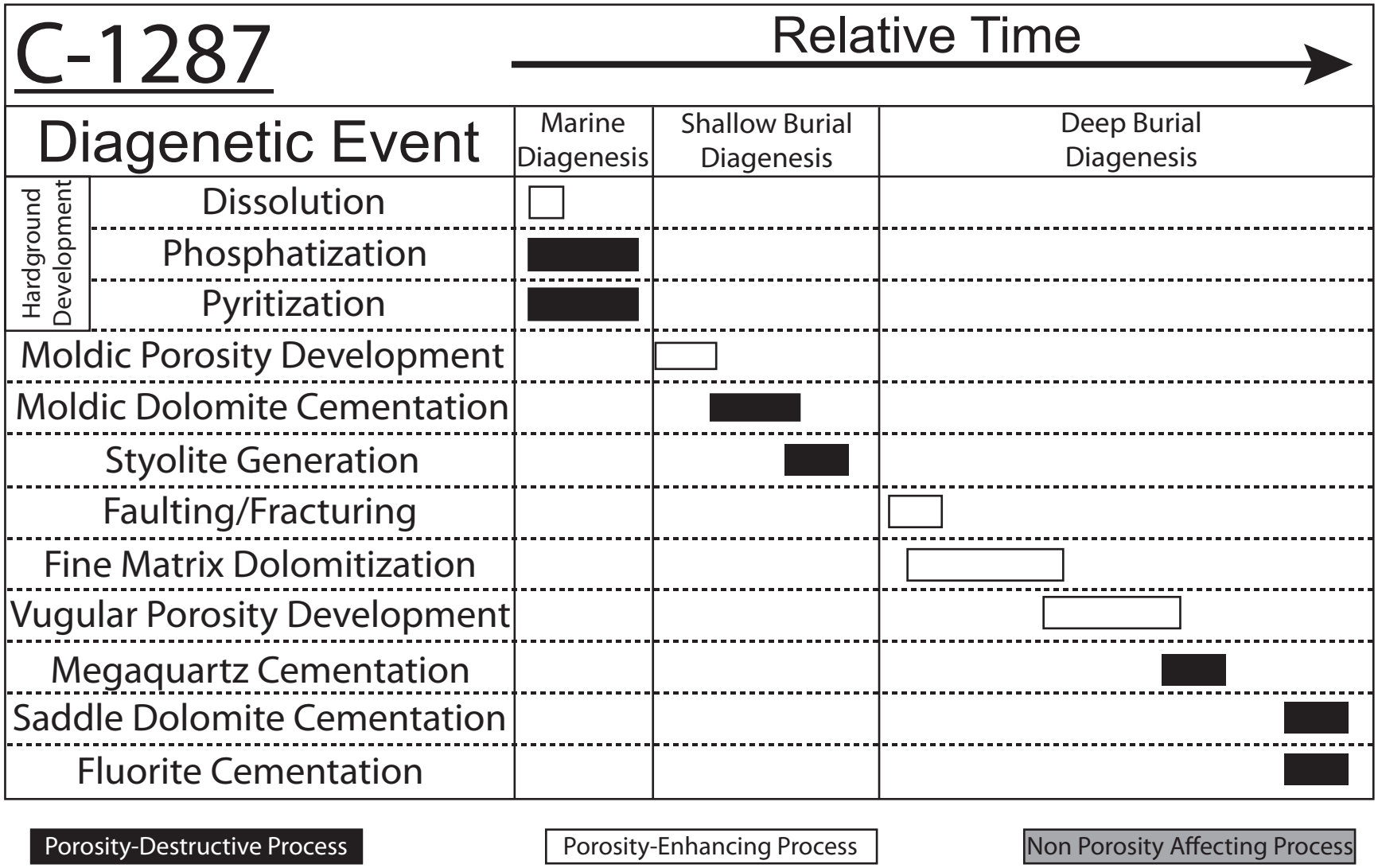

Figure 5.4 Paragenetic sequences observed in core C-1287.

5.2 NORTHERN CORES

Samples from core C-106 consist of primary fabrics that contain allochems including phosphatized echinoid plates, bryozoans, trilobites, crinoids, and brachiopods that correlate to Pope and Read's (1997) moderate energy deep ramp facies of the Millersburg member (Figure 5.5). Samples contain large fluorite and dolomite-healed fractures, however significant matrix porosity development was not observed.

Samples C-106-1 and C-106-2 are characterized by an abundance of trilobites, brachiopods, bryozoans, and echinoids that are frequently replaced by cryptocrystalline phosphate and fibrous chalcedony within a matrix of up to 10% micrite. Stylolite surfaces are frequent through both C-106-1 and C-106-2, which frequently contain limited amounts of coarsely crystalline fluorite and phosphate along the bottom of the dissolution surface. Poikilotopic calcite is highly twinned and forms where allochems are absent while minor intercrystalline porosity within the cloudy nonplanar calcite spar hosts minor amounts of ferrous calcite and fluorite. Calcite-healed microfractures offset ferrous calcite and fluorite cements while one large fracture (Stage II) is healed with finely crystalline dolomite, saddle dolomite, and coarsely crystalline fluorite progressing towards the center of the fracture (Figure 5.6 C-106-2a, C-106-2b). Saddle dolomites exhibit well-developed sweeping extinction and fluorite is isotropic under cross polarization.

The Trenton in core C-106 underwent rapid mesogenetic burial where shallow marine phosphatization of echinoids and brachiopods occurred. Mesogenetic shallow burial environments induced generation of styolite surfaces while matrix neomorphism occurred (Figure 5.7). During the waning stages of neomorphism, grain-selective chert replaced many echinoid plates. Mesogenetic stage I fractures induced minor dissolution resulting in intercrystalline porosity development, which was followed by iron-rich connate brine migration leading to precipitation of ferrous calciteand fluorite that occluded much of the resultant intercrystalline porosity. Stage II fracture development induced matrix dolomitization along the fracture margin, which graded into saddle dolomite and coarsely crystalline fluorite cements.

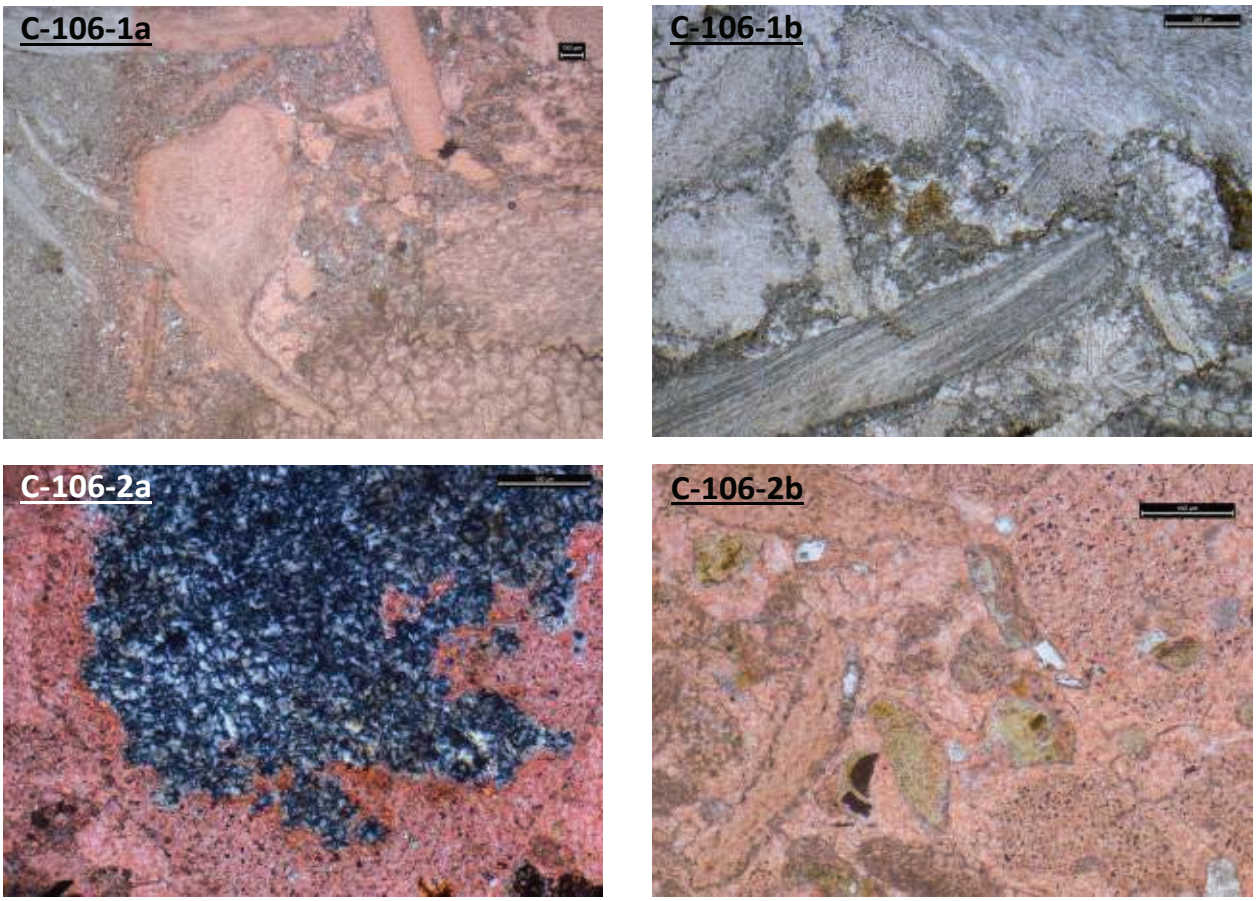

Figure 5.5 Photomicrographs of primary Millersburg fabrics that were deposited in a moderate energy deep ramp environment. (C-106-1a) Brachiopod, bryozoan, and trilobite allochems within a calcite microspar matrix that neomorphosed from primary micrite. (C-106-1b) Minor phosphatization of echinoid plates along a microfracture. (C-106-2a) Grain-selective chert replacement of a large echinoid plate exhibiting nucleation near the center of the echinoid progressing towards the outer edges. (C-106-2b) Phosphatized echinoids supplied from storm reworking from a deep ramp, phosphate-rich environment. Intraclasts commonly exhibit unit extinction and frequently occur with minor pyritization.

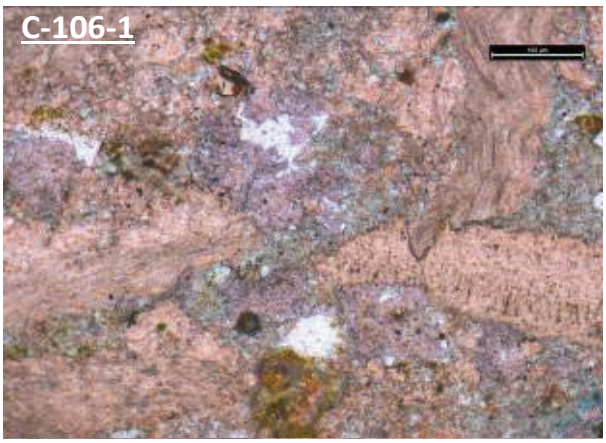

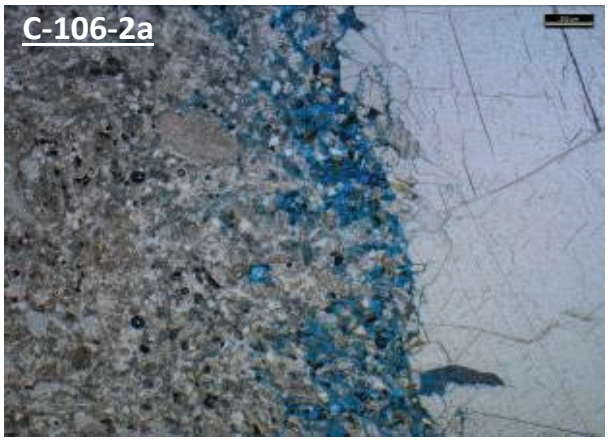

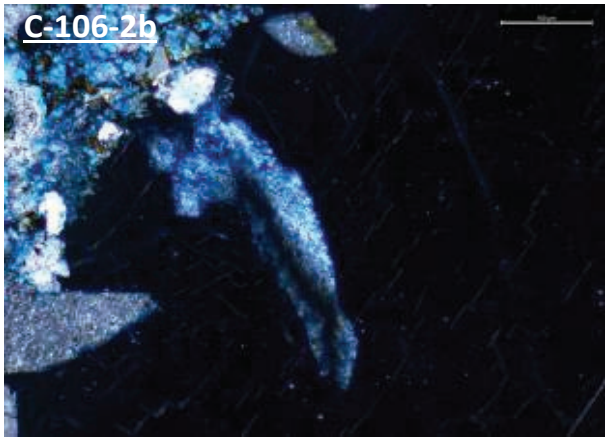

Figure 5.6 Photomicrographs illustrating paragenetic stages related to secondary mineralization that was induced by fluid migration along conjugate fractures. (C-106-1) Ferrous calcite and fluorite (Stage I) precipitation through intercrystalline porosity that marks the beginning of mesogenetic diagenesis. (C-106-2a) Intercrystalline porosity development along the margin of the fluorite-healed Stage II fracture. Coarse planar fluorite (Stage II) along the right side of the image is distinguishable from Stage I fluorite based upon crystal habit and fluid inclusion occurrence. (C-106-2b) Hydrothermal dolomite displaying sweeping extinction while Stage II fluorite exhibits isotropic extinction under cross-polarization.

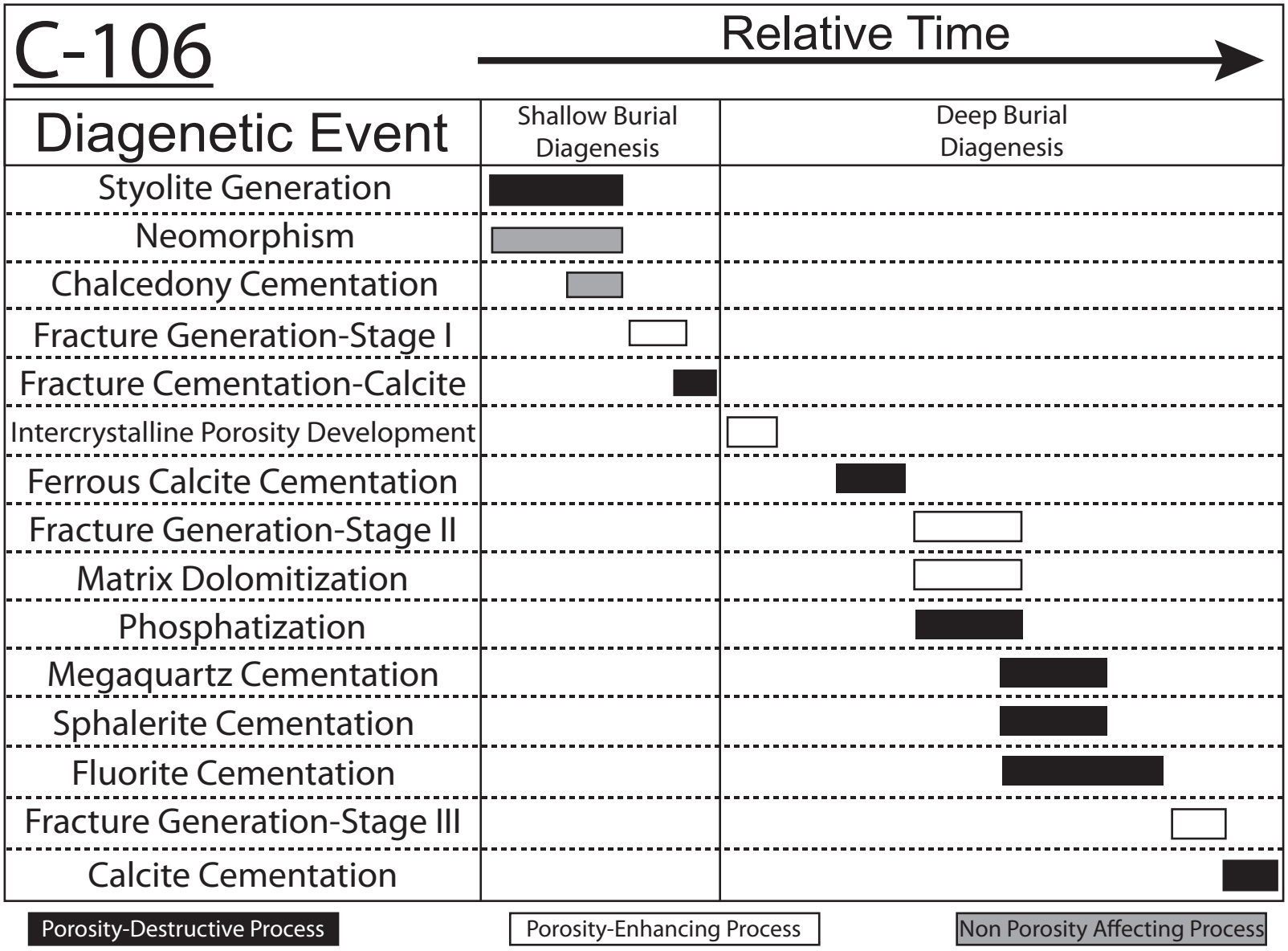

Figure 5.7 Paragenetic sequences observed in core C-106.

Sample C-200-3 is a peloidal grainstone from the Black River Group that contains abundant sponge spicules, ostracodes, bivalves, brachiopods, and peloids within a highly micritic matrix. Horizontal layering and minor geopetal fabrics (Figure 5.8 C-200-3) can be observed beneath brachiopod and bivalve fragments. Low biodiversity and the abundance of micrite is indicative of deposition in a low-energy subtidal or lagoon environment with normal to slightly saline waters while the lack of compaction structures suggests that rapid cementation in the marine phreatic realm occurred prior to deep burial (Scholle and Ulmer-Scholle, 2003). Sample C-200-2 is an echinoid wackestone of the Grier Member of the Trenton that contains echinoid plates, ostracodes, brachiopods, bryozoans, trilobites, and abundant intraclasts of phosphatized bryozoans, echinoids, and ostracodes (Figure 5.8). Sample C-200-1 contains similar grain types as in sample C-200-2, however it also exhibits more abundant geopetal and burrowed fabrics suggesting that the substrate contained more micritic mud during deposition (Figure 5.8 C-200-1a, C-200-1b). Deposition occurred in a low energy mid ramp environment where intraclast reworking during storm events occurred (Pope and Read, 1997).

Samples C-200-1 and C-200-2 both contain abundant quantities of micrite that has been neomorphosed into microspar during shallow burial. Early fracture generation (Stage I) led to fluid dissolution and vugular porosity development within geopetal fabrics. Deep burial environments allowed for magnesium-rich brine migration that led to minor hydrothermal dolomitization of the neomorphosed micritic matrix (Figure 5.9 C-200-2a). The dolomitic matrix generally contains well developed rhombic crystals that under close examination exhibit sweeping extinction (Figure 5.9 C-200-1). Phosphate was also supplied through deep burial fluids, which precipitated near fracture-matrix margins. Late-stage poikilotopic ferrous calcite vug fill is observed on the upper half of some geopetal fabrics (Figure 5.9 C-200-2b). Sample C-200-3 (Black River Group) displays minor dolomitization that parallels the margin of an open late stage fracture however pervasive (pressurized) fluid migration did not occur as a result of low primary porosity (Figure 5.9 C-200-3).

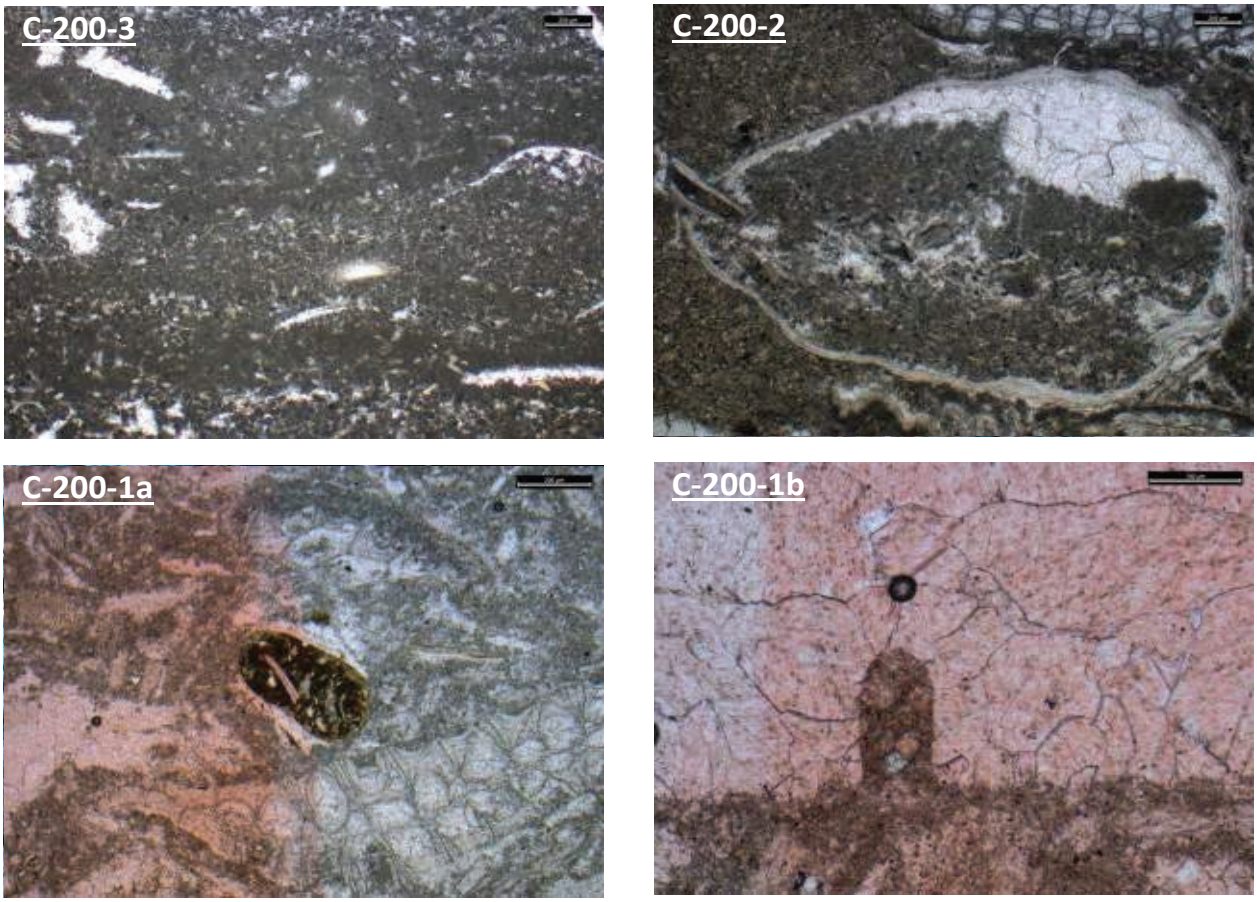

Figure 5.8 Photomicrographs of primary fabrics observed within C-200. (C-200-3) An unstained section of peloidal wackestone from the upper Black River formation that displays well-developed horizontal laminations indicating a lack of burrowing organisms and a low energy environment of deposition. (C-200-2) Geopetal fabric development within an articulated brachiopod. Nonplanar calcite cements heal the upper portion of the brachiopod while micrite and peloids encompass the lower section. (C-200-1a) A subrounded intraclast that contains fragments of ostracodes within a micritic matrix. Phosphatization is observed along the outer edge of the intraclast that likely resulted from phosphate-rich cool-water upwelling during storm events. (C-200-1b) A view of a microspar-filled bore into a large neomorphosed brachiopod. Coarse nonplanar calcite spar fills the interior of the brachiopod shell.

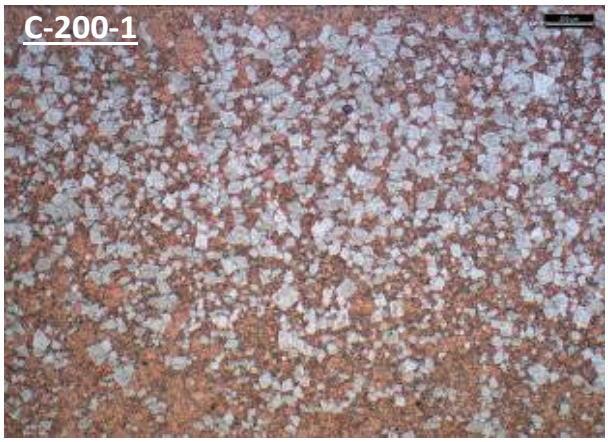

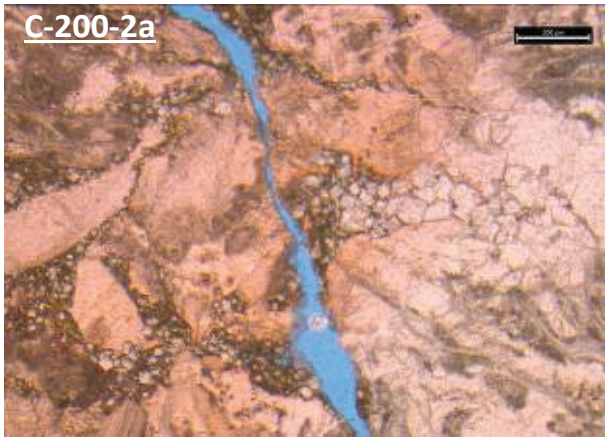

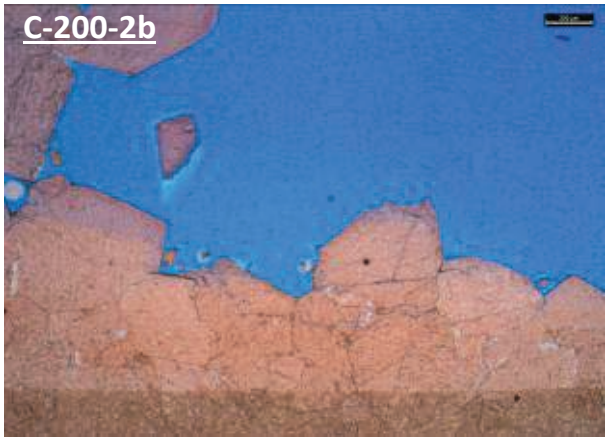

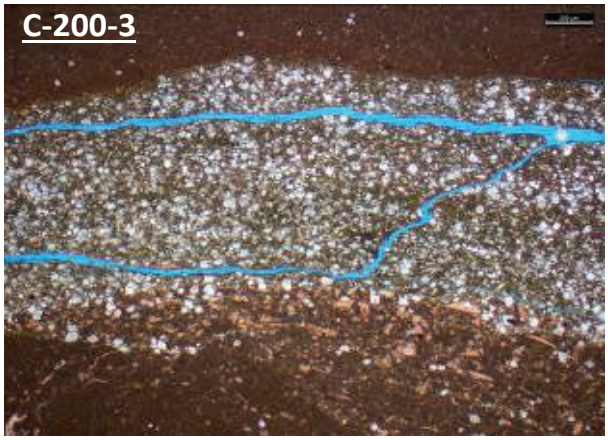

Figure 5.9 Photomicrographs illustrating diagenetic fabrics that characterize C-200. (C-200-1) Planar and subplanar dolomite dispersed through microspar that neomorphosed from micrite during early burial. (C-200-2a) Dolomitization extending away from late stage fractures. The lack of primary porosity appears to have limited fluid migration to induce significant matrix dolomitization. (C-200-2b) Late stage ferrous calcite cements extending into vugular porosity that developed within a geopetal fabric. Note the transition from clear subplanar calcite to very cloudy microspar at the base of the image, which marks the transition into a microsparry matrix with 0% porosity on the bottom half of the brachiopod. (C-200-3) Hydrothermal dolomitization along the margin of an open fracture within a low-porosity peloidal packstone from the Upper Black River.

Core C-200 experienced mesogenetic alteration in the form of stylolite generation and neomorphism of depositional cements (Figure 5.10). Fracture generation led to vugular porosity development through connate fluid dissolution. Magnesium and phosphate-rich fluid migration through open fractures allowed for matrix dolomitization in decreasing quantities away from fracture planes. Phosphate precipitation occurred along the margin of fracture planes causing a net decrease in porosity prior to final stage ferrous calcite cementation. Ferrous poikilotopic calcite cements are highly twinned and precipitate within open vugular pore spaces.

Sample C-201-2 consists of an echinoid wackestone deposited at the top of the Black River Group carbonates. Allochems such as stromatolites and extensive micritization indicate that deposition may have been in a slightly saline low energy environment such as a back barrier or lagoonal setting (Figure 5.11 C-201-2). Above the Mud Cave K-bentonite, sample C-201-3 of the Curdsville Limestone Member exhibits increased biodiversity and a complete lack of micrite within the matrix indicate deposition occurred in a high energy environment (Scholle and Ulmer-Scholle, 2003). Deposition was in a high energy mid-ramp open marine setting (Pope and Read, 1997) where well-cemented substrates developed as a result of early marine phreatic cementation. Primary porosity was largely occluded as a result of the rapid cementation following deposition in the high energy environment. Sample C-201-1 is yet another echinoid packstone; however this sample correlates to Pope and Read's (1997) high energy mid ramp facies of the Millersburg Member, which exhibits increased fine-grained siliciclastic influx resulting in increased micrite and geopetal fabric development. Phosphatization of echinoid plates and bryozoan zooecia resulted from an abundance of phosphate upwelling onto the Lexington platform (Figure 5.11 C-201-1).

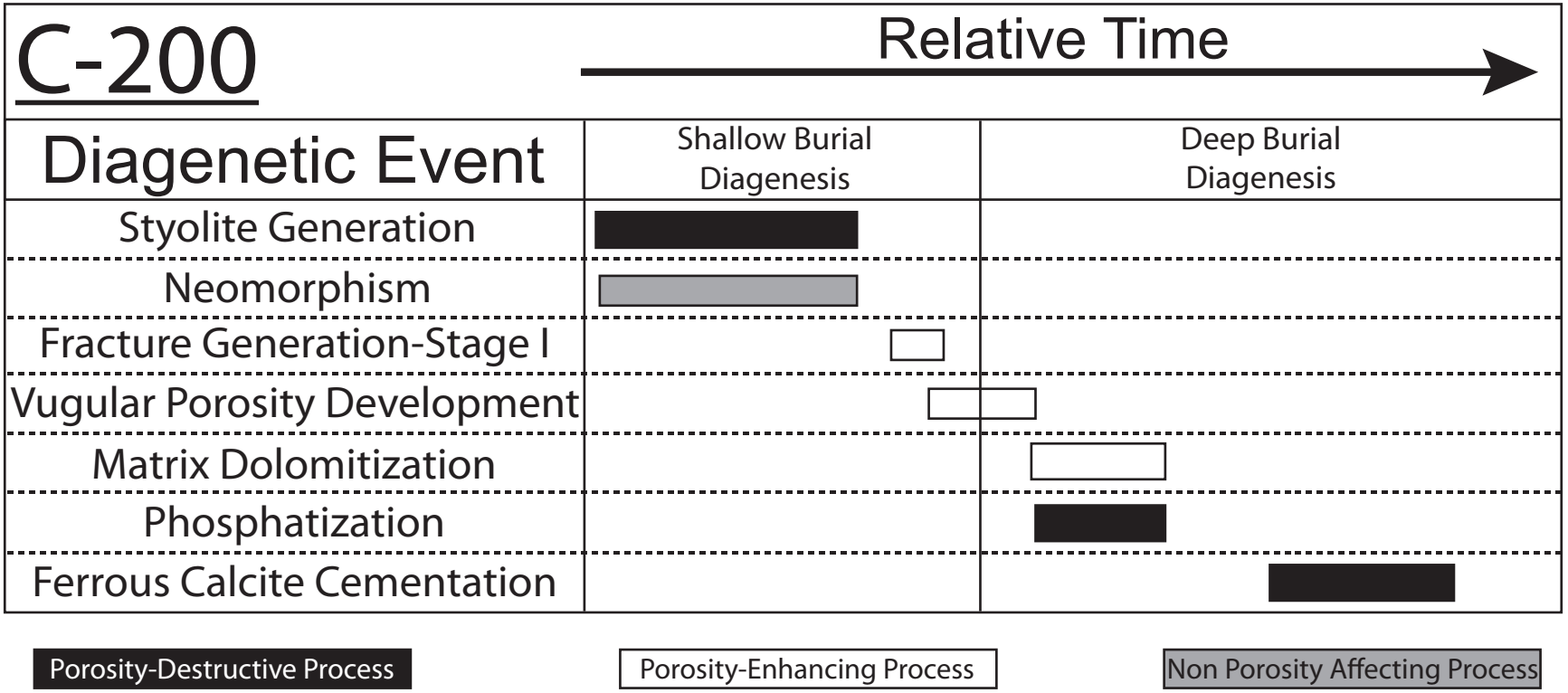

Figure 5.10 Paragenetic sequences observed in core C-200.

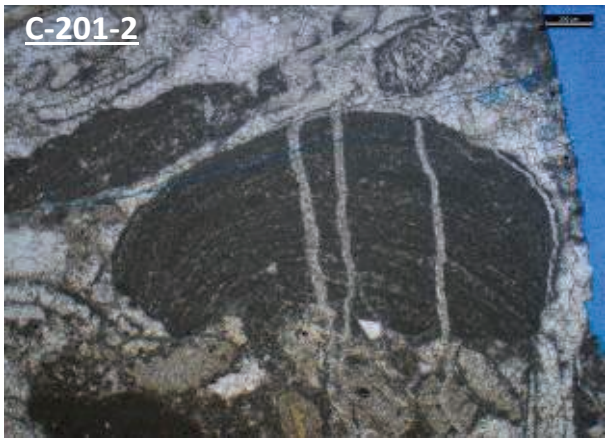

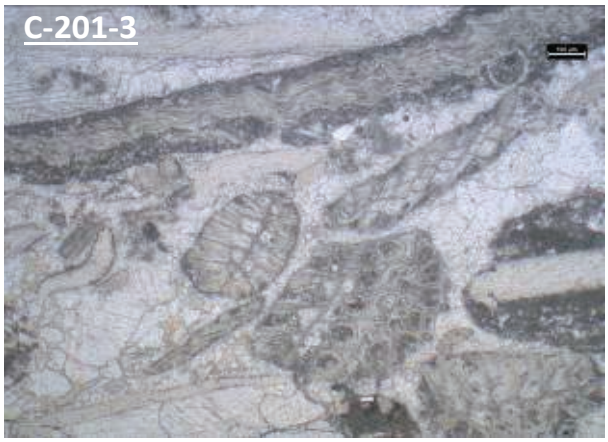

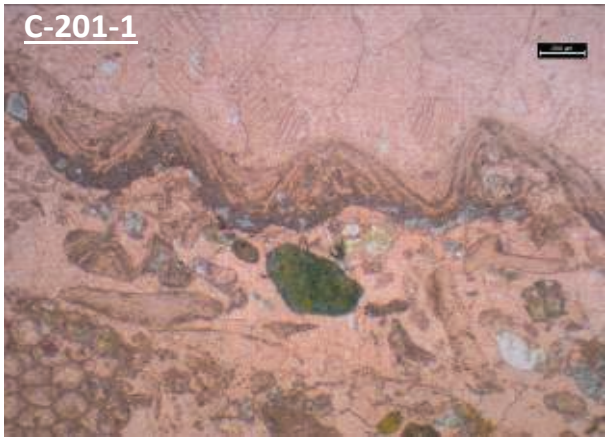

Figure 5.11 Photomicrographs of primary allochems and eogenetic alterations that affected deposition. (C-201-2) A stromatolite that contains well-developed layers of micrite and microspar indicating subtidal to intertidal deposition. (C-201-3) A micritized brachiopod stretches across the upper section of the photomicrograph while fragments of bryozoans exhibit minor amounts of micritization. The lack of phosphate within bryozoan zooecia indicates that deposition likely occurred in a shallow marine environment where phosphate upwelling did not have a significant effect on eogenetic alteration. (C-201-1) A brachiopod shell exhibits minor micritization and equant dolomitization. Underlying the brachiopod is a subrounded intraclast of a phosphatized echinoid plate that was deposited during a high-energy storm event that reworked allochems from a deep ramp environment.

Core C-201 is characterized by early moldic dolomite cements within a neomorphosed calcite matrix (Figure 5.12 C-201-1a). Many brachiopods and echinoids were preferentially replaced by fibrous chalcedony upon deep burial (Figure 5.12 C-201-1c). One significant fracture intersects the core that allowed for matrix dolomitization laterally away from the fracture. Matrix dolomitization is associated with an increase in porosity that led to vugular development. Fluorite cements precipitated in remaining un-dolomitized moldic pore spaces (Figure 5.12 C-201-1b). Bladed barite and coarsely crystalline dolomite crystal precipitation occurred in open vugs and fractures, both of which display undulose/sweeping extinction under cross polarization and occasionally occur as crystal rosettes (Figure 5.12 C-201-2a, C-201-2b). Late diagenetic precipitates of poikilotopic ferrous calcite and sphalerite generally occur in association with each other and are observed in open vugular, moldic, or fracture porosity (Figure 5.12 C-201-3).

Eogenetic hardground development in core C-201 resulted in phosphatized echinoids and bryozoans that contain minor amounts of pyrite (Figure 5.13). Low amplitude styolite development resulted from a lack of early marine cementation and rapid burial, which predated grain-selective dissolution and moldic porosity development. Planar subhedral dolomite cementation in moldic pore spaces occluded all of the mesogenetic porosity. Neomorphism during telogenetic burial led to subhedral calcite cementation and induced grain-selective chalcedony replacement within echinoid plates and brachiopod shells. Telogenetic fracturing induced hydrothermal brine migration that allowed for matrix dolomitization and subsequent vugular porosity generation. Fluorite cementation occurred within intercrystalline porosity and synchronous bladed barite and saddle dolomite precipitation occurred within vugular porosity. Late telogenetic mineralization is marked by ferrous calcite cementation and finally late stage sphalerite and megaquartz cements that occluded much of the remaining vugular and intercrystalline porosity.

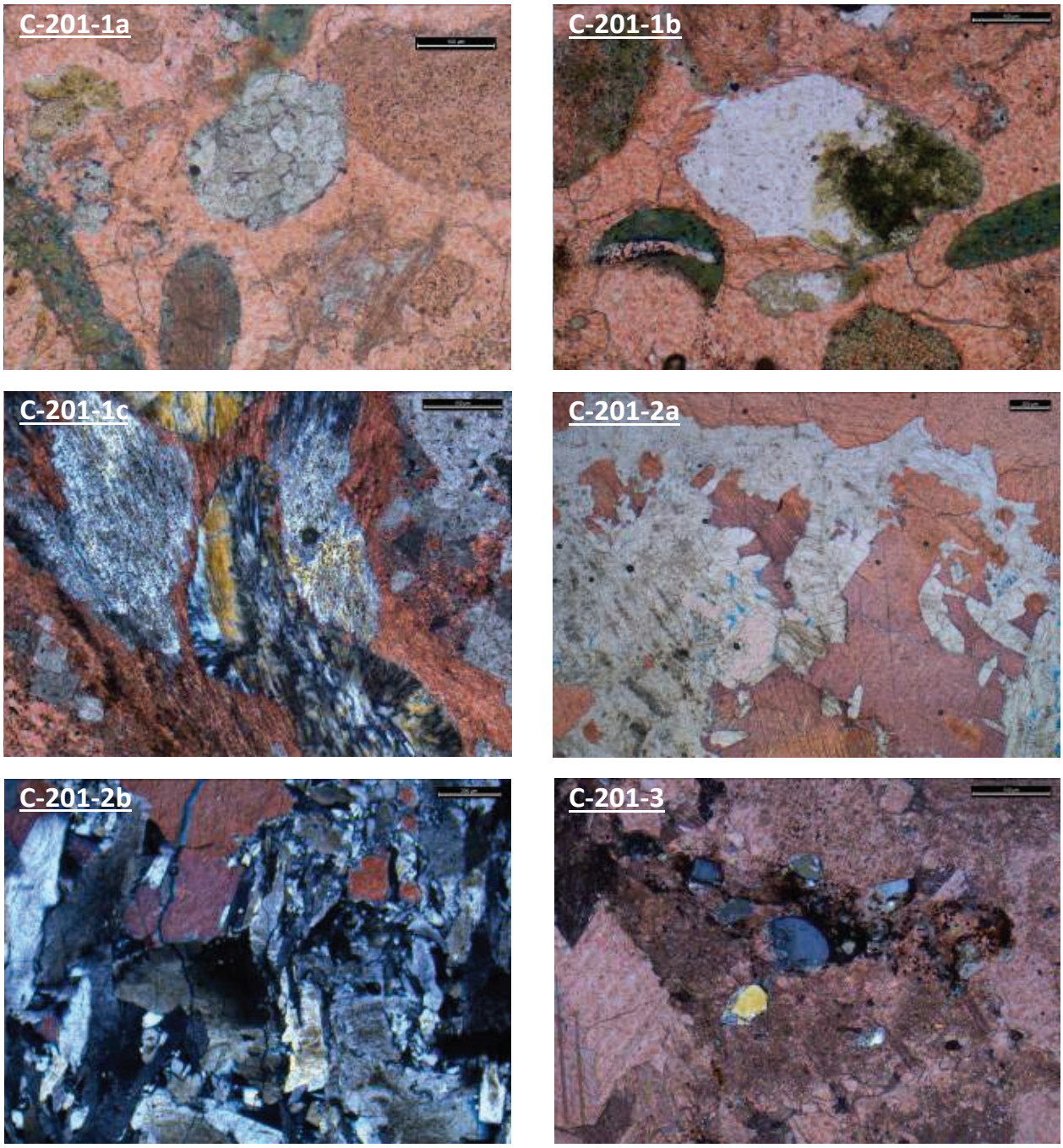

Figure 5.12 Photomicrographs illustrating diagenetic fabrics and paragenetic relationships through C-201. (C-201-1a) Moldic dolomite cements that developed in a shallow burial environment that exhibit subplanar to nonplanar crystal habit resulting in complete moldic porosity occlusion. (C-201-1b) Fluorite (unstained crystal) precipitation within open moldic pores. Phosphate is present on the right side of the fluorite cement and phosphate is also present within echinoid that surround the fluorite cement. (C-201-1c) A cross-polarization view of chalcedony replacement within a brachiopod fragment. (C-201-2a) Bladed barite has a cloudy appearance in plain transmitted light and precipitation was synchronous with coarse dolomite cements. Finally, late stage ferrous calcite occludes much of the remaining porosity surrounding

barite and dolomite cements. (C-201-2b) A view of bladed barite, dolomite, ferrous calcite, and fluorite under cross polarization. Barite blades display undulatory extinction while dolomite crystals display well developed sweeping extinction and fluorite remains isotropic. (C-201-3) Minor amounts of quartz and sphalerite precipitation within a neomorphosed microsparry matrix. Sphalerite has a dull yellow appearance under cross polarization.

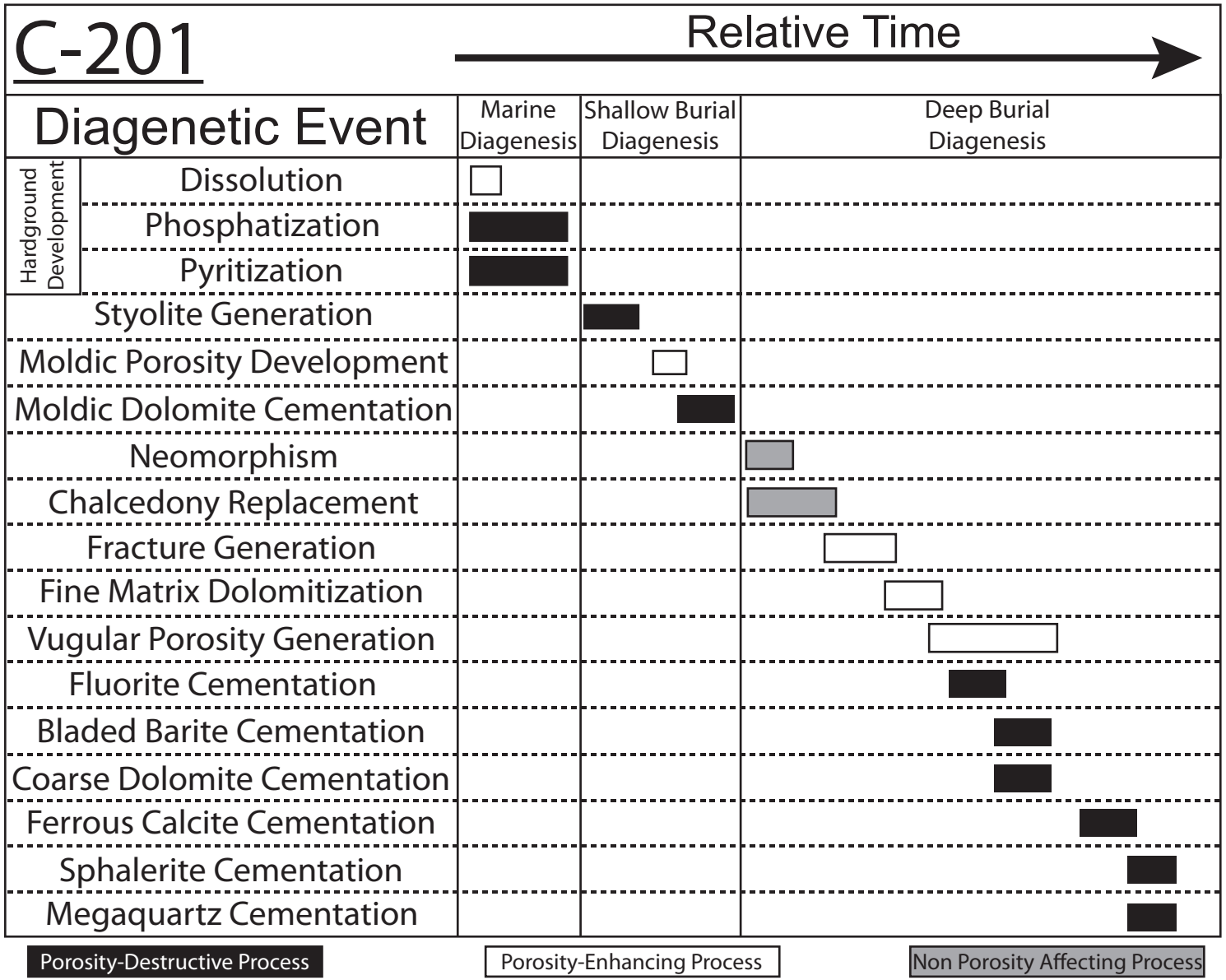

Figure 5.13 Paragenetic sequences observed in core C-201.

5.3 SOUTHERN CORES

Core C-295 begins with samples C-295-6 and C-295-5 from the basal Curdsville Member of the Trenton, which are highly neomorphosed and underwent early marine phreatic cementation in a high energy environment. The high wave energy associated with the Curdsville resulted in robust stromatoporoids that developed on hard rocky substrates (Figure 5.14 C-295-5; Pope and Read, 1997). In the overlying Grier Member (sample C-295-4) decreased wave energy resulted in a lack of encrusting stromatoporoid development and deposition of echinoids, ostracodes, gastropods, brachiopods, peloids, and intraclasts predominated (Figure 5.14 C-295-4). Deposition was likely in a low energy, normal marine mid-ramp environment within the storm wave base (Pope and Read, 1997). Sample C-295-2 contains echinoid, ostracode, brachiopod, and gastropod allochems and extraclasts of trilobite and bryozoan fragments within a micritic matrix. Deposition was in a restricted lagoon setting (Pope and Read, 1997), which characterizes the Salvisa Bed of the Perryville Limestone Member. Stylolites are present through sample C-295-2 indicating that cementation likely occurred in the meteoric phreatic or burial connate environment, which may have controlled porosity development as stylolites have a significant control over dolomitization and secondary porosity development. Extraclast deposition occurred during high energy storm events where deep ramp allochems were reworked into the back-barrier lagoon setting. Sample C-295-1 is dominated by trilobites and bryozoans and lacks a micritic matrix suggesting that deposition was between storm and normal wavebase on a hard substrate of the Millersburg Member (Figure 5.14 C-295-1). Early marine phreatic cementation is common through the Millersburg, which frequently results in a lack of horizontal laminations and stylolite surfaces.

Core C-295 underwent early burial neomorphism that led to recrystallization of the matrix into cloudy nonplanar calcite spar. During neomorphism silica sourced from solution precipitated in voids and replaced occasional echinoid plates with early fibrous chalcedony that grades into microcrystalline silica (chert) away from the origin of cementation (Figure 5.15 C-295-5, C-295-4). One fracture event allowed for fluid dissolution and vugular porosity

development. Fine equant isotropic dolomite rhombs and minor phosphate cements are observed at the vug-matrix margin that are generally more pronounced and matrix-invading stratigraphically below vugular pore spaces. Dolomitization results in an increase in matrix porosity, however much of the developed intercrystalline porosity is occluded by phosphate cements. Coarsely crystalline calcite cementation is the next vug-lining and fracture-lining cement that tends to exhibit crystal twins (caused by high temperature precipitation) and grades into ferrous poikilotopic calcite with twinned crystal faces (Figure 5.15 C-295-1a). Saddle dolomite cementation is penecontemporaneous with minor fluorite cementation that can be observed in contact with the ferrous calcite cements near the center of vugs (Figure 5.15 C-295-2a, C-295-1b). The coarsely crystalline saddle dolomites have a cloudy appearance and subtle curved growth rings can be observed through individual crystals that have sweeping extinction while isotropic fluorite appears clear under plain light and contains abundant fluid inclusions that have very high liquid-to-vapor ratios. Bladed barite occurs in very minor volumes in the center of vugular pore spaces (Figure 5.15 C-295-2b). Barite crystals have a clear-cloudy appearance and they form into one globular mass making blade distinctions difficult without the use of cross-polarization.

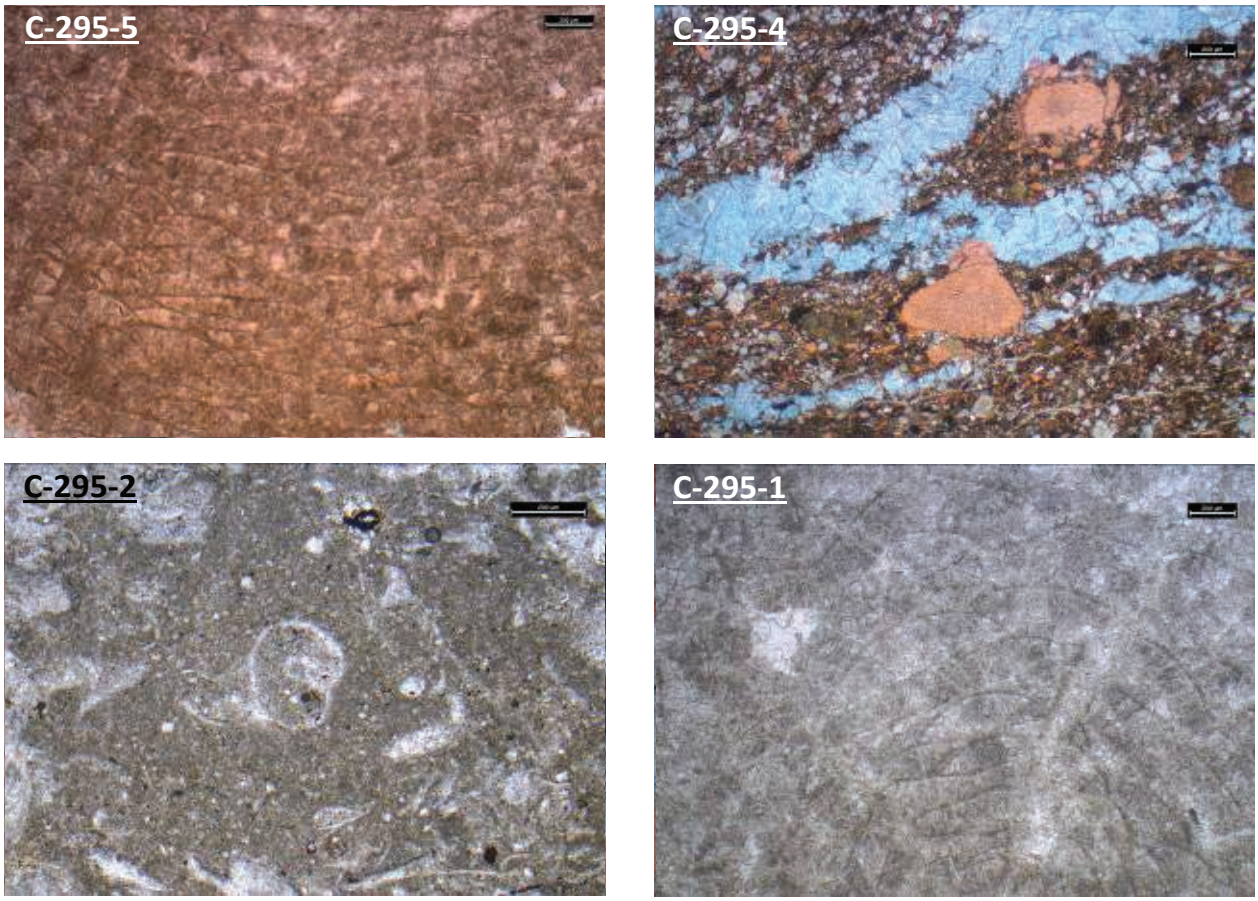

Figure 5.14 Photomicrographs of primary and neomorphosed primary fabrics within the Curdsville, Grier, Perryville Limestone and Millersburg Members. (C-295-5) A neomorphosed matrix resulted in ghost textures of a stromatoporoid with abundant peloids filling galleries. (C-295-4) Large echinoid plates within a matrix of predominantly ostracodes and peloids. Significant matrix dolomitization, matrix pyritization, and phosphatization have destroyed a significant proportion of the primary fabrics. (C-295-2) A small gastropod located in an unstained section from the Salvisa Bed of the Perryville Limestone Member that is embedded within a neomorphosed micritic matrix. (C-295-1) Ghost textures of a stromatoporoid in an unstained section from the Millersburg Member.

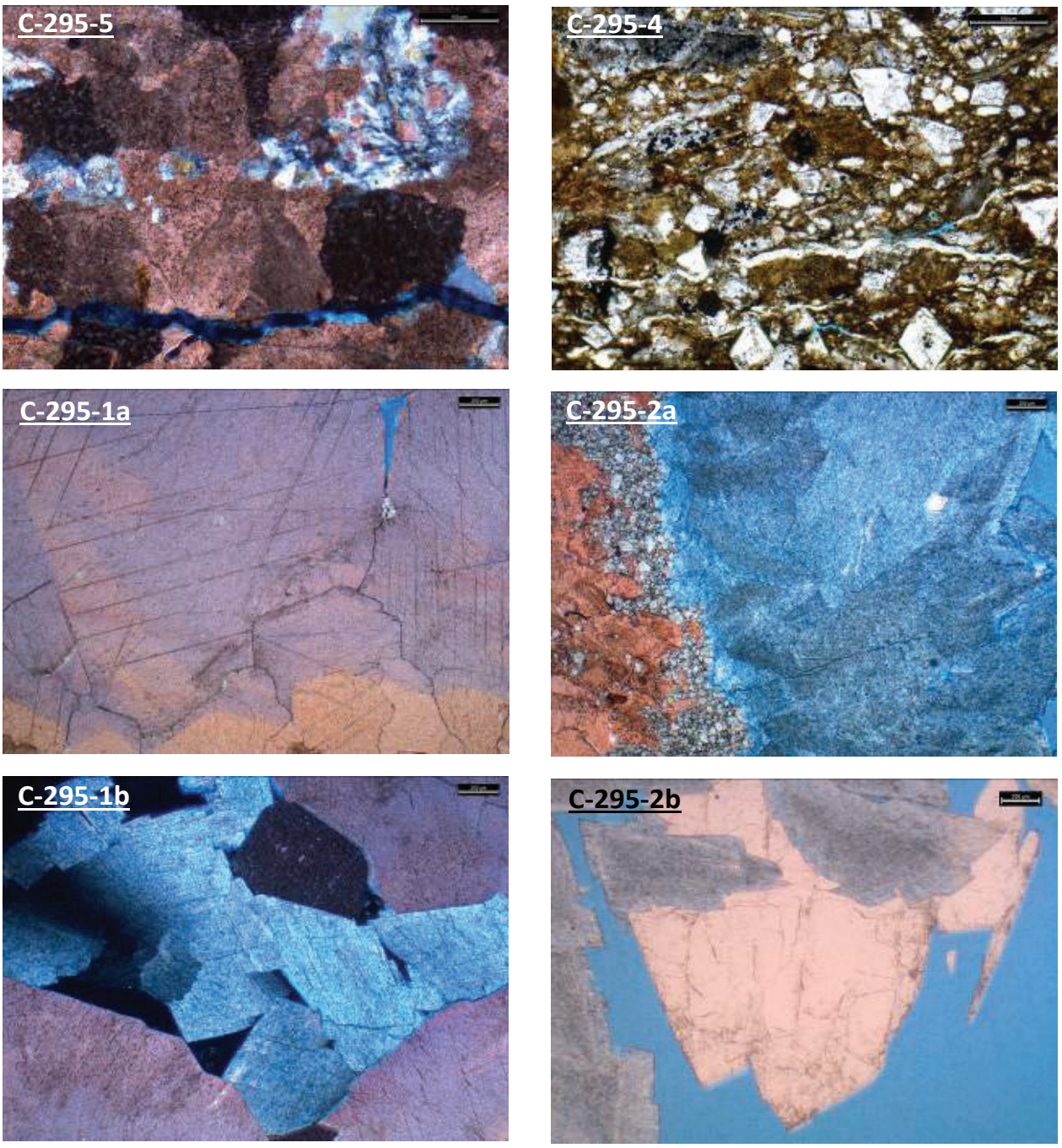

Figure 5.15 Photomicrographs demonstrating paragenetic stages of diagenesis through C-295. (C-295-5) Chalcedony replacement within an echinoid fragment. (C-295-4) Megaquartz cementation through microfractures within a highly phosphatized and dolomitized peloidal wackestone. (C-295-1a) Ferrous calcite with poikilotopic and twinned crystal habit located along the margin of matrix calcite and vugular pore spaces. (C-295-2a) Gradational variations in dolomitization transitioning from a neomorphosed matrix to a finely dolomitized matrix and then into coarse saddle dolomite cements. Saddle dolomite precipitation is synchronous with minor amounts of fluorite cements. (C-295-1b) Coarse saddle dolomite displaying sweeping extinction under cross polarization. Dolomites appear to have nucleatred on ferrous calcite crystal faces.

Core C-295 contains minor stylolite surfaces that have rather low amplitudes and are frequently highly pyritized, which developed as a result of rapid burial prior to cementation (Figure 5.16). Shallow burial was associated with matrix neomorphism that was synchronous with chalcedony cementation and replacement. Chalcedony cements predated microcrystalline quartz (chert) cementation, which was the concluding stage for shallow burial diagenesis. Deep burial was marked by fracture generation that initiated hydrothermal fluid flow that caused calcite dissolution resulting in vugular and intercrystalline porosity. Equant matrix dolomitization occurred during the final stages of dissolution and porosity development, which was simultaneous with phosphate cementation. Calcite fracture and vugular cementation followed, which graded into ferrous calcite with increasing time. Precipitation of calcite cements from hydrothermal fluids is evident due to the poikilotopic and highly twinned crystal habit. Saddle dolomite cements postdated calcite cements but was coeval with a brief period of fluorite cementation. Barite occurs as a late stage diagenetic precipitate marking the final stages of hydrothermal fluid alteration.

Sample C-511-5 is an ostracode wackestone of the Grier Limestone Member that contains ostracodes, echinoids, brachiopods, sponge spicules, peloids, and bryozoans within a matrix of micrite that neomorphosed into microspar (Figure 5.17 C-511-5). Deposition occurred on a low energy shallow shelf with a soft substrate that allowed for organisms to burrow into the sediment destroying bedding surfaces. Sample C-511-4 is a peloidal wackestone of the Faucloner Bed from the Perryville Limestone Member (Figure 5.17 C-511-4). Deposition within a restricted lagoon setting led to an abundance of gastropod and ostracode fauna through the section. Peloids and allochem micritization resulted in an abundance of micrite that underwent meteoric phreatic cementation. The post-depositional cementation led to the development of numerous stylolites through the section, which frequently show signs of oxidation and have been highly pyritized. Sample C-511-3 is an echinoid packstone of the Sulfur Well Member. Deposition in a high energy shallow shelf environment near normal wave base was conducive to

numerous niche spaces that resulted in a highly diverse fauna assemblage of echinoids, ostracodes, gastropods, brachiopods, crinoids, bryozoans, and trilobites (Figure 5.17 C-511-3). Minor micritization of grains is observed, however the high energy reworking and constant wave action limited complete micritization. The substrate was likely a well consolidated micrite that was stable enough to allow for crinoid and bryozoan anchoring and cementation occurred in the marine phreatic realm. C-511-2 is a stromatoporoid wackestone of the Devils Hollow Member. Deposition in a restricted lagoon setting resulted in limited biodiversification as is evident within stromatoporoid galleries that frequently contain peloids and ostracodes (Figure 5.17 C-511-2).

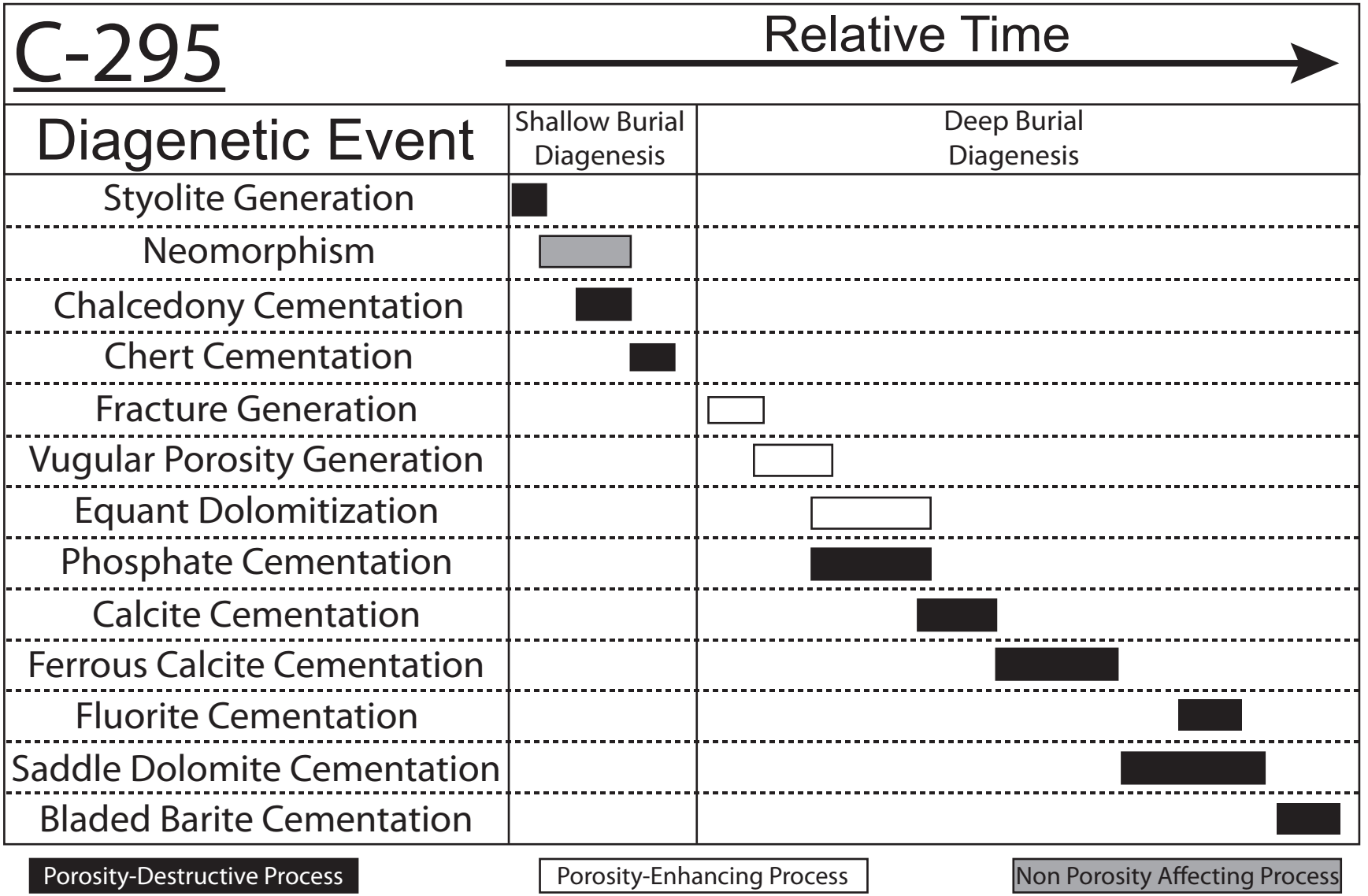

Figure 5.16 Paragenetic sequences observed in core C-295.

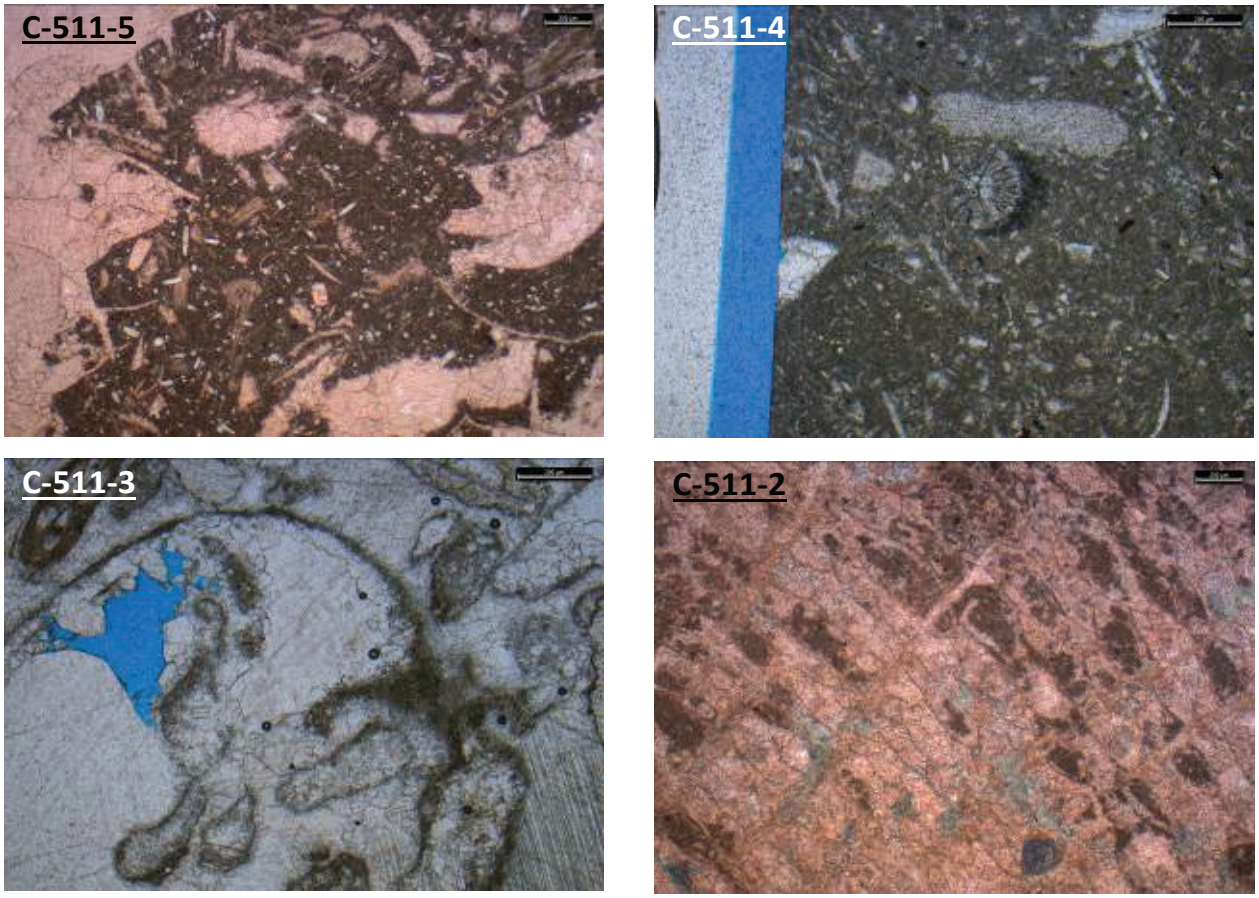

Figure 5.17 Photomicrographs illustrating primary fabrics that characterize the Grier, Perryville Limestone, Sulfur Well, and Millersburg Members of the Trenton. (C-511-5) An ostracode wackestone that contains ostracodes, sponge spicules, echinoids, brachiopods, bryozoans, and peloids within a micritic matrix. (C-511-4) Abundant sponge spicules, echinoids, ostracodes, and one bryozoan in the center of the unstained photograph hosted within a micritic matrix. The bryozoan has minor micritization forming in a pendant style that likely occurred just prior to deposition and cementation. (C-511-3) An unstained section with a neomorphosed gastropod that is filled with coarse nonplanar calcite. (C-511-2) A stained section of a peloid- encrusting stromatoporoid that has been highly neomorphosed resulting in cloudy nonplanar calcite cements as well as minor chalcedony replacement along the well-developed pillars and lamina.

The Trenton in core C-511 exhibits intense neomorphism resulting in numerous ghost textures of predominantly encrusting stromatoporoids. Neomorphism resulted in planar subhedral to nonplanar calcite cements through the majority of the matrix. During neomorphism, fibrous chalcedony cementation occurred within central portions of bryozoans and along the exterior margins of echinoid plates (Figure 5.18 C-511-3a). Near the center of chalcedony cementation extremely ferrous calcite microspar can be observed, which typically occludes any remaining porosity within the voids (Figure 5.18 C-511-2). Stage I fracturing led to moldic dissolution which created voids that are lined and partially healed by poikilotopic calcite that is highly twinned. Fluorite can also be observed healing some of the moldic pore spaces. Fluorite occurs as clear and cubic crystals that contain abundant fluid inclusions that are predominantly entirely aqueous (Figure 5.18 C-511-3b). Stage II fractures initiated hydrothermal matrix dolomitization, which consists of fine rhombic equant crystals that display sweeping extinction under close examination. Dolomitization is highly affected by stylolite surfaces, which frequently truncate vertical dolomitization (Figure 5.18 C-511-4). The associated mass balance resulted in intercrystalline and vugular porosity development. Lining vugs and remaining moldic and geopetal pore spaces is coarsely crystalline saddle dolomite that typically grades in zonation from very cloudy near the crystal nucleation sight to increasingly clear towards the interior of pore spaces (Figure 5.18 C-511-3c). The cloudy appearance of the zoned dolomites is the result of high fluid inclusion densities that commonly terminate in fir-tree patterns.

Core C-511 contains pyritized stylolite surfaces that were generated during shallow burial prior to cementation (Figure 5.19). Neomorphism of the matrix resulted in planar subhedral and nonplanar calcite cementation which was synchronous with fibrous chalcedony cementation. Chalcedony cementation grades into ferrous calcite cementation indicating that there was a transition in fluid composition (likely a decrease in silica content) towards the waning stages of mesogenetic diagenesis. Telogenetic alteration was initiated by Stage I fracturing that allowed

for moldic dissolution and porosity development that was closely followed by coarsely crystalline subhedral and poikilotopic calcite cementation. Fluorite cements are present within moldic pore spaces and Stage I fractures indicating that precipitation occurred prior to Stage II fracturing. Stage II fractures initiated magnesium-rich brine migration that led to matrix dolomitization and the associated vugular porosity development. The final stage of telogenetic alteration is evident in saddle dolomite crystal development along the margin of vugular pore spaces.

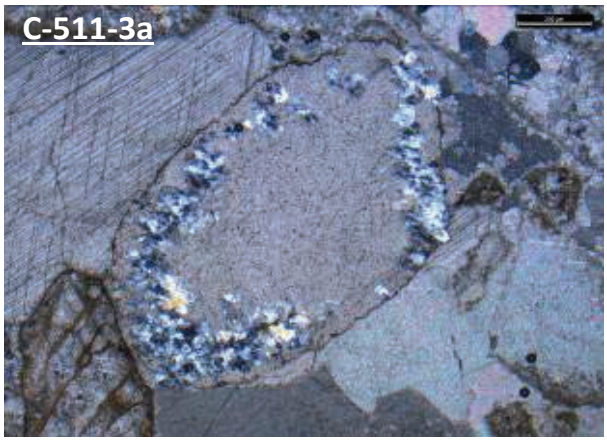

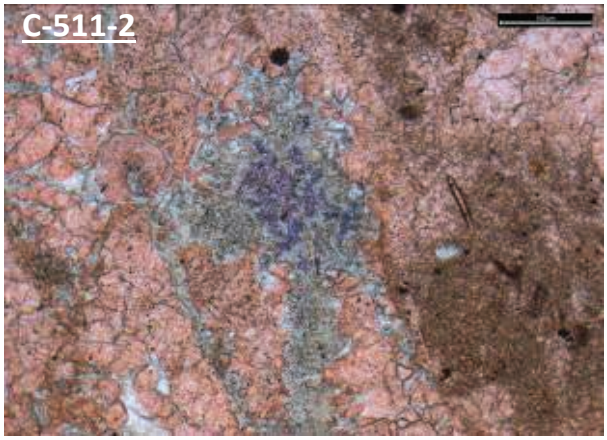

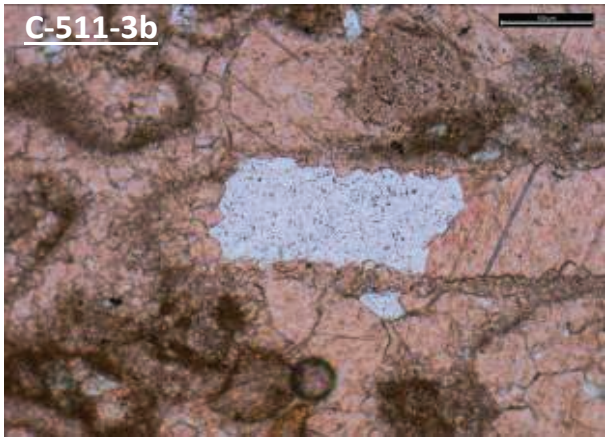

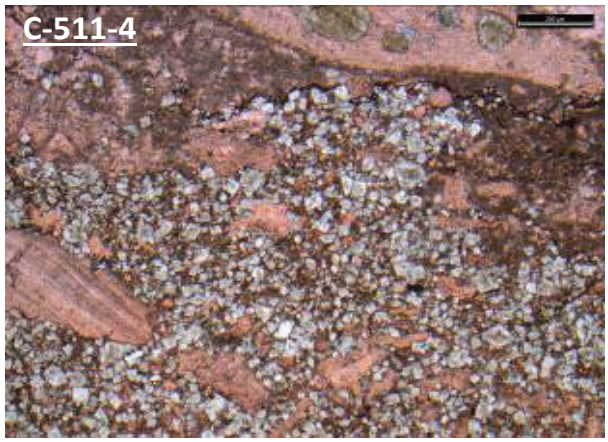

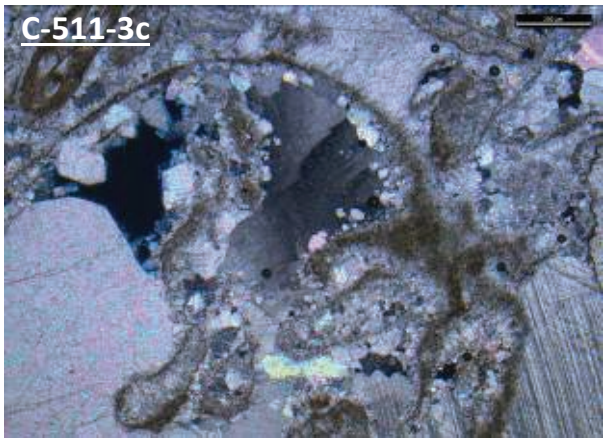

Figure 5.18 Photomicrographs from C-511 illustrating various stages of mineralization and post-depositional alteration. (C-511-3a) Chalcedony replacement along the outer margin of an echinoid plate. (C-511-2) Chalcedony cements grading into ferrous calcite near the center of intercrystalline porosity. (C-511-3b) Fluorite cements within intercrystalline porosity of a neomorphosed allochems. The fluorite is dominated by highly aqueous fluid inclusions. (C-511-4) Matrix dolomitization resulting in fine equant crystal development throughout a microsparry matrix. Stylolite surfaces near the top of the figure truncate dolomitization from migrating vertically past the stylolite. (C-511-3c) Coarse dolomite cement within a geopetal fabric that was developed within a gastropod. The dolomite exhibits sweeping extinction under cross

polarization indicating precipitation from hydrothermal fluids.

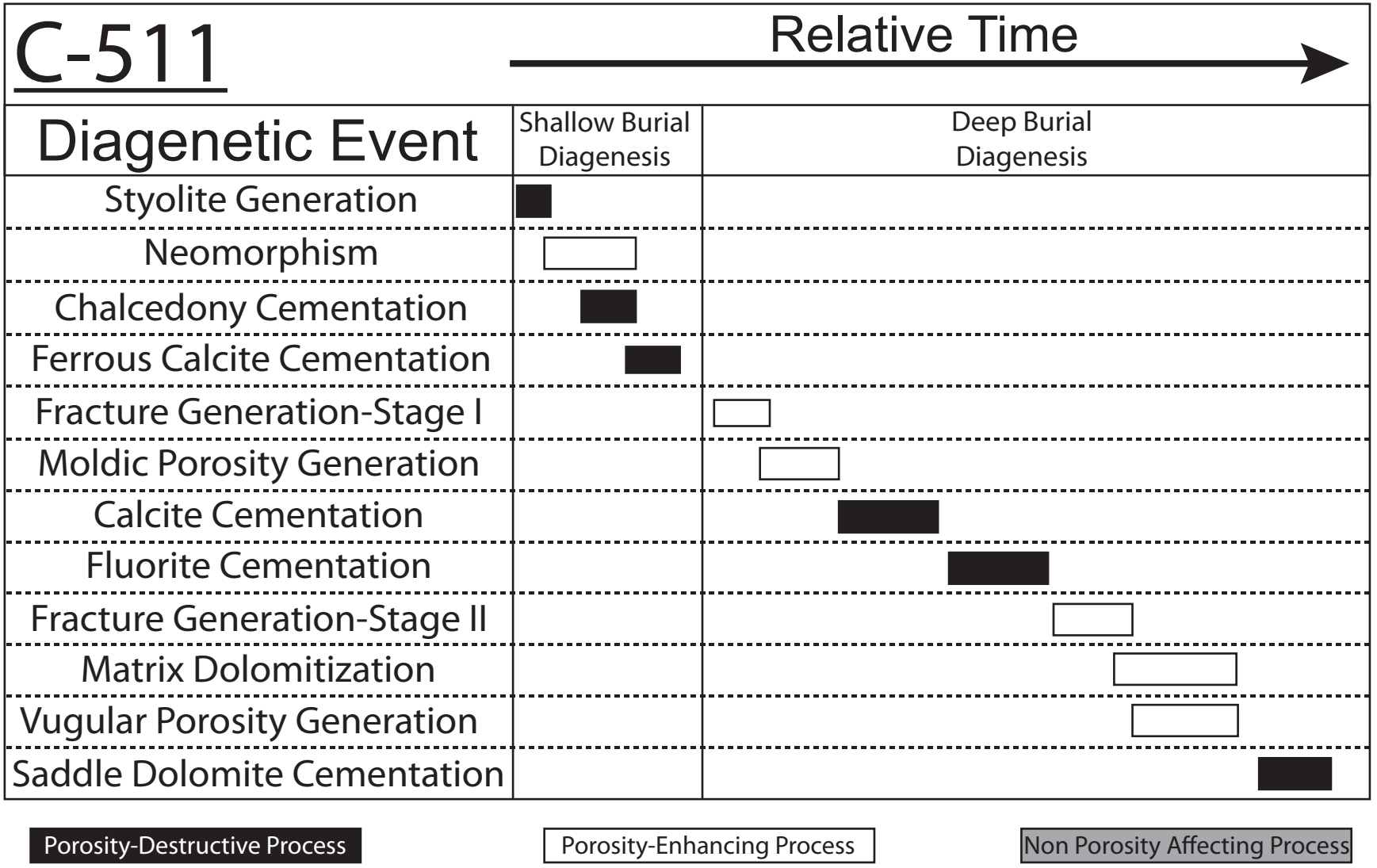

Figure 5.19 Paragenetic sequences observed in core C-511.

Sample C-1220-1 is an echinoid packstone of the Grier Member. Allochems include echinoids, ostracodes, brachiopods, crinoids, bryozoans, trilobites, and intraclasts of phosphatic bryozoan zooecia that were reworked during high energy storm events (Figure 5.20). Deposition was below normal wave base and early marine phreatic cementation occluded the majority of primary porosity.

Core C-1220 exhibits three readily distinguishable types of dolomite through the Trenton, however each stage has very limited extent of dolomitization. The first stage consists of moldic dolomite cements that have subplanar crystal habits and are porosity-destructive (Figure 5.21 C-1220-1a). Crystals are fine and appear cloudy in plain transmitted light. Matrix dolomitization is extremely limited through the core and is characterized by medium sized planar equant crystals that display sweeping extinction under close examination indicating a hydrothermal origin. The dolomites are not associated with any significant change in porosity and are not fabric-selective. The final stage of dolomitization consists of very coarsely crystalline saddle dolomite cementation within large vugular pore spaces. Dolomites have a clear to cloudy appearance and display sweeping extinction under cross polarization. Saddle dolomite precipitation is also associated with minor inclusion-rich fluorite cements within intercrystalline pore spaces that have clear appearances under plain transmitted light. Saddle dolomites generally nucleate on poikilotopic subplanar calcite crystals. Poikilotopic calcites typically are highly twinned (indicating high temperatures of formation) and tend to be the first stage of vugular cementation (Figure 5.21 C-1220-1b).

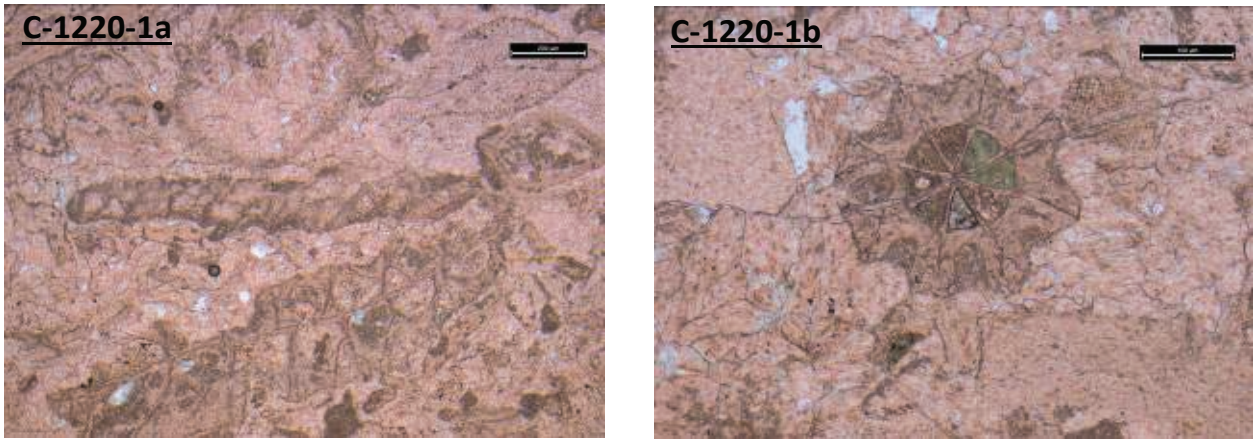

Figure 5.20 Photomicrographs showing allochems that make up the Grier Member from C-1220. (C-1220-1a) Fragments of fenestrate bryozoans, ostracodes, and echinoids that were deposited in a moderate to high energy environment. Unstained nonplanar crystals are composed of fluorite. (C-1220-1b) A phosphatized bryozoan that has subrounded edges and phosphatic chambers indicating high energy deposition in an upwelling environment while poikilotopic and syntaxial calcite indicate cementation and neomorphism in a burial connate environment.

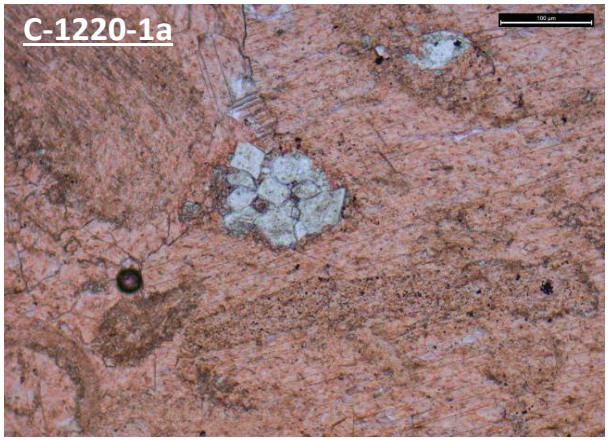

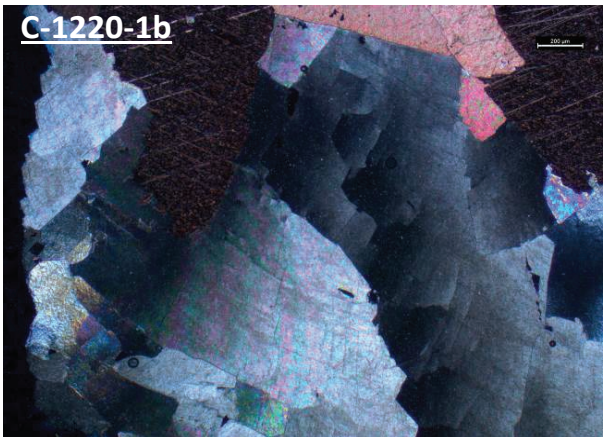

Figure 5.21 Photomicrographs illustrating variations in diagenetic alteration through C-1220. (C-1220-1a) Early stage dolomite cements within moldic pore spaces. The dolomite is porosity destructive and is planar to subplanar. (C-1220-1b) Late stage poikilotopic calcite is highly twinned and coarse saddle dolomites nucleate off of calcite crystal faces. Saddle dolomites exhibit sweeping extinction under cross polarization.

Early marine phreatic cementation in core C-1220 resisted stylolite generation that many other cores exhibit, however mesogenetic neomorphism occurred resulting in subplanar calcite (Figure 5.22). Early fracture generation allowed for fluid migration to create moldic porosity within many ostracode and echinoid allochems. Connate magnesium rich brines precipitated fine dolomites within the moldic porosity, which marked the end of mesogenetic diagenesis. Upon deep burial hydrothermal brine migration led to equant matrix dolomitization which was followed by vugular porosity development. High temperature poikilotopic calcite cements line the margin of vugular pores, which provided points of saddle dolomite nucleation towards the interior of vugs. Fluorite precipitation occurred very slowly relative to other paragenetic stages, which is evident as fluorite crystals are observed in intercrystalline pores of saddle dolomite crystals as well as within coarsely crystalline calcite crystal faces.

Sample C-1221-3 is a peloidal wackestone from the Grier Member. The micritic matrix contains abundant ostracodes and bryozoans that were deposited in a low energy shallow shelf environment (Figure 5.23 C-1221-3). Cementation occurred during deposition in the marine phreatic realm while poikilotopic calcite resulted from neomorphism in a burial connate environment. Sample C-1221-2 is a bryozoan wackestone of the Grier Member that contains red algae, bryozoans, trilobites, and intraclasts of echinoid plates that underwent rapid cementation in a marine phreatic environment (Figure 5.23 C-1221-2). Sample C-1221-4 is a bryozoan grainstone that was deposited in a high energy shallow shelf environment of the Sulfur Well Member. Nodular and encrusting masses of solenoporoid red algae (Figure 5.23 C-1221-4) are common through the section, which reinforces deposition in a high energy environment where siliciclastic influx was at a minimum. Burial connate cementation allowed for stylolite surfaces to develop, which are commonly lined with cloudy dolomite spar. Sample C-1221-5 is a bryozoan ostracode packstone that was deposited in a high energy shallow shelf environment characteristic of the Millersburg Member. Allochems include echinoids, ostracodes, brachiopods, crinoids, bryozoans, trilobites, and intraclasts of phosphatic echinoid plates that

were reworked during storm events (Figure 5.23 C-1221-5). Micritization of grains and a micritic matrix indicate that the substrate was soft that allowed for significant biological burrowing and fabric destruction. Stylolites are abundant through the interval indicating that cementation occurred in a meteoric and burial connate environment. Sample C-1221-1 is an echinoid packstone of the Millersburg that was deposited in a shallow shelf environment. The abundance of phosphatic intraclasts and encrusting nature of bryozoans suggest that deposition and cementation occurred in a high energy environment.

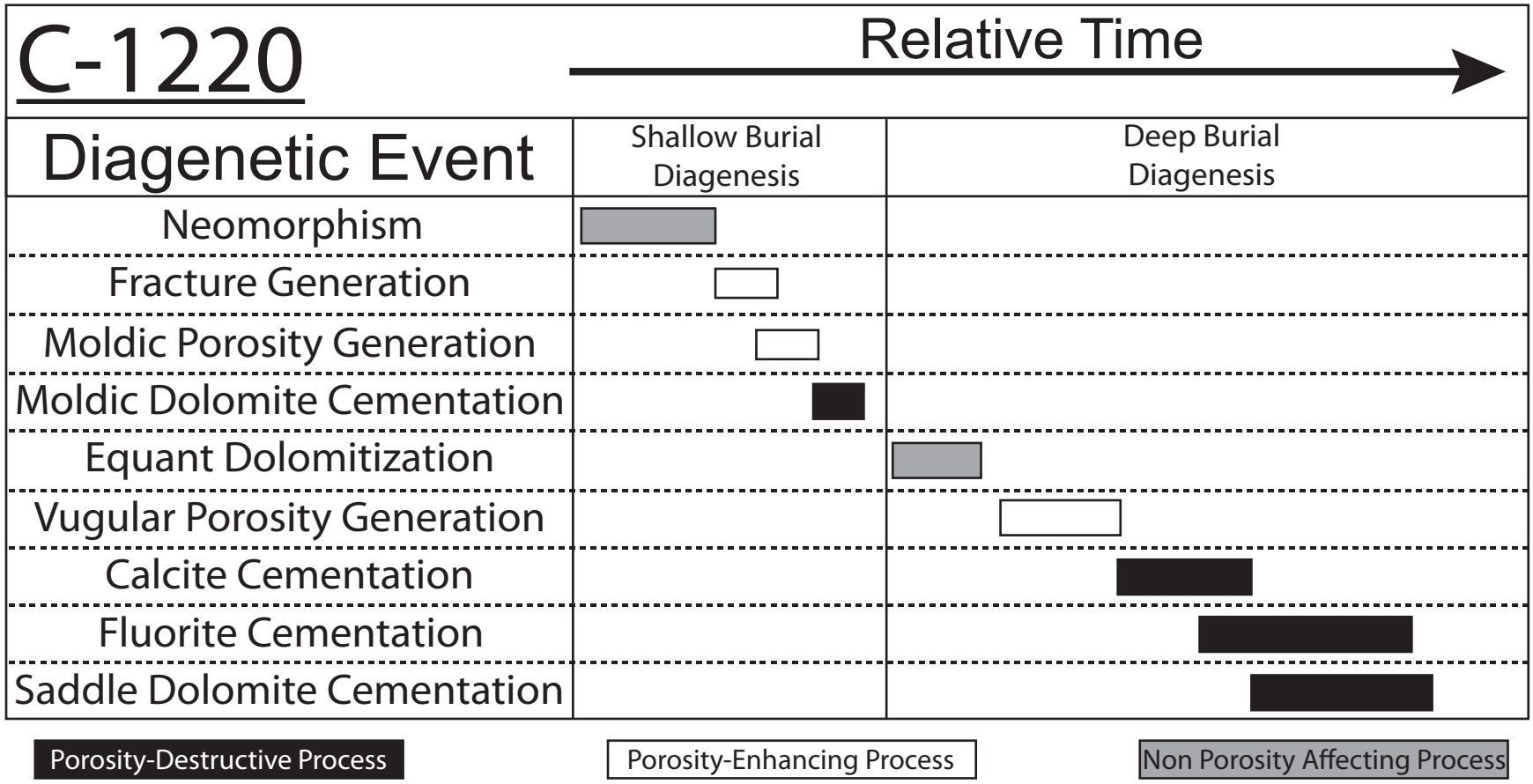

Figure 5.22 Paragenetic sequences observed in core C-1220.

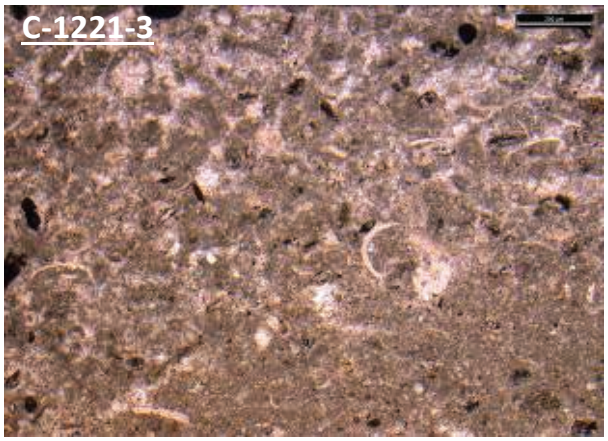

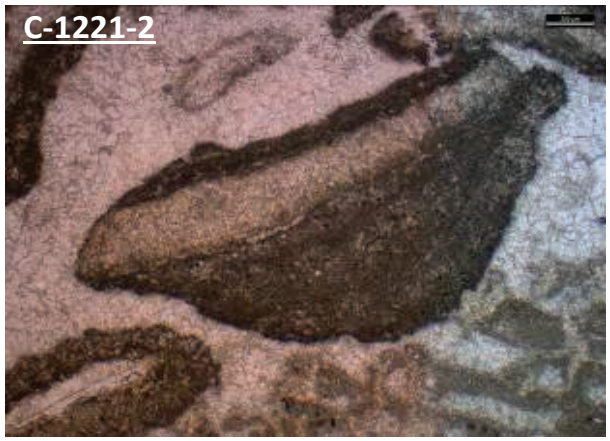

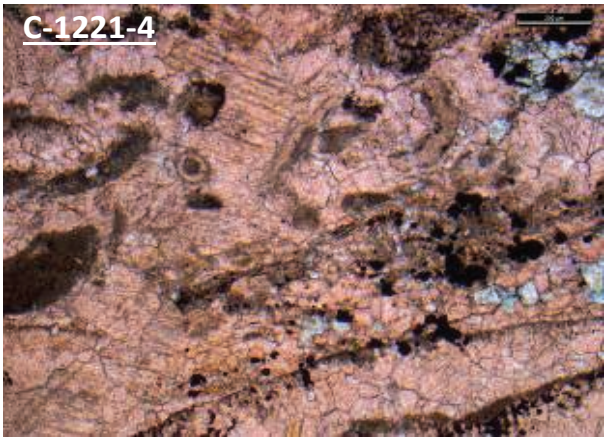

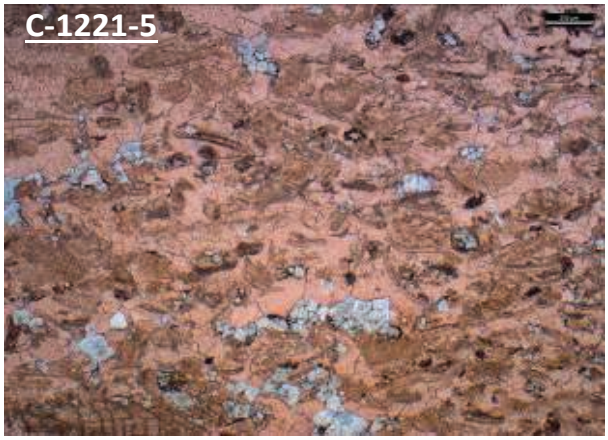

Figure 5.23 Photomicrographs illustrating primary fabrics of the Grier, Sulfur Well, and Millersburg Members in core C-1221. (C-1221-3) A peloidal wackestone that contains abundant ostracode fragments hosted within a micritic matrix. (C-1221-2) A red algal-encrusted trilobite fragment within a neomorphosed matrix of nonplanar cloudy calcite and calcite microspar from the Grier Member. (C-1221-4) A section containing highly pyritized and neomorphosed trilobites and echinoids. Additionally, the presence of a thin-walled ooid supports deposition in a high energy shallow shelf environment where wave reworking within the normal wave base resulted in concentric laminations to accrete on a fragment of well-rounded microspar. (C-1221-5) A grain-rich section of the Millersburg Member that contains echinoids, bryozoans, ostracodes, and trilobites that all appear to have been fragmented during high energy wave reworking along a shallow shelf environment.

The Trenton in core C-1221 is characterized by early eogenetic high amplitude stylolite development that is frequently lined by pyrite and equant dolomite just beneath the stylolite surface. Extensive neomorphism resulted in subplanar to nonplanar calcite cements through the core. Neomorphism appears to be both porosity enhancing as well as porosity destructive as occasional voids in geopetal fabrics were cemented by fibrous chalcedony indicating that minor amounts of silica were dissolved in solution during mesogenetic burial. Fracture generation during early telogenetic diagenesis supplied fluids that allowed for dissolution-induced vugular and intercrystalline porosity development while also supplying magnesium-rich hydrothermal brines that induced matrix dolomitization. Matrix dolomitization is associated with minor amounts of increased porosity and is characterized by fine equant rhombic dolomite crystals that are frequently found adjacent to healed fractures and along stylolite surfaces (Figure 5.24 C-1221-4a). Hydrothermal fluid flow also led to poikilotopic calcite cementation, which can be observed in vugs and in healed fractures and typically grades into ferrous calcite towards the center of healed voids (Figure 5.24 C-1221-4b, C-1221-1). Ferrous calcite is only present in minor amounts and frequently also contains fine crystalline fluorite between ferrous calcite crystal voids. The final diagenetic fabric consists of coarsely crystalline subplanar dolomite cements that are found within large vugular pores and in large geopetal pores. The dolomites exhibit sweeping extinction, have inclusion zoning, and appear to have precipitated over a prolonged period as they generally occlude the majority of the pore space where nucleation was initiated (Figure 5.24 C-1221-5).

Sample C-1221 contains numerous intraclasts from phosphatized hardground surfaces that were developed in the marine phreatic realm (Figure 5.25). Upon burial, stylolite generation resulted from poor eogenetic cementation. Following stylolite generation, matrix neomorphism led to recrystallization of the Trenton interval that provided voids for chalcedony cementation to occur. Early telogenetic diagenesis was initiated by the generation of fractures that supplied fluids to induce dissolution. Resultant porosity development provided increased fluid conduits to

induce matrix dolomitization. Late stages of matrix dolomitization were synchronous with poikilotopic calcite cementation that graded into ferrous calcite cements. Intercrystalline pores generated during ferrous calcite cementation were filled with inclusion-rich fluorite crystals indicating that precipitation was coeval. The final stage of telogenetic diagenesis is marked by coarsely crystalline subplanar dolomite cementation. Dolomites tend to fill any remaining voids and frequently nucleate either in geopetal pore spaces or on poikilotopic calcites.

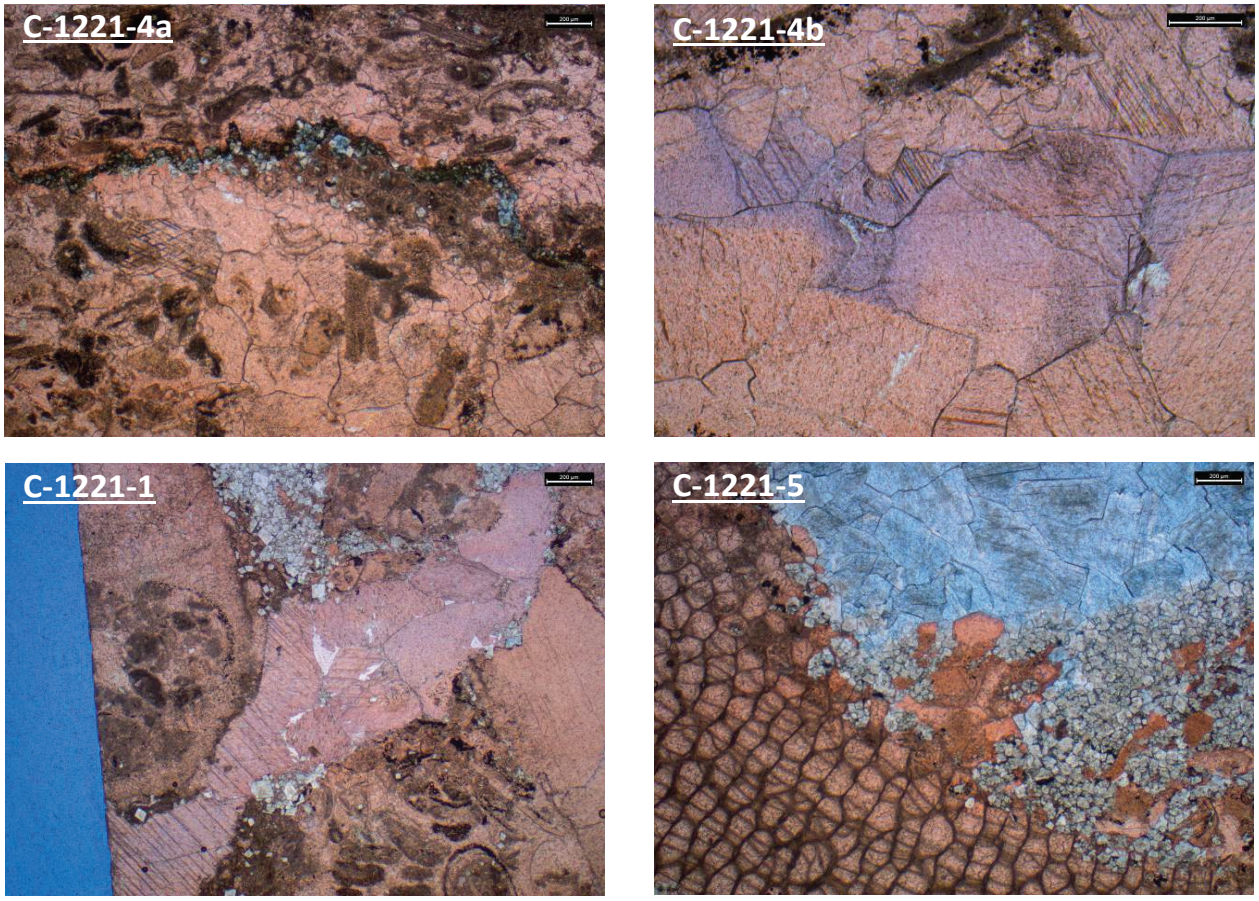

Figure 5.24 Photomicrographs demonstrating hydrothermal mineralization through C-1221. (C-1221-4a) Fine matrix dolomitization along a low-amplitude section of a pyritized stylolite surface. (C-1221-4b) Ferrous calcite and fluorite precipitates along the center of a healed fracture. (C-1221-1) Slightly ferrous calcite healing a fracture that appears to have supplied magnesium rich brines to induce hydrothermal dolomitization away from the fracture plane. Calcite is highly twinned indicating elevated temperatures of precipitation and likely resulted from depletions in magnesium content of migrating brines (Scholle and Ulmer-Scholle, 2003). (C-1221-5) Gradational dolomitization within a large bryozoan that ranged from fine subplanar dolomite into coarse subplanar dolomite that exhibits sweeping extinction.

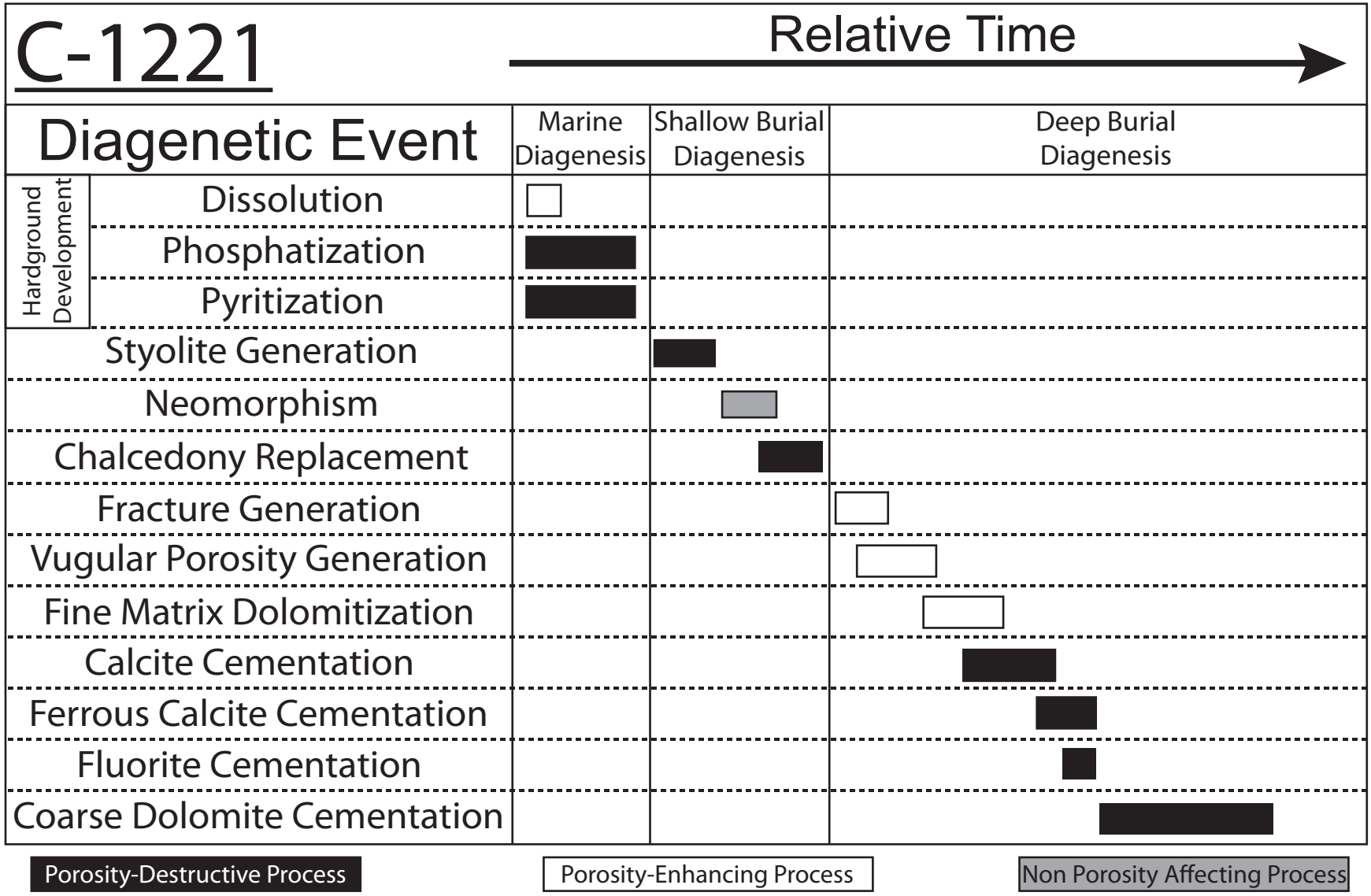

Figure 5.25 Paragenetic sequences observed in core C-1221.

Chapter 6: Stable Isotope Analysis

6.1 Oxygen Isotope ($\delta^{18}O$) Analysis

Dolomites sampled from outcrop and core in Kentucky range from -10.9‰ to -5.7‰ VPDB with an average of -7.9‰ VPDB (standard deviation of 1.28‰), which indicate that the dolomites precipitated from hydrothermal brines and do not have a primary origin (Patchen et al., 2005). Expected results of primary dolomites precipitated from Ordovician seawater in Kentucky should range from -1‰ to -4‰ VPDB (Patchen et al., 2005). A total of 23 samples of dolomites were collected ranging from early matrix dolomites to late-stage saddle dolomites. Early dolomite cements exhibit values ranging from -6.4‰ to -9‰ VPDB with an average of -8.0‰ VPDB (standard deviation of 0.78‰) whereas late saddle dolomite cements range from -7.2‰ to -7.8‰ VPDB with an average of -7.5‰ and a standard deviation of 0.25‰. Results of variations can be observed in Figure 6.1 where values are displayed in a grid that allows for spatial isotope variations around isolated vugs to be analyzed. These results confirm paragenetic sequences indicating that dissolution and matrix dolomitization occurs readily upon the initiation of hydrothermal fluid flow and saddle dolomite cements tend to precipitate during solution cooling (refer to fluid inclusion results in Chapter 7). In addition, $\delta^{18}O$ values from north-central Kentucky range from -10.9‰ to -5.7‰ VPDB and average at -8.2‰ VPDB (standard deviation of 1.93‰) whereas dolomites in south-central Kentucky range from -8.3‰ to -6.4‰ VPDB and average at -7.7‰ VPDB and a standard deviation of 0.57‰. The slight variations in values may be indicative of slightly heavier dolomitizing brines in southern Kentucky caused by variations in brine mineralogies.

Figure 6.1 Grids of $\delta^{18}O$ values in C-1221-6, C-295-3, and C-511-1 illustrating isotopic variations spatially around vugs of hydrothermal dolomite. Stable isotope trends indicate that fluid became increasingly more negative (indicating more heavy fluid) at the margin of calcite to early finely crystalline dolomite. From the margin (highly negative values) towards coarse saddle dolomite cements at the final stage of dolomitization values become slightly less negative, which may be the result of fluid cooling.

6.2 CARBON ISOTOPE ($\delta^{13}C$) ANALYSIS

Carbon isotopes of primary limestones have been a proven tool to conduct detailed sequence stratigraphic analysis on carbonate platforms through $\delta^{13}C$ variations that are directly reflect variations in geochemically distinct water masses, upwelling, ocean circulation, and primary productivity (Young et al., 2005). Detailed carbon isotope sequence stratigraphy through the Trenton in north-central Kentucky show strong shifts through facies changes in Kentucky including the M4-M5 sequence boundary that marks the beginning of Trenton deposition (shift from tropical-type to temperate-type carbonates) (Holland and Patzkowsky, 1996). The positive shift in carbon isotope values at the onset of Trenton Limestone deposition reflects the Guttenberg Carbon Isotope Excursion (GICE) that has been documented throughout much of eastern North America making $\delta^{13}C$ values a useful tool for sequence stratigraphic analysis. Measured $\delta^{13}C$ isotopes from the Grier and Millersburg Members in Kentucky range from 0.5‰ to 0.8‰ VPDB and -1.4‰ to 0.2‰ VPDB and average 0.6‰ (standard deviation of 0.16‰) and 0.5‰ VPDB (standard deviation of 0.43‰), respectively (Table 3; Table 4; Young et al., 2005). Values from 7 samples indicate that there are positive shifts through the Grier Member that may result from increased primary productivity induced by nutrient-rich upwelling onto the Lexington platform while slightly negative values from 17 samples associated with the Millersburg member may result from decreased primary productivity that may have led to increased hardground development (Figure 6.2; Young et al., 2005)

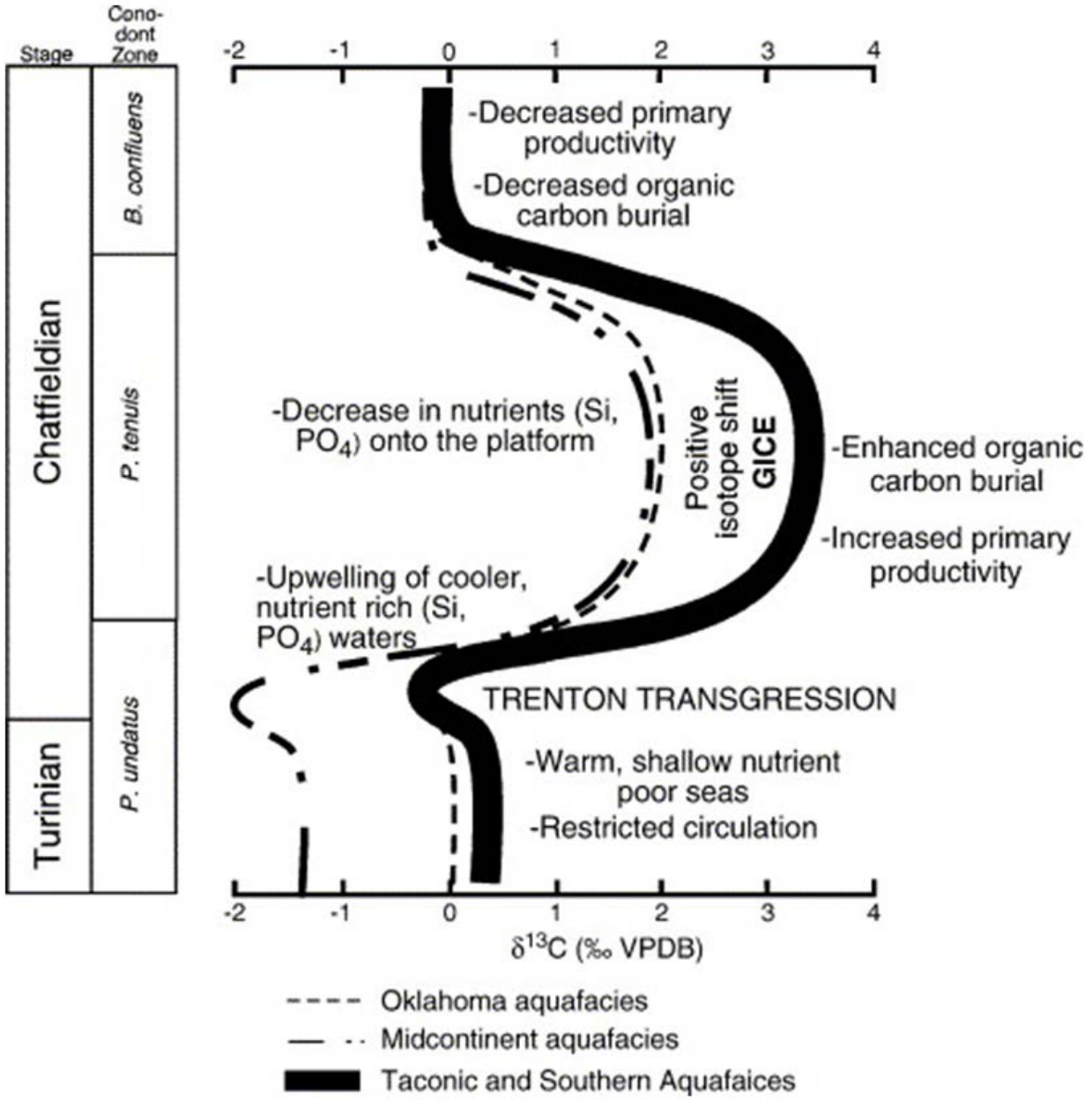

Figure 6.2 A model illustrating the use of carbon isotopes to correlate sequence stratigraphic units through the Trenton through central Kentucky (Taconic and Southern Aquafacies in figure; From Young et al., 2005).

Chapter 7: Fluid Inclusion Analysis

In accordance with Huff and Turkmenoglu (1981) who studied illite/smectite concentrations in potassium bentonites through the crest of the Cincinnati Arch, carbonates through the Trenton Limestone interval did not exceed burial temperatures exceeding 80°C. Thus any homogenization temperatures that exceed 80°C can be considered hydrothermal as they exceed burial connate temperatures.

Fluid inclusion analysis of dolomitized samples from cores C-1221, C-511, C-295, and C-106 and from the Lightbulb was conducted focusing on primary inclusions. Samples from the Drag Fold locality exhibited too great of structural deformation to conduct reliable analyses and two samples, 1221E and LB1A, appear to have been primary to a saddle dolomite recrystallization event and are not primary to the initial stages of hydrothermal dolomitization (Goldstein and Reynolds, 1994). Total ranges in homogenization temperatures were from 93.7°C to 137.8°C with an average of 115.7°C and a standard deviation of 13.4°C whereas salinities range from 14.57 wt% NaCl to 19.79 wt% NaCl with an average of 16.6 wt% NaCl (standard deviation of 1.7 wt%). Comparisons between northern and southern sample locations showed minimal variations in homogenization and eutectic temperatures indicating that fluid salinities were relatively constant across the Cincinnati arch. Evidence from 5 samples of early-stage matrix dolomite versus 5 samples of late-stage saddle dolomite precipitation conditions suggests that early dolomites precipitate at slightly increased temperatures and salinities relative to saddle dolomites. Results from the fluid inclusion analysis can be crossplot with $\delta^{18}O$ to help determine fluid isotopic compositions with the use of a graph developed by Friedman and O'Neil (1977) (Figure 7.1).

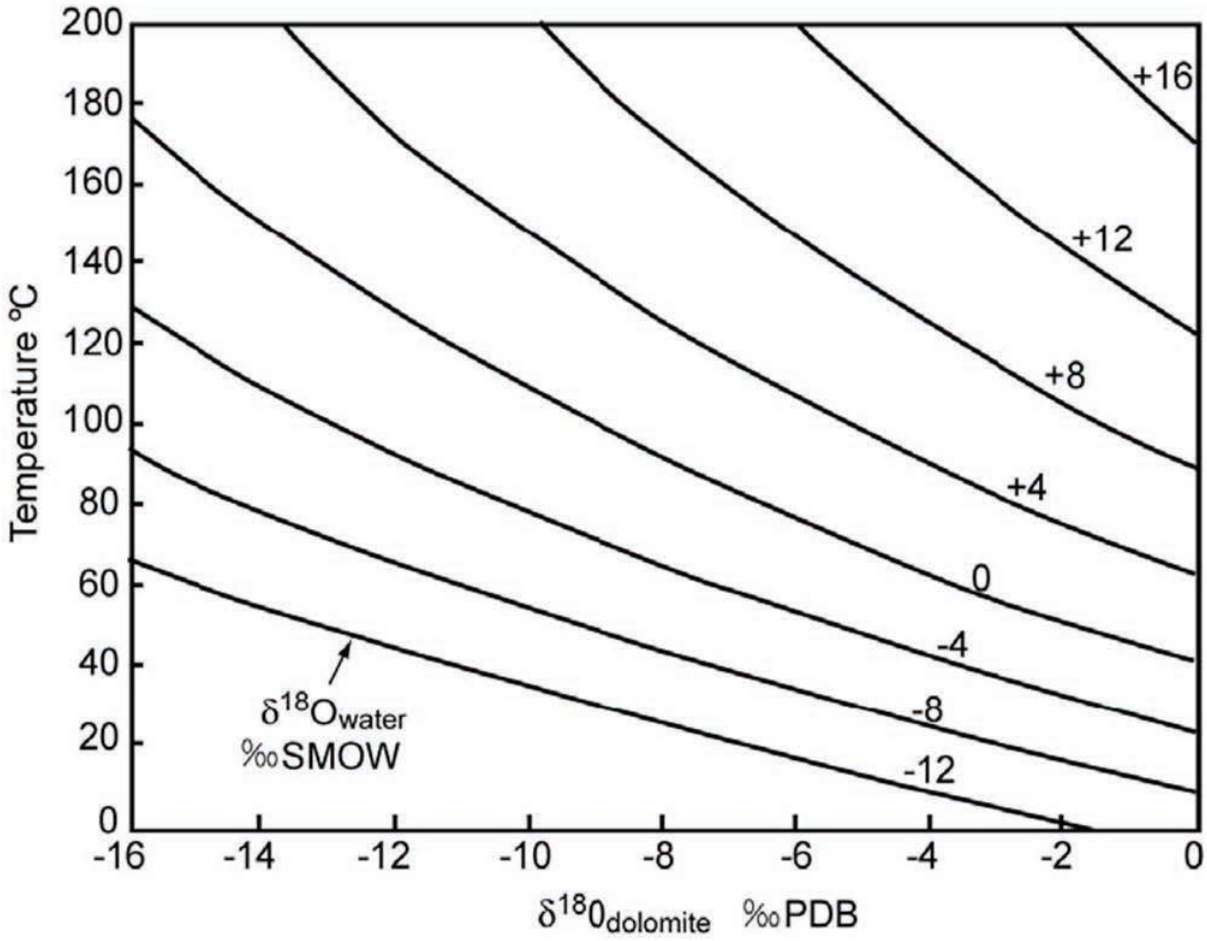

Figure 7.1 A chart utilized to determine fluid compositions through crossplotting δ18O against homogenization temperatures (From Friedman and O'Neil, 1977).

7.1 NORTHERN KENTUCKY

Three samples (LB1A, LB1B, and LB1C) from one double-polished section from the Lightbulb L2C sample location were analyzed for homogenization and eutectic temperatures. Sample LB1A inclusions are located within late-stage saddle dolomite cement that appears to have been recrystallized from a late-stage brine migration event. Inclusions are oriented parallel to each other in an elongate shape and occur in a very cloudy (inclusion-rich) section of the crystal and four inclusions with similarly high liquid-to-vapor ratios make up the analyzed assemblage (Figure 7.2a). Final results indicate homogenization temperatures of 119.4°C and final melt temperatures indicate salinities of 15.47 wt%. Sample LB1B consists of inclusions located near the cloudy nucleation site of a baroque crystal. Three primary inclusions make up the fluid inclusion assemblage (FIA), all of which have moderate-high liquid-to-vapor ratios and are oriented elongate towards the curved crystal face (Figure 7.2b). Homogenization temperatures of 103.7°C were measured and final melt temperatures suggest salinities of 15.17 wt% NaCl. Sample LB1C documents inclusions along the outer edge of an early-stage dolomite rhomb. Three inclusions make up the FIA all of which exhibit relatively low liquid-to-vapor ratios and are oriented parallel to the crystal growth zone in a minor elongate form (Figure 7.2c). Measurements indicate homogenization temperatures of 112.8°C and salinities of 16.71 wt% NaCl.

Core C-106 consists of one sample, 106A, from one double-polished thick section sampled from C-106-3. Inclusions are present within late-stage fluorite cements near the center of a healed fracture (Figure 7.2d). Inclusions are secondary in nature as the FIA (four inclusions) does not appear to follow crystal growth habits and inclusions do not appear to have formed from necking down. Inclusions within the FIA however are elongate in parallel orientations providing evidence for a possible healed microfracture, thus providing data from late-stage fluid migration. Results indicate homogenization temperatures of 101.6°C and fluid compositions are enriched with sodium chloride, calcium chloride, and water as clear globular crystals develop upon freezing (Goldstein and Reynolds, 1994). These results indicate that fluid migration is originated

from variable source beds relative to other analyzed samples that are composed primarily of saline brines, which may be the result of fluid sourcing from Precambrian basement rocks or from fluid migration within Cambrian sands.

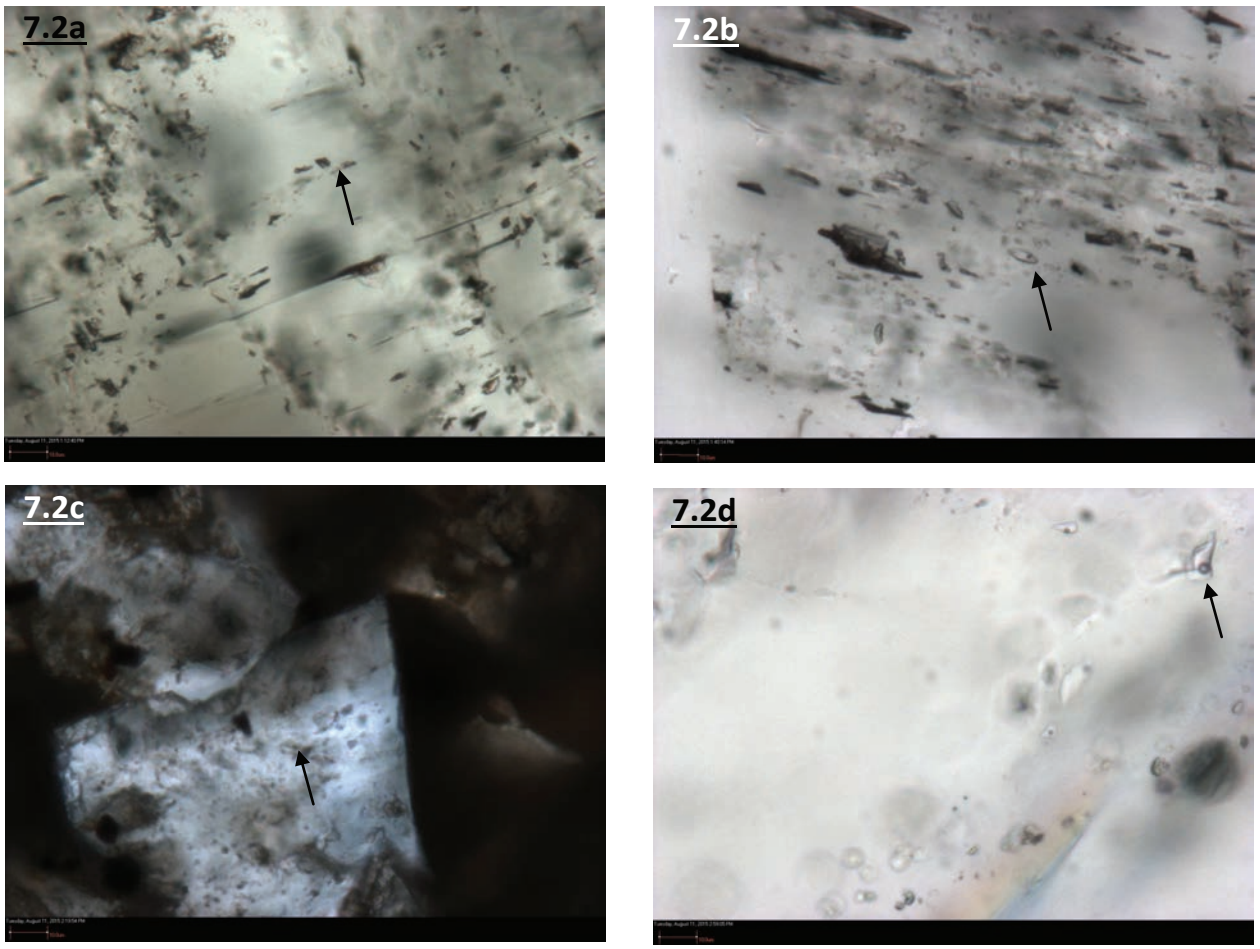

Figure 7.2 Inclusions hosted within samples from northern Kentucky's Bluegrass Region. Arrows indicate regions that contain the FIA. (Figure 7.2a) A FIA that includes three two-phase fluid inclusions that are primary to a recrystallization event within saddle dolomites from L2C. Note the elongate planes that transect the crystal from the lower left to upper right, these are results of saddle recrystallization. (Figure 7.2b) A FIA that is composed of three inclusions that are primary to early stages of saddle dolomite cementation from L2D. (Figure 7.2c) Three primary fluid inclusions make up the FIA that is hosted within an early-stage matrix dolomite. (Figure 7.2d) Four inclusions make up the FIA analyzed within fluorite from C-106. Inclusions are secondary in nature as they do not follow any growth habits that mimic crystal shape or crystal habit.

7.2 SOUTHERN KENTUCKY

Samples from core C-295 (295F and 295I) originated from one double-polished thick section sampled from C-295-3. Sample 295F consists of 4 elongate primary inclusions that mimic growth zonation within a late-stage saddle dolomite crystal (Figure 7.3a). Inclusions exhibit moderate-to-high liquid-to-vapor ratios and occur along the transition from cloudy (near crystal nucleation) to clear (near outer limit of crystal development). Results indicate a homogenization temperature of 115.2°C and fluid salinities were near 16.15 wt% NaCl. Sample 295I consists of one fluid inclusion making up the FIA that has a high liquid-to-vapor ratio and characterizes the beginning stages of dolomite cementation. The inclusion appears to have formed within growth zonation of a rhombic dolomite crystal and is primary in origin. Results indicate homogenization temperatures of 137.8°C and salinities reached 14.57 wt% NaCl.

Core C-511 consists of two samples that were utilized for fluid inclusion analysis (511I and 511J) that were derived from one double-polished thick section from C-511-1. 511I consists of three primary two and one-phase inclusions that are elongate in the direction of crystal growth (Figure 7.3b). The FIA is located at the margin of cloudy matrix dolomite and clear saddle dolomite (FIA is within a cloudy subhedral matrix dolomite) and is located within one growth zone. The FIA exhibits homogenization temperatures of 124.0°C and the final melt temperatures indicate salinities of 16.24 wt% NaCl. Sample 511J consists of two two-phase inclusions that exhibit low liquid-to-vapor ratios that are hosted within one growth zone of an early stage (near crystal nucleation) baroque dolomite crystal that is the first stage of saddle dolomite precipitation as the crystal nucleates at the matrix-saddle margin. Results indicate homogenization temperatures of 129.3°C and salinities of 16.15 wt% NaCl.

Core C-1221 consists of three samples (1221D, 1221E, and 1221F) from core sample C-1221-6 that were analyzed for fluid inclusion microthermometry. Sample 1221D consists of a FIA that contains four two-phase inclusions that are oriented perpendicular to crystal growth zones. The FIA is located within a clear early-stage saddle dolomite crystal and homogenization temperatures of 60.4°C and salinities of 19.79 wt% NaCl were observed. This sample was

removed due to the likelihood that the sample was not primary and may have formed from necking down (Goldstein and Reynolds, 1994). Sample 1221E includes a FIA consisting of three two-phase inclusions with similar sizes and orientations that are elongate towards the curved crystal face (perpendicular to growth zonation) (Figure 7.3c). Inclusions are located at the final fir-tree growth zone transition from cloudy to clear crystal appearance within a late-stage baroque dolomite crystal. Irregular lineations oriented perpendicular to crystal growth zones provides evidence that the FIA may be primary to a saddle dolomite recrystallization event and may not reflect the initial dolomite cement. Results from microthermometric analysis indicate homogenization temperatures of 119.8°C and final melt temperatures indicate that the fluid was composed of a NaCl-H_2O brine with salinities reaching 19.6 wt% NaCl during fluid entrapment. Sample 1221F consists of a FIA composed of three two-phase inclusions with high liquid-to-vapor ratios (Figure 7.3d). The inclusions are elongate towards the crystal face (perpendicular to growth zonation) and are within the final cloudy growth zone that mimics the crystal termination surface of a late-stage rhombic dolomite crystal. Results from the analysis indicate entrapment temperatures of 93.7°C and salinities of 16.15 wt% NaCl.

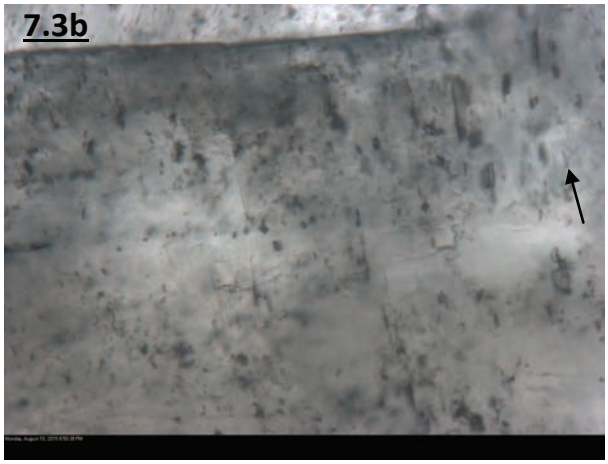

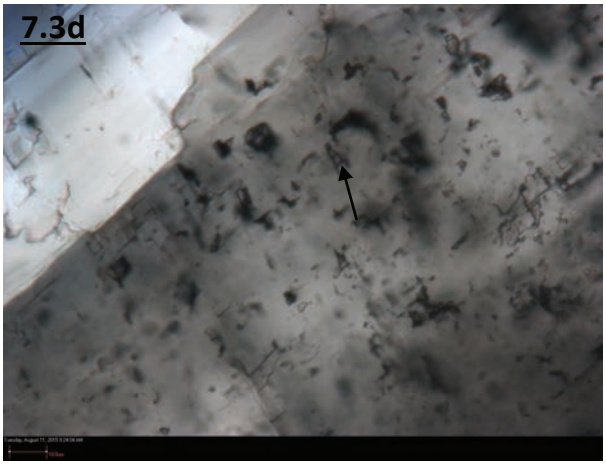

Figure 7.3 Primary fluid inclusions that make up analyzed FIA's within cores from south-central Kentucky. (Figure 7.3a) A FIA composed of four elongate inclusions that are elongate towards the direction of crystal growth from C-295-3. (Figure 7.3b) Three primary inclusions are elongate towards the direction of crystal growth within matrix dolomite from C-511-1. (Figure 7.3c) A set of three two-phase inclusions hosted within the outer portion of a late-stage saddle dolomite cement. (Figure 7.3d) Three two-phase inclusions within a late-stage rhombic dolomite cement.

7.3 REGIONAL RESULTS

With the utilization of the graph provided by Friedman and O'Neil, (1977) fluid isotopic values for samples in Kentucky were integrated with homogenization temperatures and were determined to range from 0‰ to 6‰ SMOW with a strong concentration of values averaging around 4‰ SMOW (Figure 7.4). When compared to values measured by Patchen et al. (2005) for hydrothermal dolomites from New York and Ohio, samples analyzed from Kentucky tend to exhibit similar fluids to those in Ohio, which are significantly heavier than both Ordovician, Devonian, and Silurian seawater, which range from -8‰ to -2‰ (Haeri-Ardakani et al., 2014). Fluids in New York generally exhibit isotopic values near 2‰ as dolomites tend to be more light ($\delta^{18}O_{dolomite}$ tend to range from -10‰ to -12‰ VPDB) than those hosted within carbonates from Ohio and Kentucky (Patchen et al., 2005).

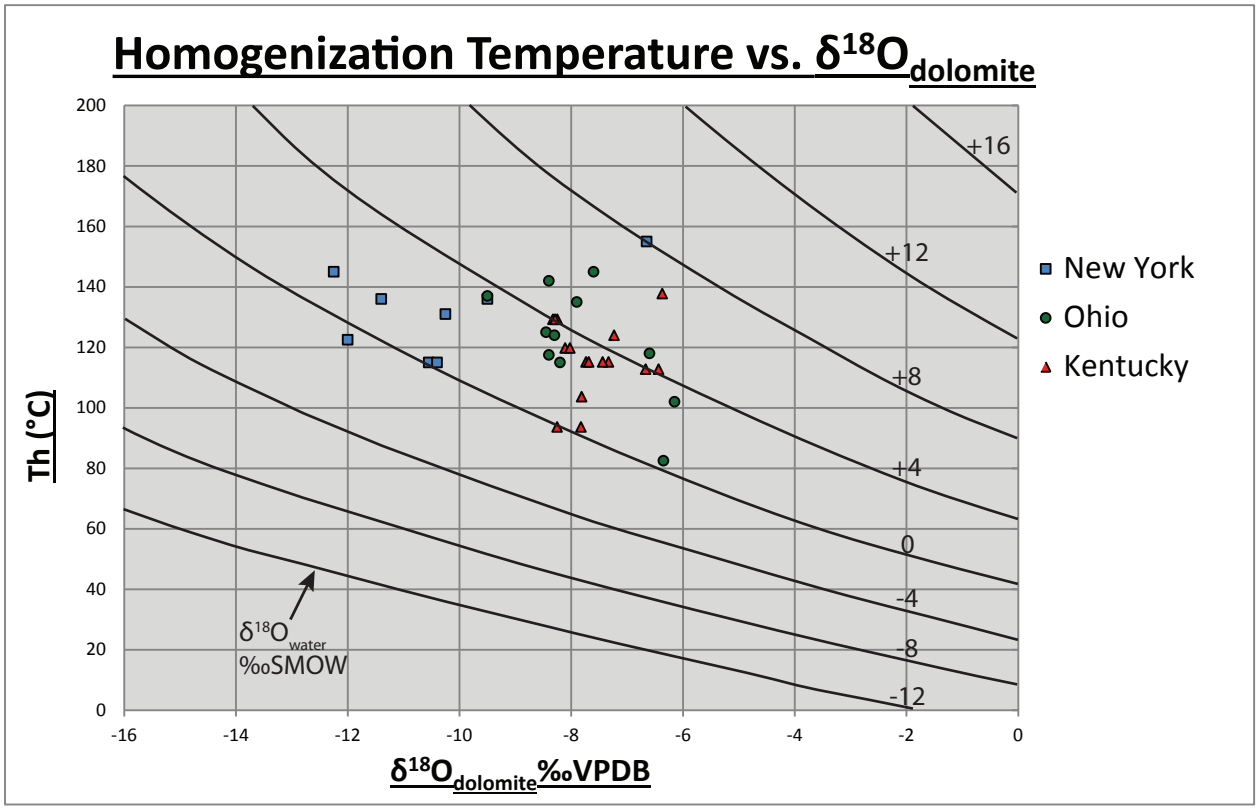

Figure 7.4 A chart illustrating values measured by Patchen et al. (2005) from New York and Ohio samples compared to those measured in samples from Kentucky. Samples in Kentucky generally concentrate around 3.5‰ to 4‰ SMOW indicating that fluids are slightly heavier than those in New York. Further, the increased isotopic values indicate that these dolomites did not precipitate from oceanic water proving that dolomites have a hydrothermal origin (From Patchen et al., 2005).

Chapter 8: Discussion

Trenton Limestone-hosted hydrothermal dolomitization is highly variable across central Kentucky and tends to lead to varying degrees of reservoir-grade porosity and permeability development. Regionally, the complex variations in cool water carbonate sedimentation along the Lexington platform have led to numerous facies ranging from high energy shallow shelf boundstones to low energy deep ramp wackestones and packstones that have hosted limited amounts of hydrothermal dolomitization. A total of twelve depositional facies from six members of the Trenton Limestone and one facies from the upper Black River Group host hydrothermally dolomitized fabrics with varying degrees of alteration.

The Curdsville, Grier Limestone, and Millersburg members of the Trenton Limestone contain hydrothermal dolomites in both northern Kentucky as well as in southern Kentucky while the Perryville Limestone (Faulconer bed) and Sulfur Well members only host dolomitization in south-central Kentucky. By far the most common hosts encountered are the Grier and Millersburg members, which is likely a result of the two making up the two thickest packages of sediments through the Trenton thus enhancing the likelihood of intersecting fracture and fault networks and is not an effect of increased primary porosity. The two members host dolomite within facies deposited in deep ramp, mid ramp, and shallow shelf settings and exhibit primary porosities generally less than 3%. In addition, the abundance of phosphatized marine hardgrounds through the two tend to act as aquitards preventing fluid migration both laterally and vertically thus inhibiting extensive reservoir development.

The frequency of marine hardgrounds through the Trenton Limestone and abundance of phosphatized allochems through the majority of the observed facies tend to have negative effects on hydrothermal alteration due to their lack of permeability. Depositional phosphate through the Lexington platform is sourced from the cool polar water upwelling from the bounding Sebree trough and Martinsburg foredeep. The physical process of upwelling onto the shallow Lexington platform results in a decrease in phosphate solubility in oceanic waters caused by increasing

water temperatures and pH thus inducing precipitation through hardground mineralization as well as echinoid and bryozoan zooecia replacement (McKelvey, 1967).

The Lightbulb dolomite exhibits extensive dolomitization that was induced by fluid migration along a small displacement oblique-normal fault; the Boonesboro Fault (Black et al., 1981). Dolomitizing fluid was likely sourced from the Grenville Province (Figure 8.1) and fluid migration was halted by the outcrop-capping marine hardground, which subsequently induced lateral fluid migration into low porosity skeletal wackestones and packstones of the Millersburg member. The Millersburg member at the Lightbulb exhibits unaltered calcite $\delta^{13}C$ values of -0.8‰, which coincides with results from Young et al. (2005). Fluid injection appears to have been under significant pressure as evidenced by bed-parallel zebra fabrics along the dolomite-limestone margin. Secondary hydrothermal mineral emplacement throughout the Lightbulb is restricted to minor amounts of fluorite; however sulfide and sulfate minerals such as sphalerite and barite were not observed indicating that fluid compositions were not enriched in dissolved solids Scholle and Ulmer-Scholle, 2003). $\delta^{18}O_{dolomite}$ from the Lightbulb average at -6.65‰ with a standard deviation of 0.87‰ indicating that fluids were depleted in O^{17} and had a hydrothermal origin. Confirmation of a hydrothermal origin was established through fluid inclusion analysis, which indicated temperatures reached 119°C, nearly 40°C above maximum burial temperatures (Huff and Turkmenoglu, 1981). Eutectic temperatures of -20.7°C indicate that fluids were composed of saline brines that were determined to reach 15.17 wt% NaCl based on methods provided by Goldstein and Reynolds (1994).

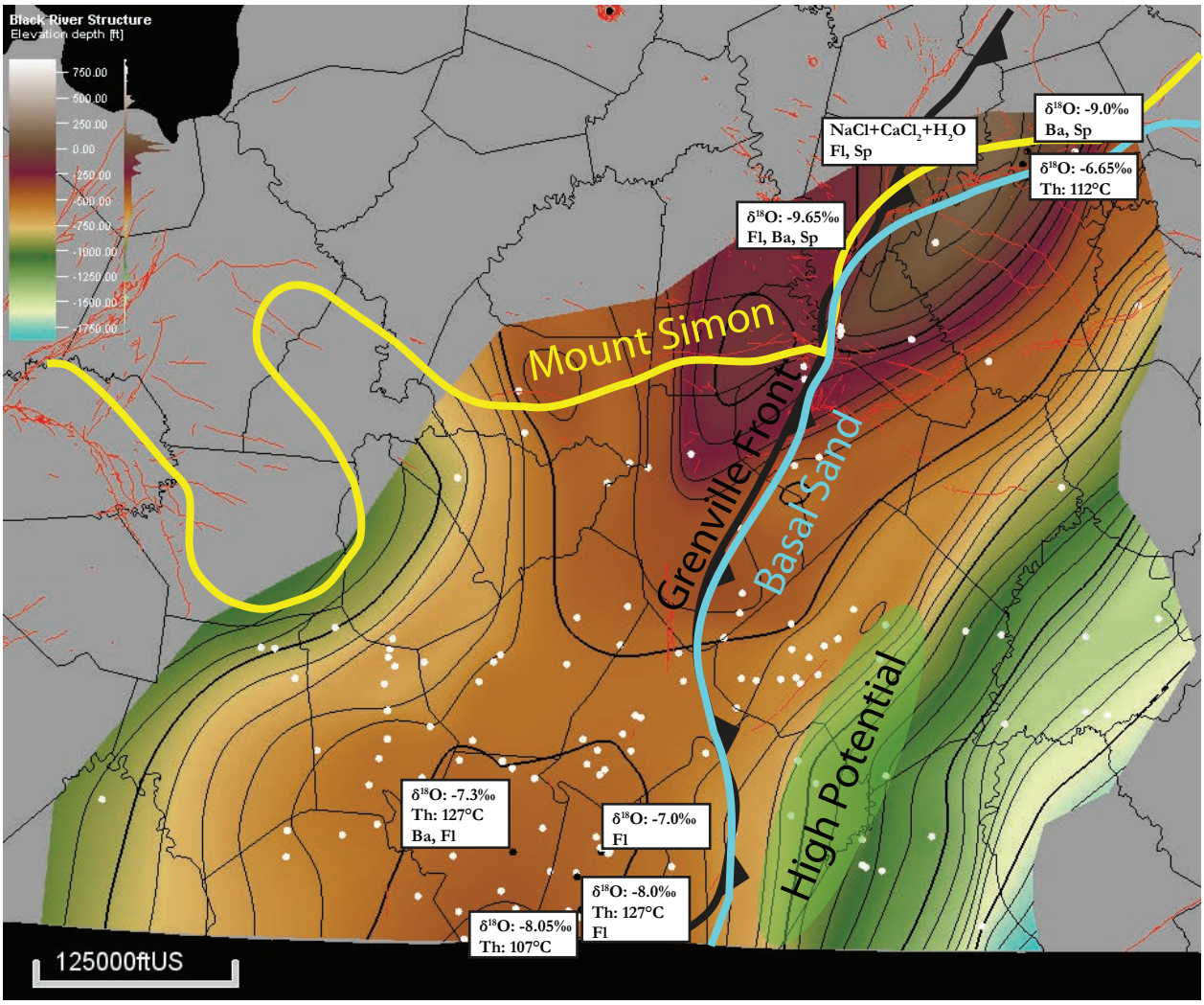

Figure 8.1 A structure contour map of the top of the Black River formation illustrating the spatial variability of hydrothermally originated minerals (Ba: barite, Fl: fluorite, Sp: Sphalerite), homogenization temperatures, and δ18Odolomite that were observed in core and outcrop analysis. Approximate limits of the Precambrian Grenville Front and Cambrian Mount Simon and Basal Sands have also been added to the figure to observe correlations between mineralogies, reservoir development, fault systems, and carrier/source beds for hydrothermal brines (Greb and Solis, 2001).

The Drag Fold locality consists of limited pervasive dolomitization, however minerals commonly observed in MVT deposits are frequently observed healing fractures and occluding intercrystalline porosity. Conjugate fracturing induced by tensional stress along the hinge of the drag fold provided fluid flow conduits that supplied mineralizing fluids. Mineralization within the Drag Fold is hosted within the Millersburg member of the Trenton, which appears to have experienced numerous phases of mineralization that were induced by three distinct stages of fracturing. The lack of an overlying low permeability aquitard and the low primary porosities through the Millersburg hindered reservoir-grade porosity development due to the lack of elevated fluid injection pressures as evidenced from the lack of zebra fabrics and the lack of pervasive matrix dolomitization. Dolomites within the Drag Fold locality are confined to fracture margins and healed fractures and exhibit $\delta^{18}O_{dolomite}$ values with average mean values of -9.65‰ with standard deviations of 1.73‰ indicating hydrothermal origin. The variability of emplaced minerals (bladed barite, sphalerite, fluorite, and ferroan calcite) is indicative of reducing conditions during mineral precipitation (Scholle and Ulmer-Scholle, 2003). Further, mineral variations may have been caused by basement fluid sourcing as the Drag Fold lies along the margin of the Grenville Front and overlies the Cambrian Mount Simon sandstone, a possible carrier bed for hydrothermal migration (Figure 8.1; Greb and Solis, 2001).

Cores from northern Kentucky (C-200, C-201, and C-106) are located along the Kentucky River fault system and host mineralization in the Millersburg, Grier, and Curdsville members of the Trenton as well as within lagoon facies from the Black River Group. Cores exhibit variable mineralization ranging from matrix dolomitization and vugular porosity development through C-200 to the more variable and complex mineralization hosted within C-201 and C-106. Both C-106 and C-201 contain fluorite, ferrous calcite, dolomite, and sphalerite, which were likely supplied from fractures produced by reactivation of the Kentucky River fault system. The Black River-hosted dolomite in C-201 exhibits $\delta^{18}O_{dolomite}$ values of -9.0‰ and secondary fluid inclusions from C-106 indicate fluid homogenization temperatures of 101.6°C.

Eutectic temperatures from fluorite-hosted inclusions within C-106 indicate that fluid compositions were enriched with NaCl, $CaCl_2$, and H_2O based upon Table 1. All of the cores are located above the Grenville Province and lie east of the Grenville Thrust in a region that does not contain basal Cambrian sandstones, however the basal sands are positioned just down dip of the core locations making the basal undifferentiated sands possible carrier beds for mineralizing fluids (Figure 8.1, Greb and Solis, 2001). The lack of confining beds through the cores combined with the lack of HTD fabrics such as zebra fabrics and brecciation indicate that fluid injection pressures were likely not extensive enough to initiate pervasive matrix dolomitization and reservoir development.

Northwestern cores from the Jeptha Knob structure (C-1286 and C-1287) exhibit extensive dolomitization throughout the Trenton interval that resulted in excellent porosity and permeability development. Accessory minerals are limited to fluorite cements that occlude portions of intercrystalline porosity. The abundance of faulting and fracturing in the region likely induced rapid pervasive dolomitization of the Trenton. Primary fabrics are no longer distinguishable due to the extent of dolomitization, which have homogenization temperatures ranging from 70° to 123°C (Patchen et al., 2005). Mineralization appears to have occurred rapidly as saddle dolomite development is minimal (suggesting rapid solution cooling). The lack of variable mineralogies such as those presented in MVT deposits may be the result of fluid sourcing from the Cambrian Mount Simon sandstone or from the Middle Run Formation (Figure 8.1; Greb and Solis, 2001). Previous interpretations of the Jeptha Knob feature suggest that the brecciated fabrics resulted from fluid injection (a characteristic trait of HTD reservoirs) under elevated hydrostatic pressures (Thompson, 2005).

Cores located within Clinton and Cumberland counties of south-central Kentucky exhibit secondary minerals that include barite, fluorite, dolomite, and ferrous calcite, which indicate mineral formation under reducing conditions (Scholle and Ulmer-Scholle, 2003). Mineralization is hosted within the Millersburg, Devils Hollow, Sulfur Well, Perryville Limestone, Grier, and

Curdsville members of the Trenton and is linked to one or two stages of fracturing through the Trenton interval. Homogenization temperatures of dolomites (without the use of 60.4°C due to the likelihood of a bad data point) average at 120°C with standard deviations of 15°C while eutectic and final melt temperatures indicate that fluids were composed of NaCl and H_2O with average salinities reaching 17 wt% NaCl. Samples from south-central Kentucky are positioned west of the Grenville Front and overlie the Middle Run formation and Granite-Rhyolite Province in Clinton and Cumberland counties, respectively based on maps generated by Greb and Solis (2001). Further, Cambrian sands in Clinton and Cumberland counties are not present suggesting that fluids are sourced from Precambrian basement rocks (Greb and Solis, 2001). Due to the lack of significant dormant faults in the subsurface of Clinton and Cumberland counties, relatively low potential exists for significant fault-induced dolomitization.

Based upon results from fluid inclusion microthermometric analysis, fluids tend to increase in temperature south along the Cincinnati arch, which is confirmed with increasing $\delta^{18}O_{dolomite}$ values. Intergration of $\delta^{18}O_{dolomite}$ and homogenization temperature data, $\delta^{18}O_{fluid}$ was determined to exhibit $\delta^{18}O_{fluid}$ values of +4‰SMOW, which indicates that foreland dewatering and fluid migration onto the Cincinnati arch forebulge did not occur suggesting that fluids were sourced from deep Precambrian basement rocks ($\delta^{18}O_{fluid}$ from Ordovician, Silurian, and Devonian seawater generally contain values of -8‰ to -2‰SMOW (Haeri-Ardakani et al., 2014).

Chapter 9: Conclusions

9.1 Extent of Dolomitization in South-Central Kentucky

Dolomitization through south-central Kentucky is extensive, and locally forms nonmimetic fabrics. Spatially, hydrothermal dolomitization is present in both north-central and south-central Kentucky along the Cincinnati arch, but it occurs with varying degrees of pervasiveness, accessory minerals, and subsequent reservoir development. Dolomites were observed within six of the eleven members in both core and outcrop, which all displayed variable degrees of dolomite pervasiveness as well as the presence of HTD fabrics.

Matrix dolomitization is the dominant requisite to allow for reservoir development through the Trenton Limestone in Kentucky, which tends to be nonmimetic and produces large volumes of intercrystalline porosity. Reservoir-grade porosity development was observed in the Lightbulb locality and in the Northwestern cores (C-1286 and C-1287), however the development of isolated vugular porosity occurred within southern cores C-511, C-295, and C-1221 indicating that connate fluids in south-central Kentucky are conducive to potentially induce pervasive matrix dolomitization given the proper conditions. Hydrothermal dolomitization was spatially observed along the Lexington and Kentucky River fault systems in north-central Kentucky, however the decreased structural influence progressing south in Kentucky limited subsurface dolomite occurrences.

Dolomites exhibit trends such as increasing homogenization temperatures and increased $\delta^{18}O_{dolomite}$ values south across the Cincinnati arch indicating that southern samples are likely to have matrix dolomitization. Dolomites all exhibit increased temperatures of formation as homogenization temperatures exceed the maximum burial temperature of 80°C (Huff and Turkmenoglu, 1981). Fluid compositions are highly variable across Kentucky, which have a significant influence on observed MVT-type minerals such as ferrous calcite, fluorite, barite, and sphalerite. The majority of observed dolomites generally had eutectic temperatures indicating that compositions were composed of NaCl and H_2O brines with salinities ranging from 14.57

wt% NaCl to 19.79 wt% NaCl with an average of 16.6 wt% NaCl and a standard deviation of 1.7 wt% NaCl. Measured fluid isotope values of ($\delta^{18}O_{fluid}$) +4‰SMOW indicate that fluid sourcing is not from ocean water reflux (expected fluid compositions from Ordovician, Devonian, or Silurian seawater range from -2‰ to -8‰) based on results from Haeri-Ardakani et al. (2014) or foreland sediment dewatering designating deep fluid sourcing from underlying formations. Fluid compositions are likely caused by variability in deep fluid source rocks such as the Precambrian basement and Cambrian sands that are spatially variable across Kentucky.

9.2 CONTROLS ON DOLOMITIZATION

The overriding primary control on hydrothermal dolomitization through central Kentucky is the presence of basement fault systems to reactivate and initiate vertical fluid migration into Ordovician strata. Basement weaknesses such as the Grenville Front and the abundance of normal faults that transect basement rocks of central Kentucky provide excellent zones of weakness to allow for reactivation during the Taconic, Acadian, and Alleghanian orogenies. Continental rifting of the supercontinent Pangea during Triassic time does not appear to have influenced central Kentucky. Typically HTD reservoir development is most extensive in oblique-thrust faults as they tend to favor development of negative flower structures that frequently occur in en echelon pairs (Smith and Nyahay, 2005).

Additional controls on reservoir development in Kentucky are the abundance of phosphate through primary fabrics of the Trenton. Phosphatization associated with cool water carbonate deposition in a nutrient upwelling foreland leads to grain-selective replacement with cryptocrystalline phosphate (collophane), a process that tends to occlude primary porosity and replace with microporosity resulting in an apparent net decrease in permeability. This limitation on permeability is not conducive to host reservoir development, but instead provides for vertical aquitards to limit vertical fluid migration. Vertical aquitards are essential to induce lateral hydrothermal dolomitization and reservoir development through their abilities to cause increased fluid injection pressures below impermeable beds.

Fluid injection pressure is another key factor that affects reservoir-grade porosity development in Kentucky. High-pressure injection is recognized in HTD reservoirs through bed-parallel zebra fabrics and injection breccias, which frequently result in nonmimetic dolomitization illustrating a natural hydro-frac of host carbonates. The nonmimetic dolomites commonly occur as results of a lack of crystal nucleation sites due to the pervasive dissolution induced by high temperature fluid flow. Hydrostatic pressure gradients may also have significant controls on the generation of high-pressure fluid migration.

Homogenization temperatures in dolomites through Kentucky indicate that matrix dolomitization and maximum porosity/permeability development occurs during maximum fluid temperatures while solution cooling frequently results in porosity-destructive cementation with saddle dolomites and coarsely crystalline subplanar to nonplanar dolomitization.

Complexities among fluid compositions also result in variable accessory mineral cements including fluorite and ferrous calcite, which likely result from deep carrier and source bed fluid migration. The increase in MVT-type deposits in western Kentucky likely result from the Precambrian basement Granite-Rhyolite province (Figure 2.1) while decreasing abundancies of large scale MTV deposits in eastern Kentucky may result from decreased sulfate and sulfide supply from the metamorphic Grenville Province (Greb and Solis, 2001). Mineralization in MVT hosted regions frequently exhibit more abundant sources to supply porosity-destructive cements and thus are commonly late stage reservoir-degrading cements.

9.3 IMPLICATIONS FOR HYDROCARBON EXPLORATION

Hydrocarbon exploration in central Kentucky for hydrothermally dolomitized reservoirs proves to be a valid model that has very high potential in Kentucky. High potential exists in the underlying Black River Formation while cool-water carbonates through the Trenton do not appear to be conducive to extensive reservoir development. Due to primary HTD controls including faulting, primary porosity in host carbonates, fluid injection pressures, homogenization temperatures, and secondary mineral cements, high potential for Black River Group carbonate

alteration lies along the eastern margin of the Cincinnati arch (Figure 8.1). Along the eastern margin of the Cincinnati arch increased tension along the transition of relatively low-dipping bedding along the crest of the Cincinnati arch into the steep east dipping carbonates (towards the Appalachian Basin) provides for zones where fracturing and faulting may be more easily achieved. Increased hydrostatic pressures are also predicted to lie along the margin of the Cincinnati arch due to the increased depth-to-basement and potential for fluid sourcing from deep within the Appalachian Basin that may produce an increased regional fluid-pressure gradient. Increased homogenization temperatures south through Kentucky create more favorable conditions to initiate matrix dolomitization in southern Kentucky where homogenization temperatures reach 127°C. Finally, secondary MVT-type mineral cements tend to occlude porosity in northern Kentucky while concentrations of fluorite generally decrease south along the Cincinnati arch, a result of variable fluid source and carrier beds (Precambrian basement and Cambrian sands). In conclusion, Figure 8.1 illustrates the region where increased potential for Black River HTD reservoir development exists. This region overlies the Precambrian Grenville Province and is located in a region where dormant basement faults may be more susceptible to oblique-thrust reactivation during compressional events including the late Taconic, Acadian, and Alleghanian orogenies.

References

Anderson, W., and Dever, G., 2001, Mineral and Fuel Resources Map of Kentucky: Kentucky Geological Survey Map and Chart 26, Series XII.

Black, D.F.B., MacQuown, W.C., and DeHaas, R.J., 1981, Relation of Dolomite Associated with Faults to the Stratigraphy and Structure of Central Kentucky:.

Blakey, R., 2011, Middle Ordovician (470Ma): Northern Arizona University Geology North American Paleogeographic Maps.

Borella, P.E., and Osborne, R.H., 1978, Late Middle and early Late Ordovician history of the Cincinnati arch province, central Kentucky to central Tennessee: Geological Society of America Bulletin, v. 89, no. 10, p. 1559–1573, doi: 10.1130/0016-7606(1978)89<1559:LMAELO>2.0.CO;2.

Brett, C., McLaughlin, P., Schramm, T., Sullivan, N., Thomka, J., Cramer, B., and Gerke, T., 2012, Middle Paleozoic Sequence Stratigraphy and Paleontology of the Cincinnati Arch: Part 1 Central Kentucky and Southern Ohio: International Geoscience Programme, Cincinnati, Ohio.

Cable, M.S., and Beardsley, R.W., 1984, Structural controls on Late Cambrian and Early Ordovician carbonate sedimentation in eastern Kentucky: American Journal of Science, v. 284, no. 7, p. 797–823, doi: 10.2475/ajs.284.7.797.

Catacosinos, P.A., Dickas, A.B., Forsyth, D.A., Hinze, W.J., and Pluijm, B.A. van der, 1996, Basement and basins of eastern North America: A research conference summary: Geological Society of America Special Papers, v. 308, p. 1–6, doi: 10.1130/0-8137-2308-6.1.

Cressman, E.R., 1973, Lithostratigraphy and depositional environments of the Lexington Limestone (Ordovician) of central Kentucky: U.S. Govt. Print. Off., Professional Paper USGS Numbered Series 768.

Davies, G.R., and Smith, L.B., 2006, Structurally controlled hydrothermal dolomite reservoir facies: An overview: AAPG Bulletin, v. 90, no. 11, p. 1641–1690, doi: 10.1306/05220605164.

Douglas Patchen, Taury Smith, Ron Riley, Mark Baranoski, David Harris, John Hickman, John Bocan, and Michael Hohn, 2005, Creating a Geologic Play Book for Trenton-Black River Appalachian Basin Exploration: 895657.

Eby, D., Chidsey, T., Morgan, C., McClure, K., Humphrey, J., Moore, J., Taylor, L., and Weyland, V., 2005, Dolomitization of the Mississippian Leadville Reservoir at Lisbon Field, Paradox Basin, Utah:.

Folk, R.L., 1987, Detection of organic matter in thin-sections of carbonate rocks using a white card: Sedimentary Geology - SEDIMENT GEOL, v. 54, no. 3, p. 193–200, doi: 10.1016/0037-0738(87)90022-4.

Friedman, I., and O'Neil, J.R., 1977a, Compilation of stable isotope fractionation factors of geochemical interest: Professional Paper USGS Numbered Series 440-KK.

Friedman, I., and O'Neil, J.R., 1977b, Data of Geochemistry: Compilation of stable isotope fractionation factors of geochemical interest: U.S. Government Printing Office.

Goldstein, R., and Reynolds, J., 1994, Systematics of Fluid Inclusions in Diagenetic Minerals: Society for Sedimentary Geology.

Grammer, G.M., and Harrison, W.B., 2013, Evaluation and Modeling of Stratigraphic Control on the Distribution of Hydrothermal Dolomite away from Major Fault Planes: Western Michigan University Research Partnership to Secure Energy for America Final Technical Report 08123.12.Final, 284 p.

Grammer, G.M., Schultz, J., Barnes, D.A., Gillespie, R., Harrison, W.B., and Thornton, J.E., 2010, Stratigraphic Control on the Lateral Distribution of Hydrothermal Dolomites away from Major Fault Zones:.

Greb, S., and Solis, M., 2010, Chapter 4: Geologic Carbon Storage (Sequestration) Potential in Kentucky, *in* Kentucky Geological Survey, University of Kentucky, p. 55–212.

Haeri-Ardakani, O., Al-Aasm, I., and Coniglio, M., 2014, Hydrothermal Dolomitization and a Fluid Flow Model: An Example from the Middle Ordovician Trenton Group, Southwestern Ontario, Canada*: AAPG Bulletin Search and Discovery,.

Hamilton-Smith, T., Nuttall, B., Gooding, P., Walker, D., and Drahovzal, J., 1990, High-Volume Oil Discovery in Clinton County Kentucky: Kentucky Geological Survey, v. 33.

Harris, D., Hickman, J., and Kincheloe, J., 2006, High Matrix Porosity in a Dolomitized Black River Reservoir, Clinton County, Kentucky:.

Hatcher, R., 2005, Final Report of Results for the Project "Geologic controls of hydrocarbon occurrence in the southern Appalachian basin in eastern Tennessee, southwestern Virginia, eastern Kentucky, and southern West Virginia: University of Tennessee-Knoxville Final Technical Report 896540.

Holland, S.M., and Patzkowsky, M.E., 1996, Sequence Stratigraphy and Long-Term Lithologic Change in the Middle and Upper Ordovician of the eastern United States: Geological Society of America, p. 117–130.

Huff, W., and Gunal Turkmenoglu, A., 1981, Chemical Characteristics and origin of Ordovician K-bentonites along the Cincinnati Arch: Clays and Clay Minerals, v. 29, no. 2, p. 113–123.

Kim, S.-T., Coplen, T.B., and Horita, J., 2015, Normalization of stable isotope data for carbonate minerals: Implementation of IUPAC guidelines: Geochimica et Cosmochimica Acta, v. 158, p. 276–289, doi: 10.1016/j.gca.2015.02.011.

Kolata, D.R., Huff, W.D., and Bergström, S.M., 2001, The Ordovician Sebree Trough: An oceanic passage to the Midcontinent United States: Geological Society of America Bulletin, v. 113, no. 8, p. 1067–1078, doi: 10.1130/0016-7606(2001)113<1067:TOSTAO>2.0.CO;2.

Machel, H.G., 1991, Causes and Emission of Luminescence in Calcite and Dolomite:.

McDowell, R., 1986, The Geology of Kentucky- A Text to Accompany the Geologic Map of Kentucky: U.S. Geological Survey Professional Paper 115-H.

McKelvey, V.E., 1967, Phosphate Deposits, *in* Contributions to Economic Geology, Geological Survey Bulletin, Washington D.C., p. 21.

McLaughlin, P.I., Brett, C.E., Taha McLaughlin, S.L., and Cornell, S.R., 2004, High-resolution sequence stratigraphy of a mixed carbonate-siliciclastic, cratonic ramp (Upper Ordovician; Kentucky–Ohio, USA): insights into the relative influence of eustasy and tectonics through analysis of facies gradients: Palaeogeography, Palaeoclimatology, Palaeoecology, v. 210, no. 2–4, p. 267–294, doi: 10.1016/j.palaeo.2004.02.039.

Ong, S.-E., Blagoev, B., Kratchmarova, I., Kristensen, D.B., Steen, H., Pandey, A., and Mann, M., 2002, Stable Isotope Labeling by Amino Acids in Cell Culture, SILAC, as a Simple and Accurate Approach to Expression Proteomics: Molecular & Cellular Proteomics, v. 1, no. 5, p. 376–386, doi: 10.1074/mcp.M200025-MCP200.

Patchen, D., Hickman, J., Harris, D., Drahovzal, J., Lake, P., Smith, L., Nyahay, R., Schulze, R., Riley, R., Baranoski, M., Wickstrom, L., Laughrey, C., Kostelnik, J., Harper, J., et al., 2006, A geologic play book for Trenton-Black River Appalachian Basin exploration: West Virginia University Research Corporation, 1–582 p.

Pope, M.C., Holland, S.M., and Patzkowsky, M.E., 2009, The Cincinnati Arch: A Stationary Peripheral Bulge during the Late Ordovician, *in* Swart, P.K., Eberli, G.P., McKenzie, J.A., Editor, I.J.S., and Co-Editor, T.S.S. eds., Perspectives in Carbonate Geology, John Wiley & Sons, Ltd, p. 255–275.

Pope, M., and Read, F., 1997, High resolution stratigraphy of the Lexington Limestone (Late Middle Ordovician), Kentucky, U.S.A.: Society for Sedimentary Geology: Cool Water Carbonates, v. 56, p. 411–429.

Potter, C.J., Goldhaber, M.B., Heigold, P.C., and Drahovzal, J.A., 1995, Structure of the Reelfoot-Rough Creek rift system, Fluorspar area fault complex, and Hicks Dome, southern Illinois and western Kentucky; new constraints from regional seismic reflection data: Geological Survey (U.S.) Professional Paper USGS Numbered Series 1538-Q.

Reid, W., Harris, D., Drahovzal, J., and Woolery, E., 2004, Origin and Distribution of Fault-Related Dolomites in Central Kentucky: Imaging of Near-Surface Reservoir Analogs: Kentucky Geological Survey.

Rowan, E.L., 2006, Burial and thermal history of the central Appalachian basin, based on three 2-D models of Ohio, Pennsylvania, and West Virginia: Open-File Report Report 2006-1019, 37 p.

Ryder, R. Oil and Gas Resources of the Cincinnati Arch, Ohio, Indiana, Kentucky, and Tennessee: U.S. Geological Survey Final Technical Report 87-450Y.

Scholle, P.A., and Ulmer-Scholle, D.S., 2003, A Color Guide to the Petrography of Carbonate Rocks: Grains, Textures, Porosity, Diagenesis, AAPG Memoir 77: AAPG.

Slater, B.E., and Smith, L.B., 2012, Outcrop analog for Trenton–Black River hydrothermal dolomite reservoirs, Mohawk Valley, New York: AAPG Bulletin, v. 96, no. 7, p. 1369–1388, doi: 10.1306/10041110200.

Smith, L.B., 2006, Origin and reservoir characteristics of Upper Ordovician Trenton–Black River hydrothermal dolomite reservoirs in New York: AAPG Bulletin, v. 90, no. 11, p. 1691–1718, doi: 10.1306/04260605078.

Smith, T., and Nyahay, R., 2005, Wrench Fault Architecture of Trenton Black River Hydrothermal Dolomite Reservoirs:.

Swart, P.K., Eberli, G.P., and McKenzie, J.A., 2012, Perspectives in Carbonate Geology: A Tribute to the Career of Robert Nathan Ginsburg (Special Publication 41 of the IAS): John Wiley & Sons.

Thompson, M., 2005, The Jeptha Knob Cryptoexplosive Structure, Shelby County, Kentucky, and Buffalo Trace Distillery, Franklin County, Kentucky: American Institute of Professional Geologists.

Twiss, R., and Moores, E., 1992, Structural Geology: W. H. Freeman and Company.

Weir, G.W., Peterson, W.L., and Swadley, W.C., 1984, Lithostratigraphy of Upper Ordovician Strata Exposed in Kentucky, *in* Contributions to the Geology of Kentucky, U.S. Geological Survey.

Witzke, B.J., Ludvigson, G.A., and Day, J., 1996, Paleozoic sequence stratigraphy; views from the North American Craton: Geological Society of America.

Young, S.A., Saltzman, M.R., and Bergström, S.M., 2005, Upper Ordovician (Mohawkian) carbon isotope (δ13C) stratigraphy in eastern and central North America: Regional expression of a perturbation of the global carbon cycle: Palaeogeography, Palaeoclimatology, Palaeoecology, v. 222, no. 1–2, p. 53–76, doi: 10.1016/j.palaeo.2005.03.008.

Appendix A

List of tables illustrating results from stable isotope and fluid inclusion analysis.

SYSTEM	First Melting - T_e T °C ----------> lower
$NaCl-H_2O$	stable -21.2 metastable -28 observed (-21.1 to -21.2) (-28 to -35)
$NaCl-CaCl_2-H_2O$	stable -52 metastable -70 observed (-47 to -53) (-70 to -85) -90
$NaCl-MgCl_2-H_2O$	stable -35 metastable (-37 to -55) -80 observed (-33 to -40) (-45 to -50) (-70 to -80)
$NaCl-KCl-H_2O$	stable -22.9 metastable -28 observed (-23.0 to -23.4)
$NaCl-CaCl_2-MgCl_2-H_2O$	stable -57 metastable observed

(From Goldstein and Reynolds, 1994)

Table 1 A table that is utilized in conjunction with Te (eutectic temperatures) to determine fluid compositions within fluid inclusions (From Goldstein and Reynolds, 1994).

FPD	.0	.1	.2	.3	.4	.5	.6	.7	.8	.9
0.	0.00	0.18	0.35	0.53	0.71	0.88	1.05	1.23	1.40	1.57
1.	1.74	1.91	2.07	2.24	2.41	2.57	2.74	2.90	3.06	3.23
2.	3.39	3.55	3.71	3.87	4.03	4.18	4.34	4.49	4.65	4.80
3.	4.96	5.11	5.26	5.41	5.56	5.71	5.86	6.01	6.16	6.30
4.	6.45	6.59	6.74	6.88	7.02	7.17	7.31	7.45	7.59	7.73
5.	7.86	8.00	8.14	8.28	8.41	8.55	8.68	8.81	8.95	9.08
6.	9.21	9.34	9.47	9.60	9.73	9.86	9.98	10.11	10.24	10.36
7.	10.49	10.61	10.73	10.86	10.98	11.10	11.22	11.34	11.46	11.58
8.	11.70	11.81	11.93	12.05	12.16	12.28	12.39	12.51	12.62	12.73
9.	12.85	12.96	13.07	13.18	13.29	13.40	13.51	13.62	13.72	13.83
10.	13.94	14.04	14.15	14.25	14.36	14.46	14.57	14.67	14.77	14.87
11.	14.97	15.07	15.17	15.27	15.37	15.47	15.57	15.67	15.76	15.86
12.	15.96	16.05	16.15	16.24	16.34	16.43	16.53	16.62	16.71	16.80
13.	16.89	16.99	17.08	17.17	17.26	17.34	17.43	17.52	17.61	17.70
14.	17.79	17.87	17.96	18.04	18.13	18.22	18.30	18.38	18.47	18.55
15.	18.63	18.72	18.80	18.88	18.96	19.05	19.13	19.21	19.29	19.37
16.	19.45	19.53	19.60	19.68	19.76	19.84	19.92	19.99	20.07	20.15
17.	20.22	20.30	20.37	20.45	20.52	20.60	20.67	20.75	20.82	20.89
18.	20.97	21.04	21.11	21.19	21.26	21.33	21.40	21.47	21.54	21.61
19.	21.68	21.75	21.82	21.89	21.96	22.03	22.10	22.17	22.24	22.31
20.	22.38	22.44	22.51	22.58	22.65	22.71	22.78	22.85	22.91	22.98
21.	23.05	23.11	23.18							

(From Goldstein and Reynolds, 1994)

Table 2 Table used to determine weight percent salinity based on measured freezing point depressions (FPD) within fluids composed of NaCl-H_2O. Temperatures of Tm (final melt) correspond to FPD's (From Goldstein and Reynolds, 1994).

Member	Source	Sample	Mineralogy *	Mean δ13C vs VPDB (permil)	Mean δ18O vs VPDB (corrected mineralogy)(permil)
Grier	C-295-3	1A	calcite	0.5	-6.5
Grier	C-295-3	1B	calcite	0.5	-6.4
Grier	C-295-3	1C	calcite	0.5	-6.4
Grier	C-295-3	1D	calcite	0.7	-6.0
Grier	C-295-3	1E	calcite	0.7	-5.7
Grier	C-295-3	1F	calcite	0.9	-5.0
Grier	C-295-3	1G	calcite	0.8	-5.1
Grier	C-295-3	1H	dolomite	0.8	-6.4
Grier	C-295-3	1I	dolomite	1.1	-7.7
Grier	C-295-3	1J	dolomite	1.2	-7.3
Grier	C-295-3	1K	dolomite	1.1	-7.4
Grier	C-295-3	1L	dolomite	1.1	-7.7
Millersburg	C-511-1	2A	calcite	-0.4	-5.1
Millersburg	C-511-1	2B	calcite	0.1	-4.5
Millersburg	C-511-1	2C	calcite	0.0	-5.0
Millersburg	C-511-1	2D	calcite	-0.5	-5.3
Millersburg	C-511-1	2E	calcite	-0.6	-6.0
Millersburg	C-511-1	2F	dolomite	0.3	-8.3
Millersburg	C-511-1	2G	dolomite	0.7	-7.2
Millersburg	C-511-1	2H	dolomite	0.4	-8.2
Millersburg	C-511-1	2I	calcite	-0.5	-5.4
Millersburg	C-511-1	2H	calcite	0.2	-4.0
Millersburg	C-511-1	2K	dolomite	0.2	-8.3
Millersburg	C-511-1	2L	calcite	-0.5	-5.5
Millersburg	C-1221-6	3A	calcite	-0.9	-5.5
Millersburg	C-1221-6	3B	calcite	-0.5	-4.0
Millersburg	C-1221-6	3C	dolomite	-1.5	-8.1
Millersburg	C-1221-6	3D	calcite	-0.8	-5.3
Millersburg	C-1221-6	3E	calcite	-0.8	-5.0
Millersburg	C-1221-6	3F	dolomite	-1.3	-7.8
Millersburg	C-1221-6	3G	dolomite	-1.4	-8.0
Millersburg	C-1221-6	3H	calcite	-0.4	-3.8
Millersburg	C-1221-6	3I	calcite	-1.4	-7.0
Millersburg	C-1221-6	3J	dolomite	-1.3	-8.3
Millersburg	C-1221-6	3K	calcite	-0.4	-3.8
Millersburg	C-1221-6	3L	calcite	-1.0	-5.4
NA	C-1286-1	4	calcite	-0.3	-3.7
Grier	C-1220-1	5	dolomite	2.1	-7.0
Black River	C-201-2	6	dolomite	-0.6	-9.0
NA	C-1287-1	7	calcite	0.3	-3.2
Millersburg	DRF3	8	calcite	0.1	-6.2
Millersburg	DRF3	9	dolomite	-0.9	-10.9
Millersburg	DRF4	10	dolomite	-1.1	-10.2
Millersburg	DRF4	11	dolomite	0.7	-7.1
Millersburg	DRF5A	12	dolomite	-0.5	-10.4
Millersburg	LBA	13	dolomite	-0.7	-6.4
Millersburg	LBB	14	dolomite	-0.4	-7.8
Millersburg	LBC	15	dolomite	-0.7	-6.7
Millersburg	LBD	16	calcite	-0.8	-5.4
Millersburg	LBE	17	dolomite	-0.9	-5.7

Table 3 Table listing results from stable isotope analyses with $\delta^{18}O_{dolomite}$ corrections applied.

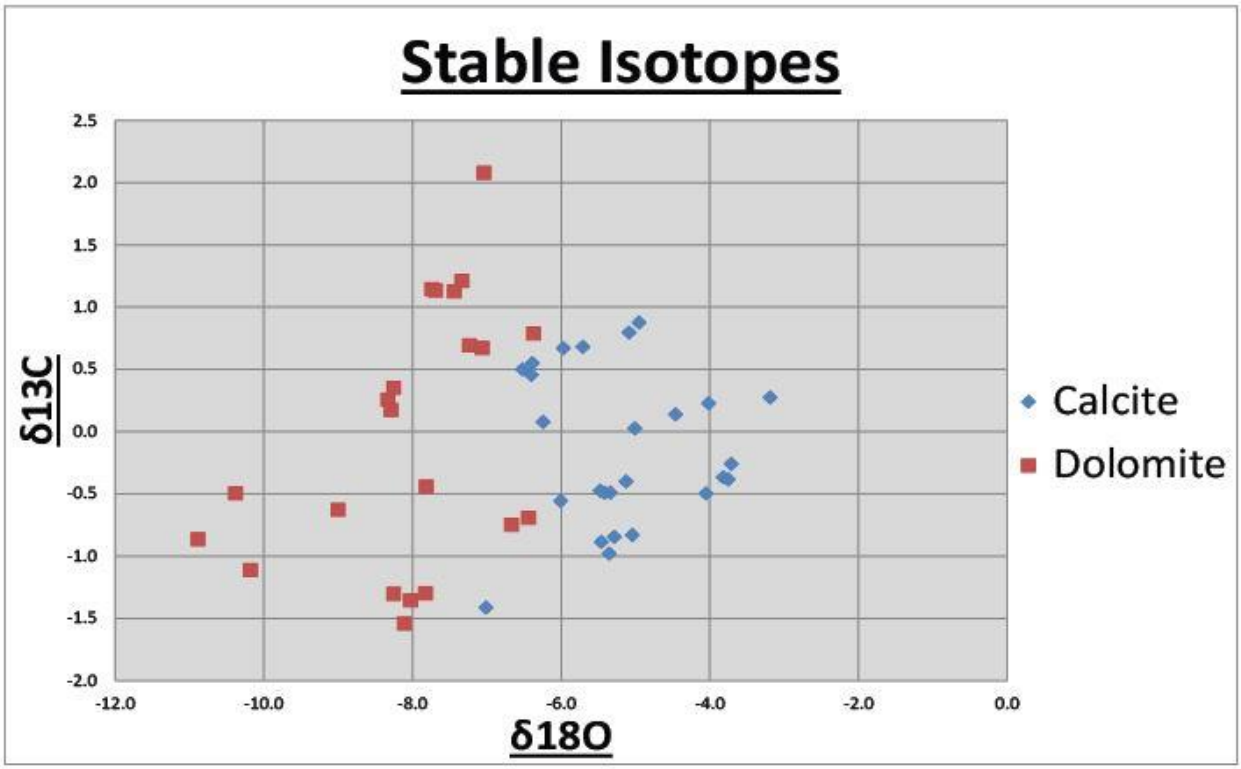

Millersburg Calcite δ13C	δ13C (‰)
Minimum	-1.40
Maximum	0.20
Average	-0.50
Standard Deviation	0.43

Early Dolomite	δ18O (‰)
Minimum	-9.00
Maximum	-6.37
Average	-7.96
Standard Deviation	0.78

North-Central Dolomite	δ18O (‰)
Minimum	-10.88
Maximum	-5.69
Average	-8.23
Standard Deviation	1.93

Grier Calcite δ13C	δ13C (‰)
Minimum	0.50
Maximum	0.80
Average	0.64
Standard Deviation	0.16

Late Dolomite	δ18O (‰)
Minimum	-7.83
Maximum	-7.23
Average	-7.54
Standard Deviation	0.25

South-Central Dolomite	δ18O (‰)
Minimum	-8.33
Maximum	-6.37
Average	-7.71
Standard Deviation	0.57

Dolomite δ18O	δ18O (‰)
Minimum	-10.88
Maximum	-5.69
Average	-7.91
Standard Deviation	1.28

Table 4 Plots illustrating $\delta^{18}O$ versus $\delta^{13}C$ of calcites and dolomites and numerous tables demonstrating variations in the Millersburg and Grier Members, between early versus late-stage dolomites, and between northern and southern Kentucky samples.

Appendix B

Petrographic analysis of depositional and diagenetic facies from outcrop and core samples itemizing abundances of grain types, cements, depositional fabrics, diagenetic fabrics, members, depositional facies, and porosities.

Group	Slide	Facies	Member	Lithology	% Micrite Matrix	Other	Well Log API
Lightbulb	L1C	Moderate Energy Mid-Ramp Dolomite	Millersburg	Crystalline Dolomite	0		
Lightbulb	L1D	Moderate Energy Mid-Ramp Dolomite	Millersburg	Crystalline Dolomite	0	Py	
Lightbulb	L1E	Moderate Energy Mid-Ramp Dolomite	Millersburg	Crystalline Dolomite	0		
Lightbulb	L2B	Moderate Energy Deep Ramp Dolomite	Millersburg	Crystalline Dolomite	0		
Lightbulb	L2C	Moderate Energy Deep Ramp Dolomite	Millersburg	Crystalline Dolomite	0	Py	
Lightbulb	L2D	Moderate Energy Deep Ramp Dolomite	Millersburg	Crystalline Dolomite	0	Py	
Lightbulb	L2E	Moderate Energy Deep Ramp Dolomite	Millersburg	Crystalline Dolomite	0		
Lightbulb	L3A	Dolomite	Millersburg	Crystalline Dolomite	0	Py, Qtz	
Lightbulb	L3B	Dolomite	Millersburg	Crystalline Dolomite	0	Py	
Lightbulb	L3C	Dolomite	Millersburg	Crystalline Dolomite	0	Py	
Lightbulb	L3D	Dolomite	Millersburg	Crystalline Dolomite	0	Py	
Lightbulb	L1A	Moderate Energy Mid-Ramp	Millersburg	Echinoid-Bivalve-Ostracode-Wackestone	0		
Lightbulb	L1B	Moderate Energy Mid-Ramp	Millersburg	Bryozoan-Ostracode-Echinoid-Packstone	0	Py	
Lightbulb	L1F	Moderate Energy Mid-Ramp	Millersburg	Ostracode-Echinoid-Bryozoan-Packstone	0	Py	
Lightbulb	L1G	Moderate Energy Mid-Ramp	Millersburg	Bivalve-Echinoid-Bryozoan-Packstone	0	Py	
Lightbulb	L4A	Moderate Energy Mid-Ramp	Millersburg	Ostracode-Bryozoan-Wackestone	0	Py	
Lightbulb	L4B	Moderate Energy Mid-Ramp	Millersburg	Bryozoan-Echinoid-Brachiopod-Wackestone	0	Py	
Lightbulb	L4C	Moderate Energy Mid-Ramp	Millersburg	Bryozoan-Ostracode-Echinoid-Wackestone	0	Py	
Lightbulb	L4D	Moderate Energy Mid-Ramp	Millersburg	Echinoid-Bryozoan-Wackestone	0	Py	
Lightbulb	L2A	Moderate Energy Deep Ramp	Millersburg	Echinoid-Bryozoan-Ostracode-Wackestone	0		
Lightbulb	L2F	Moderate Energy Deep Ramp	Millersburg	Bivalve-Ostracode-Echinoid-Wackestone	0	Py	
Lightbulb	L2G	Moderate Energy Deep Ramp	Millersburg	Ostracode-Echinoid-Wackestone	0		
Lightbulb	L5A	Moderate Energy Deep Ramp	Millersburg	Ostracode-Brachiopod-Bryozoan-Packstone	0	Py	
Drag Fold	D5C	High Energy Mid-Ramp	Millersburg	Gastropod Wackestone	10	Ch	
Drag Fold	D5D	High Energy Mid-Ramp	Millersburg	Echinoid Wackestone	10	Ch, Fl	
Drag Fold	D6A	High Energy Mid-Ramp	Millersburg	Bryozoan Wackestone	20	Ch, Fl	
Drag Fold	D6B	High Energy Mid-Ramp	Millersburg	Echinoid Wackestone	20		
Drag Fold	D1A	Moderate Energy Deep Ramp	Millersburg	Trilobite-Brachiopod Wackestone	10	Fl, Sp	
Drag Fold	D1B	Moderate Energy Deep Ramp	Millersburg	Brachiopod Wackestone	25	Py,Ba	
Drag Fold	D2A	Moderate Energy Deep Ramp	Millersburg	Brachiopod -Trilobite Wackestone	25	Ch, Sp	
Drag Fold	D2B	Low Energy Deep Ramp	Millersburg	Peloidal Wackestone	50	Ch	
Drag Fold	D3A	Low Energy Deep Ramp	Millersburg	Peloidal Wackestone	50	Ch, Sp	
Drag Fold	D3B	Low Energy Deep Ramp	Millersburg	Brachiopod Packstone	50	Ch	
Drag Fold	D4A	Low Energy Deep Ramp	Millersburg	Brachiopod Packstone	25	Sp	
Drag Fold	D4B	Low Energy Deep Ramp	Millersburg	Peloidal Packstone	30	Ch, Fl, Sp	
Drag Fold	D5A	Low Energy Deep Ramp	Millersburg	Peloidal Packstone	35	Ch, Sp	
Drag Fold	D5B	Low Energy Deep Ramp	Millersburg	Peloidal Packstone	35	Sp	
Drag Fold	D4C	High Energy Shallow Shelf	Millersburg	Bryozoan Boundstone	15	Sp	
106	C-106-1 (24')	Moderate Energy Deep Ramp	Millersburg	Echinoid Wackestone	10	Fl, Ch, Sp	16049000330000
106	C-106-2 (27.5')	Moderate Energy Deep Ramp	Millersburg	Echinoid Wackestone	10	Fl, Ch, Qtz, Sp	16049000330000
C-200	C-200-1 (57')	Low Energy Mid-Ramp	Grier	Echinoid Packstone	40	Py	16049000330000
C-200	C-200-2 (82.5')	Low Energy Mid-Ramp	Grier	Echinoid Wackestone	65	Py	16049000330000
C-200	C-200-3 (176')	Lagoon	Black River	Peloidal Packstone	90		16049000330000
C-201	C-201-1 (48')	High Energy Mid-Ramp	Millersburg	Echinoid Packstone	10	Ch	16049000330000
C-201	C-201-3 (228')	Mid-Ramp Open Marine	Curdsville	Echinoid Packstone	0	Ch, Sp, Qtz	16049000330000
C-201	C-201-2 (230.5')	Lagoon	Black River	Echinoid Wackestone	75	Ch, Fl, Ba, Sp	16049000330000
	C-1286-1 (806.5')	Dolomite	NA	Crystalline Dolomite	0	Fl	NA
128	C-1287-1 (647')	Dolomite	NA	Crystalline Dolomite	0	Fl, Qtz	NA
128	C-1287-2 (679.5')	Dolomite	NA	Crystalline Dolomite	0	Fl	NA
C-295	C-295-1 (708.25')	Moderate Energy Deep Ramp	Millersburg	Trilobite Wackestone	0	Qtz	16057001420000
C-295	C-295-2 (754.75')	Lagoon	Perryville Limestone (Faulconer Bed)	Ostracode Packstone	70	Ch	16057001420000
C-295	C-295-4 (781')	Low Energy Mid-Ramp	Grier	Peloidal Wackestone	60	Fl, Qtz	16057001420000
C-295	C-295-5 (843.5')	Mid-Ramp Open Marine	Curdsville	Stromatoporoid Wackestone	0	Ch, Fl, Py	16057001420000
C-295	C-295-6 (872.5')	Mid-Ramp Open Marine	Curdsville	Crystalline Carbonate	0	Ch, Fl	16057001420000
C-511	C-511-2 (710')	Lagoon	Devils Hollow	Stromatoporoid Wackestone	40	Py, Fl, Ch	16053053770000
C-511	C-511-3 (867.5')	High Energy Shallow Shelf	Sulfur Well	Echinoid Packstone	10	Ch, Fl	16053053770000
C-511	C-511-4 (882.25')	Lagoon	Perryville Limestone (Faulconer Bed)	Peloidal Wackestone	80	Ch	16053053770000
C-511	C-511-5 (901.5')	Low Energy Mid-Ramp	Grier	Ostracode Wackestone	40	Py	16053053770000
C-511	C-1220-1 (900.6')	Moderate Energy Mid-Ramp	Grier	Echinoid Packstone	10	Fl	16053023920000
C-1221	C-1221-2 (559.2')	Moderate Energy Mid-Ramp	Grier	Bryozoan Wackestone	25	Py	16053051510000
C-1221	C-1221-5 (512.25')	Moderate Energy Deep Ramp	Millersburg	Bryozoan Ostracode Packstone	10		16053051510000
C-1221	C-1221-1 (496')	High Energy Deep Ramp	Millersburg	Echinoid Packstone	10	Fl, Py	16053051510000
C-1221	C-1221-4 (529')	High Energy Shallow Shelf	Sulfur Well	Bryozoan Grainstone	20	Py	16053051510000
C-1221	C-1221-3 (605.75')	Low Energy Mid-Ramp	Grier	Peloidal Wackestone	50	Py	16053051510000

Color-coded columns: Hydrothermal Dolomitization; Echinoids; Ostracodes; Foraminifera; Bivalves; Gastropods; Brachiopods; Dasycladacean Green Algae (*Mastopora*); Radiolarians; Stromatoporoids; Red Algae (Solenoporaceae); Crinoids; Carophytes; Calcispheres; Sponges; Tabulate Corals; Rugose Corals; Bryozoans; Cephalopods; Trilobites; Grapestones; Ooids; Pellets; Peloids; Extraclasts; Intraclasts; Worm Tubes; Syntaxial Overgrowth; Pendant Overgrowth; Isopachous; Coarsen Inwards; Poikilotopic; Clear; Cloudy; Equant; Drusy; Blocky; Ferrous Calcite; Baroque; Sweeping Extinction; Fractured Grain; Sutured Boundaries; Spalling Ooids; Cementation; Micritization; Neomorphism; Compaction; Dolomitization; Phosphatization-Fracture; Phosphatization-Depositional; Burial Connate; Meteoric Vadose; Meteoric Phreatic; Marine Vadose; Marine Phreatic; Horizontal Laminations; Fenestral; Stylolites; Geopetal; Burrowed; Total Porosity; Moldic Porosity; Intercrystalline Porosity; Intracrystalline Porosity; Vugular Porosity; Fracture Porosity

2%	Low Abundance	Sp: Sphalerite	Qtz: Quartz
10%	Moderate Abundance	Fl: Fluorite	Ba: Barite
30%	High Abundance	Ch: Chalcedony	Py: Pyrite
50%	Very High Abundance		

Vita

Collin James Gray was born and raised in Traverse City, Michigan. The third of three children of Michael and Deborah Gray, he graduated from Traverse City West Senior High School in 2008 and enrolled at Sault Ste Marie: Lake Superior State University, Sault Ste Marie, Michigan. While pursuing a Bachelor of Science degree in geology, he worked as an intern for West Bay Exploration Company during semester breaks from 2012 to 2013 and conducted undergraduate research focusing on geomagnetics in the ID/OR region. Collin qualified for the Dean's List in 2011, 2012, and 2013, and received the Lake Superior State Geology Club Scholarship in 2012 and 2013 and the Outstanding Geology Graduate Award in 2013. After graduating *cum laude* from Lake Superior State University in 2013, he enrolled at the University of Texas at El Paso, Texas in the fall of 2013 to pursue a Master of Science degree in geological sciences. While a graduate student, he received a research sponsorship from West Bay Exploration Company and completed internships with West Bay Exploration Company in Traverse City, Michigan, and with ConocoPhillips in Houston, Texas while receiving scholarships and grants from the American Association of Petroleum Geologists, the Geological Society of America, the West Texas Geological Society, the Southwest Section of the American Association of Petroleum Geologists, and the Society of Petrophysicists and Well Log Analysts. Collin also received an Award of Excellence for presenting a "Top 10" Poster Presentation at the June 2015 AAPG Annual Convention and Exhibition, and received the honor of serving as the Graduate Marshall of Students during UTEP's fall 2015 commencement ceremony.

Permanent address: 9979 Terra West
Traverse City, MI 49685

This thesis was typed by Collin James Gray.